Mechanisms of BAR Protein Function in Brush Border Assembly

By

Meagan Marie Postema

Dissertation

Submitted to the Faculty of the

Graduate School of Vanderbilt University

in partial fulfillment of the requirements

for the degree of

DOCTOR OF PHILOSOPHY

in

Cell and Developmental Biology

September 30, 2019

Nashville, TN

Approved:

Kathleen L. Gould, Ph.D.

Irina Kaverina, Ph.D.

Robert J. Coffey, M.D.

Matthew J. Tyska, Ph.D.

For Izzy and Teddy

ACKNOWLEDGEMENTS

First and foremost, I would like to thank my wonderful mentor, Matt Tyska, for the tremendous amount of support and guidance he has provided me. Because of the countless hours Matt has spent helping me improve my writing and presentation skills and discussing my project, I am a better writer, public speaker, and critical thinker. Matt is a tremendous teacher, and his passion and enthusiasm for science is contagious; it has been a privilege to have trained with such an amazing scientist and mentor.

I am also thankful for my supportive and encouraging committee members, Drs. Kathy Gould, Bob Coffey, and Irina Kaverina. They have always been accessible when I need them and have provided much needed advice, guidance and recommendation letters. Furthermore, I must acknowledge the Vanderbilt Microtubules and Motors Club and Epithelial Biology Center for thoughtful discussions on my research. As well as the Nikon Center of Excellence and the Electron Microscopy Core, especially Evan Krystofiak who has helped me perfect my SEM technique and provided guidance on KO tissue experiments. I also thank the CDB staff members, especially Susan and Kristi, who work diligently to keep our department running and are always available when needed.

I must also acknowledge Tyska lab members, as I am beyond fortunate to have worked with such wonderful and amazing people. Past lab members Nathan and Meredith were exceptionally helpful mentors and provided the guidance I needed to excel with my project. Moreover, my experience as a graduate student would not have been the same without the current lab members Suli, Caroline, Bella, Leslie, Angelo, Colbie and Gill. I will forever be grateful for all the amazing conversations, lunches, and coffee breaks I've had with my lab mates; they provided many necessary distractions, as well as incredible

support over the last few years. I am confident that the friends I have made in the lab will be friends for life, and I look forward to seeing their many future successes.

I must acknowledge my friends in the department and IGP program who have provided an enormous amount of support and love over the last five years. Also, my “murderino” group who have become lifelong friends and have immensely enriched my time living in Nashville. Finally, I must thank my family for the love and support they have provided, without them I would not be where I am today. My parents have always been there for me and I’m grateful for the number of times they have come to Nashville to visit me over the last few years. Additionally, I need to thank my younger sister, Melanie, my beautiful and bright nieces, Grace and Caroline, and my older sister, Nichole, who have all been extremely supportive through this entire process and I am continually grateful for their love and understanding.

TABLE OF CONTENTS

Page

LIST OF FIGURES

LIST OF ABBREVIATIONS

^{o}C	degrees Celsius
Δ	delta, deletion
α-HD	alpha- helical domain
aa	amino acids
AB	actin-binding domain
ADP	adenosine diphosphate
A/E	attaching/effacing
AH	alpha helix
ATP	adenosine triphosphate
BAIAP2L1	brain-specific angiogenesis inhibitor 1-associated protein 2 like 1
BAR	Bin-Amphiphysin-Rvs
BB	brush border
BMP	bone morphogenetic protein
BSA	bovine serum albumin
CIP4	Cdc4- Interacting Protein 4
CL4	LLC-PK1-CL4 cells
CO_2	carbon dioxide
COBL	cordon bleu
CRIB	Cdc42/Rac interactive binding
CRISPR	clustered regularly interspaced short palindromic repeats
C-terminal	carboxy-terminal

DAPI	4’,6-diamidino-2-phenylindole
DMSO	dimethyl sulfoxide
DOX	doxycycline
EGF	epidermal growth factor
EGFP	enhanced green fluorescent protein
EHEC	enterohemorrhagic *Escherichia coil*
EPEC	enteropathogenic *Escherichia coii*
ERM	ezrin, radixin, moesin protein family
EPS8	epidermal growth factor receptor pathway substrate 8
F-BAR	Fes-CIP4 homology Bin-amphiphysin-Rvs161/167
FBS	fetal bovine serum
FFT	fast Fourier transform
FL	full-length
FRAP	fluorescence recovery after photobleaching
GAPDH	glyceraldehyde 3-phosphate dehydrogenase
GTP	guanosine triphosphate
H&E	hematoxylin and eosin staining
HET	heterozygous
Hs	*Homo sapiens*
I-BAR	Inverse Bin-Amphiphysin-Rvs
IMAC	intermicrovillar adhesion complex
IRTKS	Insulin receptor tyrosine kinase substrate
IRSp53	Insulin receptor substrate 53 kDa

KD	knockdown
K_D	equilibrium dissociation constant
kDa	kilodaltons
KO	knockout
LKB1	liver kinase B1
Max I.P.	maximum intensity projection
mCh	mCherry
Mena	mammalian enabled
min	minute
MIM	missing in metastasis
MV	microvilli
NIH	National Institutes of Health
NMR	nuclear magnetic resonance
NND	nearest neighbor distance
NPF	nucleation promoting factor
ns	not significant
N-terminal	amino-terminal
N-WASP	Neural Wiskott–Aldrich Syndrome protein
ON	overnight
PACSIN	protein kinase C and casein kinase substrate in neurons
PBS	phosphate buffered saline
PC	Paneth cells
PCDH24/CDHR2	protocadherin-24

PCR	polymerase chain reaction
PFA	paraformaldehyde
PH	pleckstrin homology domain
Phall	phalloidin
Pinkbar	planar intestinal and kidney specific BAR domain protein
PIP(4,5)P_2	phosphatidylinositol (4,5)-bisphosphate
PM	plasma membrane
PR	proline rich
ROI	region of interest
RT	room temperature
SAH	single α-helix
Scr	scramble
SD	standard deviation
SDCM	spinning disk confocal microscopy
SIM	structured illumination microscopy
sec	second
SEM	scanning electron microscopy
SH3	SRC homology 3
shRNA	short hairpin ribonucleic acid
STRADα	STE20-related kinase adapter protein alpha
t	time
T3SS	type 3 secretion system
TBS	tris buffered saline

TEM	transmission electron microscopy
Tir	translocated intimin receptor
TIRF	total internal reflection fluorescence
UtrCH	Utrophin
VAMP4	vesicle associated membrane protein 4
VASP	vasodilator-stimulated phosphoprotein
W4	Ls174T- W4 cells
WGA	wheat germ agglutin
WH2	Wiskott-Aldrich homology 2
WT	wild-type
ZO-1	zona occludens-1

CHAPTER I

INTRODUCTION

Polarized Epithelial Cells

Polarized epithelial cells form sheets that line the external surfaces of the body and all internal cavities and glands. They provide a barrier between the inside and outside worlds and are the first line of defense against physical, chemical, and biological perturbations. Epithelial cells also act as gatekeepers of the body through their functions in secretion, absorption, and filtration; any substance that enters the body must first pass through an epithelial cell (Guillot and Lecuit, 2013). Tight junctions between cells promote this barrier function by forming an impenetrable surface to unwanted substances. A defining characteristic of epithelial cells is their ability to polarize into distinct apical and basal domains that help aid their functions (Roignot et al., 2013). The apical domain is exposed to the outside world and thus contains specialized proteins and organelles necessary to perform cellular functions, e.g. filtration in the liver and solute transport in the intestine. In contrast, the basal domain is attached to the basement membrane which serves to anchor the epithelium to underlying connective tissue. The morphology of an epithelial cell is critical for its function and it is often detrimental when the processes that control cell shape are lost. For instance, a carcinoma is a type of malignant cancer that derives from epithelial cells. This often occurs when cells lose the signals responsible for maintaining their shape, leading to a loss of normal function and uncontrollable growth. Thus, it is

important to understand the molecules that control cell shape to prevent disease when normal shape is compromised.

Cell shape and organization is controlled by the cytoskeleton, which consists of three main components - microtubules, intermediate filaments, and actin. All three cytoskeletal proteins form filaments that interact with the plasma membrane to provide structure to cellular processes. This introduction will focus on the actin cytoskeleton and how it is assembled and regulated by actin-binding proteins. The model system that we use to study the actin cytoskeleton, the enterocyte brush border, will first be introduced along with linear actin-bundled protrusions. Then, the classes of actin-binding proteins that assemble outward protrusions will be discussed with an emphasis on the specific molecules necessary for microvillar growth. Finally, we will focus on BAR domain-containing proteins and how they link the actin cytoskeleton to the plasma membrane in a majority of cellular processes that require membrane dynamics. The goal of this introduction is to provide perspective on the BAR domain proteins IRTKS and PACSIN2, and how our studies on these BAR proteins have advanced the field of epithelial cell biology.

Epithelial cell classifications

Epithelial sheets come in many different shapes and morphologies to simplify their functions. There are three main classes of epithelial cells based on their overall shape; 1) columnar epithelial cells, 2) flat and scale-like squamous epithelial cells, and 3) cuboidal epithelial cells (Fig. 1-1). These classifications can be further broken down according to the number of epithelial layers the tissue contains. A simple epithelium has

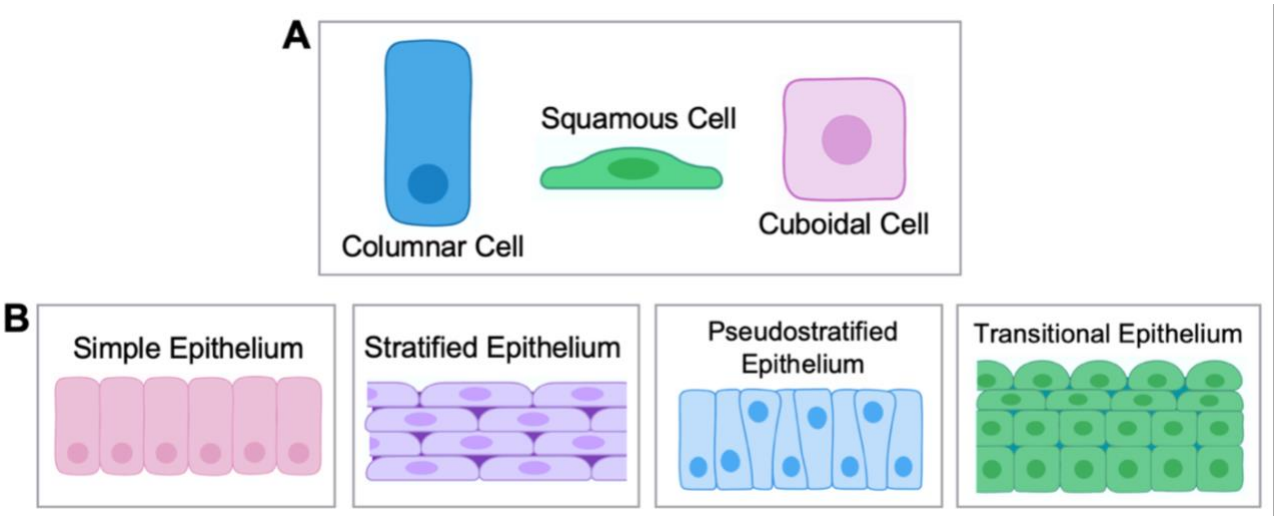

Figure 1-1. Epithelial cell shape and tissue organization. Cartoon schematics depicting **(A)** the three basic shapes epithelial cells take - columnar, squamous and cuboidal, and **(B)** the four classification of epithelial tissue from the number and shape of the cell layers. Images from BioRender.com.

one layer of cells with every cell in contact with the basement membrane. These tissues are usually involved in solute transfer, diffusion, and secretion and reside in areas of the body where large amounts of absorption and filtration are needed. A stratified epithelium has multiple layers of cells and are usually in areas of the body where large amounts of mechanical or chemical stress occur. Two additional, rarer categories are the pseudostratified epithelium, with contains one layer of cells with nuclei positioned to resemble multiple layers, and the transitional epithelium, which contains a mix of squamous and cuboidal cells (Fig. 1-1). Transitional epithelium is only seen in the urinary organs where the combination of cell shapes allows for expansion; transitional cells in the bladder appear cuboidal in shape when resting and take on a squamous appearance when distended (Apodaca, 2004). Most epithelial nomenclature states the number of layers followed by the cell shape. For example, a stratified squamous epithelium contains

multiple layers of squamous cells that protect the tissue against physical and chemical abrasion, such as the mouth and esophagus.

Apical surface specializations

In addition to general cell and tissue morphology, epithelial cells can be further specialized through cytoskeleton-based apical surface modifications. There are three main classes of surface specializations – cilia, microvilli, and stereocilia. All three structures protrude out of the apical surface of the epithelium they derive from to facilitate interactions with the external environment. Cilia are highly motile structures found on the surface of the respiratory tract and the female reproductive tract where they clear mucus and debris off of the cell surface. They contain a core of microtubule filaments and are usually between 5 and 10 μm in length. Microvillar protrusions are relatively short and are around 30-40 bundled actin filaments and aid in increasing epithelial surface area for solute transport (Ohta et al., 2012). Stereocilia are arranged in rows of graded height on the apical surface of cochlear and vestibular epithelial cells to promote hearing and balance (Tilney and Saunders, 1983). They are originally derived from microvilli and range from 1 μm to 100 μm in length depending on the specific epithelium (Prost et al., 2007). As we study the actin cytoskeleton in our lab, we will only focus on the two actin-based surface modifications, stereocilia and microvilli, going forward.

Both stereocilia and microvilli are supported by a core bundle of actin filaments that generates the rigidity needed for membrane deformation. These filaments are oriented in the same direction with their fast- growing barbed ends embedded in a dense tip complex of proteins that likely consists of actin nucleators and elongators. The filament

pointed ends of each protrusion are embedded in an underlying meshwork of filaments – the terminal web for microvilli (Hirokawa et al., 1982), and the cuticular plate for stereocilia (Pollock and McDermott, 2015). These underlying networks of filaments anchor microvilli and stereocilia into the cell to provide stability to the protrusions.

The main difference between microvilli and stereocilia are in the density of the protrusions and their lifetimes. Microvilli are all of a uniform length and densely packed on the apical surface of intestinal epithelial cells. Furthermore, they are maintained for the entire lifetime of the cell, roughly 3-5 days in enterocytes. In contrast, stereocilia are in graded arrays on the surface of inner ear epithelial cells and have to be preserved for the entire lifespan of the organism. Therefore, the actin-binding proteins and their regulation are highly specific to each structure. Nevertheless, even though the individual molecules may differ, the steps leading to protrusion and elongation between both structures are relatively similar. These general steps towards membrane protrusion and actin elongation are as follows: 1) GTPase signaling molecules need to establish the apical domain and sites of protrusion, 2) individual actin filaments need to nucleate, 3) actin filaments need to associate with the plasma membrane, 4) actin filaments need to bundle into actin cores, and 5) actin cores need to elongate and provide the force to protrude the membrane. Though the exact mechanisms, and even the order, of the preceding steps are not completely understood, recent studies are shaping our understanding of the protrusion process and how the actin cytoskeleton is regulated. Some of these molecules and their role in microvillar protrusions will be discussed in the following sections.

Enterocytes as a model to study apical specializations

The intestine is the main site of nutrient absorption in the body and functions to protect underlying peripheral tissue from bacteria and toxins. The intestinal epithelium is subdivided into two main domains – villi and the crypts of Lieberkühn (crypts). Villi are finger-like folds of tissue that protrude into the intestinal lumen; they function to increase the intestinal surface area for maximal uptake of solutes (Helander and Fandriks, 2014). Crypt domains are tissue invaginations that sit between villar protrusions and contain the intestinal stem cells. Enterocytes, the main type of intestinal epithelial cell, are initially born at the base of the crypts from asymmetric division of stem cells. They then undergo several additional rounds of division and differentiation within the crypt transit amplifying zone, and emerge onto the villus once fully differentiated. The enterocytes then continue to migrate upward until they reach the top of the villus and are sloughed off into the intestinal lumen (van der Flier and Clevers, 2009). This entire process takes approximately 3-5 days and allows for continuous renewal of the intestinal epithelium (Fig. 1-2B).

Enterocytes are simple columnar epithelial cells that form a highly specialized structure on their apical surface called the brush border (Fig. 1-2C). Every brush border is composed of thousands of actin filled protrusions called microvilli that point into the gastrointestinal lumen, functioning to further increase the intestinal nutrient absorbing surface area (Mooseker, 1985). Microvilli must be of a uniform length and densely packed into hexagonal patterns with little free space between adjacent protrusions (Helander and Fandriks, 2014). Perturbations to the structure or packing of microvilli can significantly decrease nutrient absorption, often leading to malnutrition and osmotic diarrhea (Bailey et al., 1989). Numerous gastrointestinal diseases are also associated with the disruption

of brush border structure and function, similarly resulting in diarrhea and nutrient malabsorption. These include microvillus inclusion disease, celiac disease, and infections with the attaching and effacing bacteria enteropathogenic (EPEC) and enterohemorrhagic (EHEC) *Escherichia coli* (Khubchandani et al., 2011; Vallance et al., 2002; Wilson et al., 2001)**,** which will be discussed in more detail in a later section.

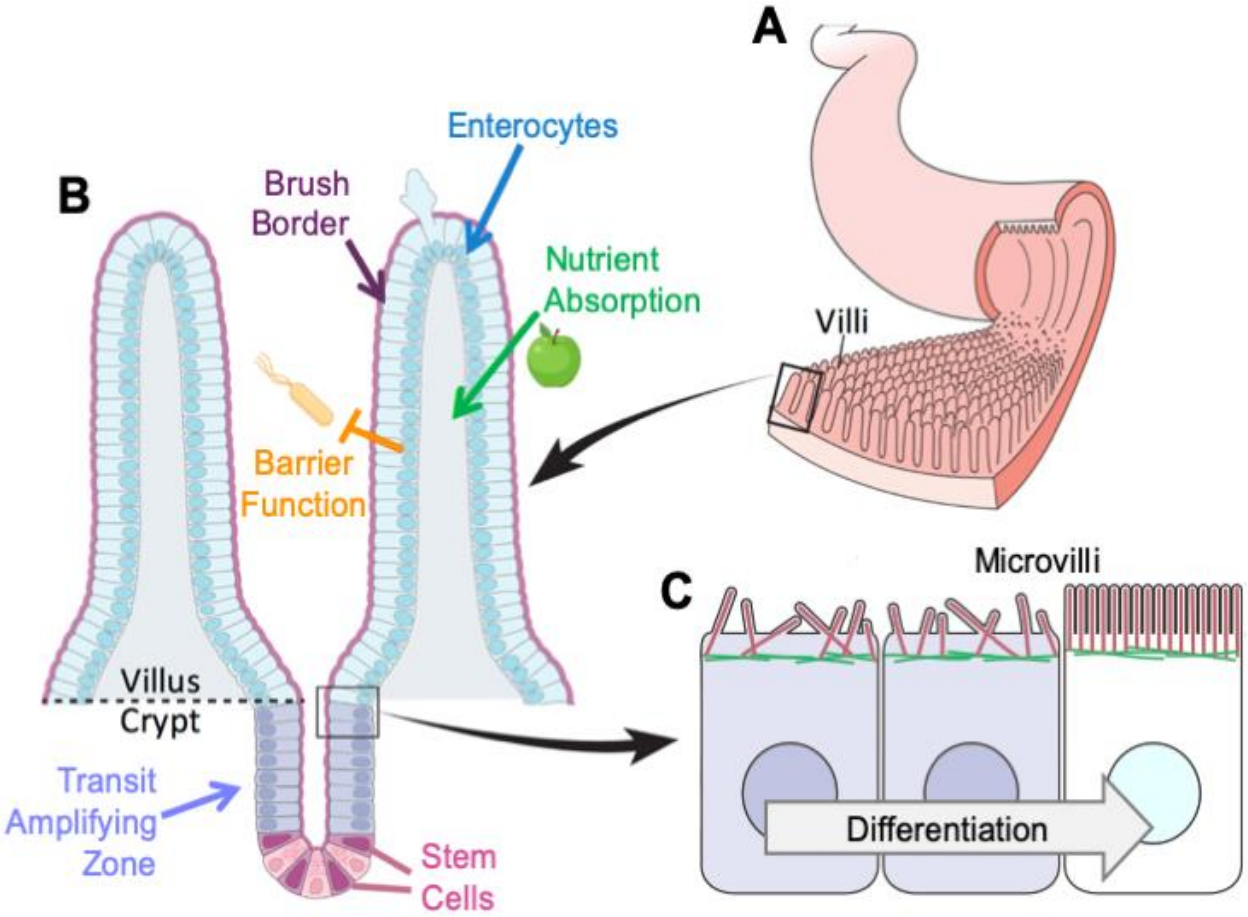

Figure 1-2. Architecture of the small intestinal epithelium. Schematic representation of **(A)** the small intestine showing the finger-like folds of tissue called villi, **(B)** a cross section through the intestine along the crypt-villus axis, showing the pit-like crypt domains between villi, and **(C)** the differentiation of an enterocyte with the associated formation and organization of the brush border within the crypt domain. Adapted from (Crawley et al., 2014a).

Mechanisms of microvillar protrusion

Microvillar protrusion and growth occur as enterocytes differentiate within the crypt domain; with microvilli transitioning to their characteristic uniformity as a mature brush border when enterocytes migrate onto the villus (Fig. 1-2C). Initial actin nucleation is thought to involve the WH2 domain-containing protein cordon bleu (COBL), which localizes to the base of microvillar actin bundles and uses its WH2 domains to form an actin nucleation core (Grega-Larson et al., 2015; Wayt and Bretscher, 2014). Another molecule involved in both promoting outward membrane curvature and in elongation of microvilli is the I-BAR domain-containing protein IRTKS (Fig. 1-3). Through its lipid binding I-BAR domain, IRTKS associates with the plasma membrane to promote outward

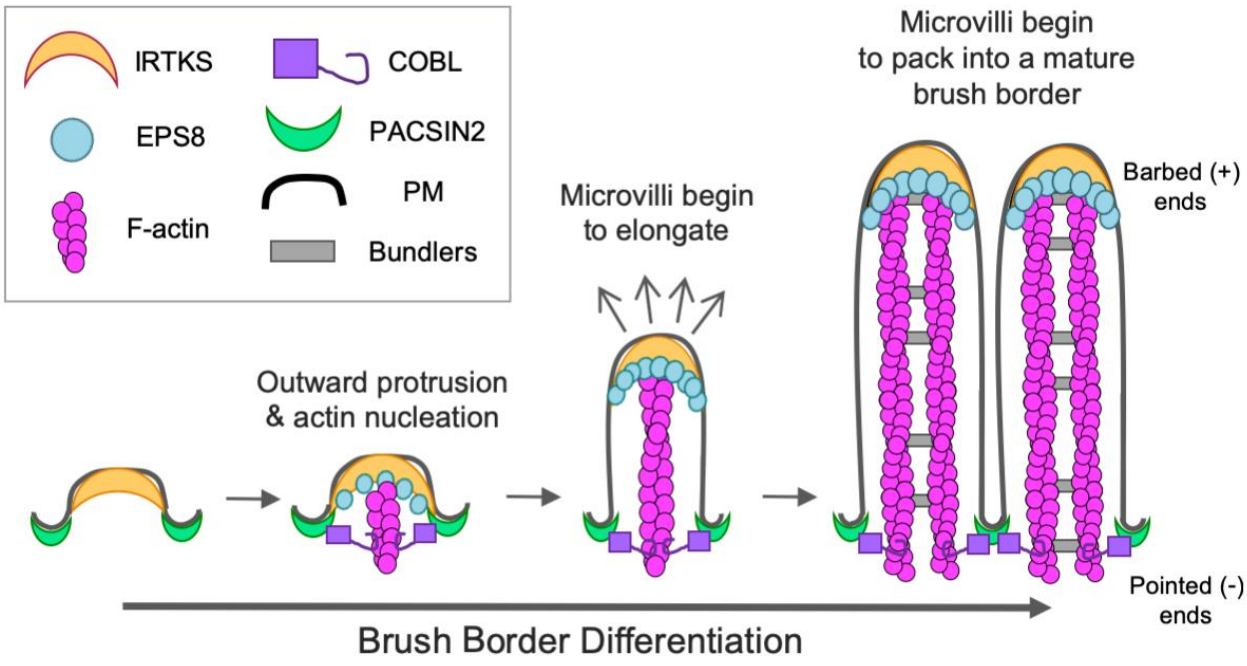

Figure 1-3: Mechanism of microvillar protrusion and growth. Schematic depiction of the molecules involved and their prospective order of action in promoting microvillar outward protrusion. The BAR domain proteins PACSIN2 and IRTKS first localize to the apical membrane before recruiting in the actin-binding proteins COBL and EPS8, respectively. Actin polymerization can then occur with subsequent actin elongation as enterocytes differentiate along the crypt/villar axis.

protrusion; it then stays associated at the distal tips of microvilli throughout their elongation within the crypt domain (Postema et al., 2018). IRTKS also associates with the actin-binding protein EPS8 (Postema et al., 2018; Sudhaharan et al., 2016), which has differential roles in microvillar assembly from capping the barbed ends, to elongation and actin bundling (Croce et al., 2004; Disanza et al., 2006; Manor et al., 2011). There are also actin-bundling proteins, villin, espin, and fimbrin that stabilize the microvillar core and potentially contribute to microvillar elongation (Bartles et al., 1998; Bretscher and Weber, 1979, 1980). More details on each of these classes of actin-binding proteins and how they facilitate microvillar protrusions will be discussed in detail in the following sections.

Actin Assembly

The cytoskeleton is a series of filamentous structures composed of three categories of proteins that assemble into large polymers – microtubules, intermediate filaments, and actin. Microtubules are the largest polymer at around 25nm in diameter and are composed of assemblies of alpha and beta tubulin dimers. Intermediate filaments have a diameter of around 10nm and are constructed from several different types of proteins, but mainly keratin in epithelial cells. Actin filaments are the smallest polymer at around 6-7nm in diameter and are the primary cytoskeletal filament that will be discussed going forward. Actin is assembled from globular actin monomers (termed G-actin) that form filaments (termed F-actin) in a process called polymerization. G-actin assembles into a double helical structure through head to tail interaction of individual monomers, resulting in an actin filament with inherent polarity (Fig. 1-4) (Pollard and Borisy, 2003). In epithelial cells,

actin gives shape to the cell cortex, stability to the junctions, and structure to protrusions such as microvilli.

There are many actin-binding proteins that facilitate actin polymerization in a highly controlled spatial and temporal manner. These proteins assist with actin nucleation, elongation, filament bundling and capping, monomer sequestration, and many additional processes (Pollard, 2016). Controlled interactions of these proteins with actin and each other give rise to the dynamic actin networks and structures necessary for the function of various cell types. The next sections will focus on a few categories of regulatory proteins involved in the formation of actin-based protrusions, and the specific proteins within each category necessary for microvillar assembly. There will be an emphasis on the structure of BAR domain-containing proteins and their regulation in cellular processes as BAR proteins are the focus of the studies in the following chapters.

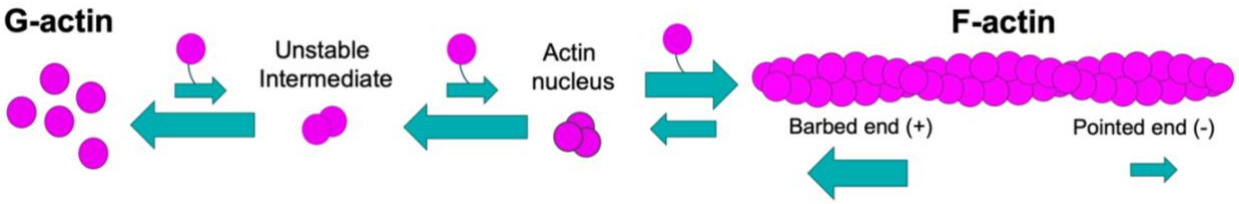

Figure 1-4. Cartoon depicting actin polymerization. A stable nucleus of 3 G-actin monomers needs to form before F-actin polymerization can occur.

Nucleating proteins

De novo actin filament formation is a slow and energetically unfavorable process due to the energy needed to generate an actin nucleus, which is a stable core of 2-3 G-actin subunits off which subsequent monomers bind (Skau and Waterman, 2015). Nucleating proteins help overcome this energy barrier by binding to and bringing in actin monomers to form a stable nucleus. This is done through the actin of several domains that nucleation

proteins contain, one of which is the WH2 domain. WH2 domains are 17-20 amino acids long and form an alpha helix that binds to the hydrophobic cleft at the barbed end of an actin monomer, between the subdomains 1 and 3 (Carlier et al., 2011). The three main classes of actin nucleators found in a cell are the Arp2/3 complex, the tandem WASP-homology 2 (WH2) domain-containing nucleators and formins. These three classes express and localize to different areas of a cell where specific actin nucleation is required.

Tandem WASP- homology 2 (WH2) domain-containing nucleators are a family of proteins that contain several WH2 domains to perform their nucleation functions (Ahuja et al., 2007; Quinlan et al., 2005). The two main mammalian proteins in this category are Spire and Cordon Bleu (COBL). COBL is mainly expressed in neurons and the gastrointestinal tract (Ahuja et al., 2007) where it localizes to the terminal web of enterocytes; it is thought to nucleate microvillar actin filaments while in this position (Grega-Larson et al., 2015; Grega-Larson et al., 2016; Wayt and Bretscher, 2014). COBL has a span of three WH2 domains that it uses to nucleate actin filaments; all three of these WH2 domains are necessary for the full nucleation potential of COBL in vitro (Ahuja et al., 2007). The way the three WH2 domains are arranged suggests that COBL forms a trimeric nucleus, different from the elongated nucleus that is produced by Spire (Quinlan et al., 2005). Moreover, deletion of a single WH2 domain drastically lowers the ability of COBL to being together actin monomers to form a viable nucleus. Interestingly, both Spire (Bosch et al., 2007) and COBL (Husson et al., 2011) have also been shown to have filament severing capabilities. But this is likely a mechanism used in other processes and not in the early formation of linear-based actin structures like microvilli. Currently, COBL is the only nucleating protein that has been found to localize to the intestinal brush border

(Grega-Larson et al., 2015; Wayt and Bretscher, 2014). However, knocking down COBL only leads to ~50% reduction in brush border formation (Grega-Larson et al., 2015), suggesting a potential role for additional actin nucleating proteins, perhaps facilitating actin monomer addition at microvillar tips.

Capping protein and EPS8

Capping proteins bind to the ends of actin preventing addition of new monomers or depolymerization of existing filaments. Perhaps the most ubiquitous of these proteins in capping protein (CP) itself. CP functions as a heterodimer composed of one α and one β subunit, and binds stoichiometrically to the barbed ends of actin filaments with pico-molar affinity (Cooper and Sept, 2008), and regulates the formation of protruding filopodia, as well as the formation of stereocilia and microvilli. Although capping protein effectively eliminates barbed end elongation, knockdown of capping protein can lead to distinct cellular phenotypes depending on the type of protrusion. Knockdown of capping protein in the motile B16F1 cell model leads to a dramatic elongation of filopodia (Mejillano et al., 2004), leaving barbed end elongation factors free to incorporate new actin monomers. However, knockout of capping protein leads to a shortened stereocilia phenotype (Avenarius et al., 2017), as capping protein is theorized to stabilize developing stereocilia. CP has also been detected in brush border proteomics screen (McConnell et al., 2011) and purified microvillar fractions, yet its role in the development of brush border microvilli remains unknown.

Another putative capping protein in microvilli is EPS8, which exhibits actin bundling and capping activities through its C-terminal region (Disanza et al., 2004; Hertzog et al.,

2010). It has been shown to bind to and cap the barbed end of actin filaments (Disanza et al., 2004), as well as exhibit bundling activity *in vitro*, which has been found to rescue viability of *C. elegans* in EPS8 null animals (Hertzog et al., 2010). Studies suggest that EPS8 targets to the tips of intestinal microvilli (Croce et al., 2004; Tocchetti et al., 2010), hair cell stereocilia (Behlouli et al., 2014; Manor et al., 2011; Zampini et al., 2011), and filopodia (Disanza et al., 2006) where it controls the length of these protrusions. It has also been shown to be a necessary component of intestinal microvillar morphology, KD in intestinal W4 cells leads to reduced brush border formation (Postema et al., 2018). However, significant questions remain regarding the mechanism of targeting and action of EPS8 in microvillar protrusions.

Bundling proteins

Single filaments of actin are not strong enough to protrude out of the cell on their own. This is because the downward forces of the membrane are higher than the protrusive force of one actin filament, leading to filament bucking. To overcome these high membrane forces, actin filaments are usually bundled together in higher order actin structures like microvilli. Actin bundling proteins have multiple actin-binding sites as well as additional domains that help control their regulation. Intestinal microvilli contain the three known and well-studied actin bundling proteins, villin, espin and fimbrin that exist in a graded pattern throughout the microvillar actin core (Bartles et al., 1998; Bretscher and Weber, 1979, 1980). Espin is localized through the actin core, while villin is concentrated in the upper two thirds and fimbrin is concentrated at the base. However, there are likely additional bunding proteins involved in microvillar assembly as loss of all three of these

bundlers, villin, espin and plastin, does not eliminate brush border formation, although they have reduced length and transverse area (Revenu et al., 2012). This suggests the existence of alternate bundling proteins that could be compensating for this loss, with one candidate being EPS8, which was discussed in the previous section. However, EPS8 localizes very specifically to the distal tips of microvillar protrusions (Postema et al., 2018), suggesting a capping role for its actin-binding domain rather than a bundling role. Studies are currently being performed in our lab to tease out the functions of EPS8 in the brush border. Thus, it is likely that additional, currently unknown actin bundlers are playing a role in microvillar formation.

BAR domain-containing proteins

BAR (Bin/Amphiphysin/Rvs) domain-containing proteins are a large family of protein scaffolds that link a cell's signaling pathways between the plasma membrane and the actin cytoskeleton. They are known to play a role in membrane deformation through their crescent-shaped, N-terminal BAR domains that directly associate with negatively charged phospholipids. The link between the membrane and downstream signaling pathways is generated through additional domains within BAR proteins, including protein binding SH3 domains and Rho GTPase binding domains. The BAR domain was first classified as a conserved sequence in 1996 when the mammalian protein Bin1 was found to contain the same sequence previously seen in two other proteins, Amphiphysin and the yeast Rvs167 (Lichte et al., 1992; Sakamuro et al., 1996; Sivadon et al., 1995). The functional capacity of BAR domains towards membrane binding and deformation was determined a few years later through studies on Amphiphysin (Takei et al., 1999). Since then, up to 50 different

proteins have been found to contain a BAR domain and to participate in countless numbers of cellular processes from filopodial protrusions and neurite growth, to endocytosis and vesicle trafficking. In the context of this dissertation, the BAR domain proteins IRTKS and PACSIN2 are required molecules in brush border microvillar assembly.

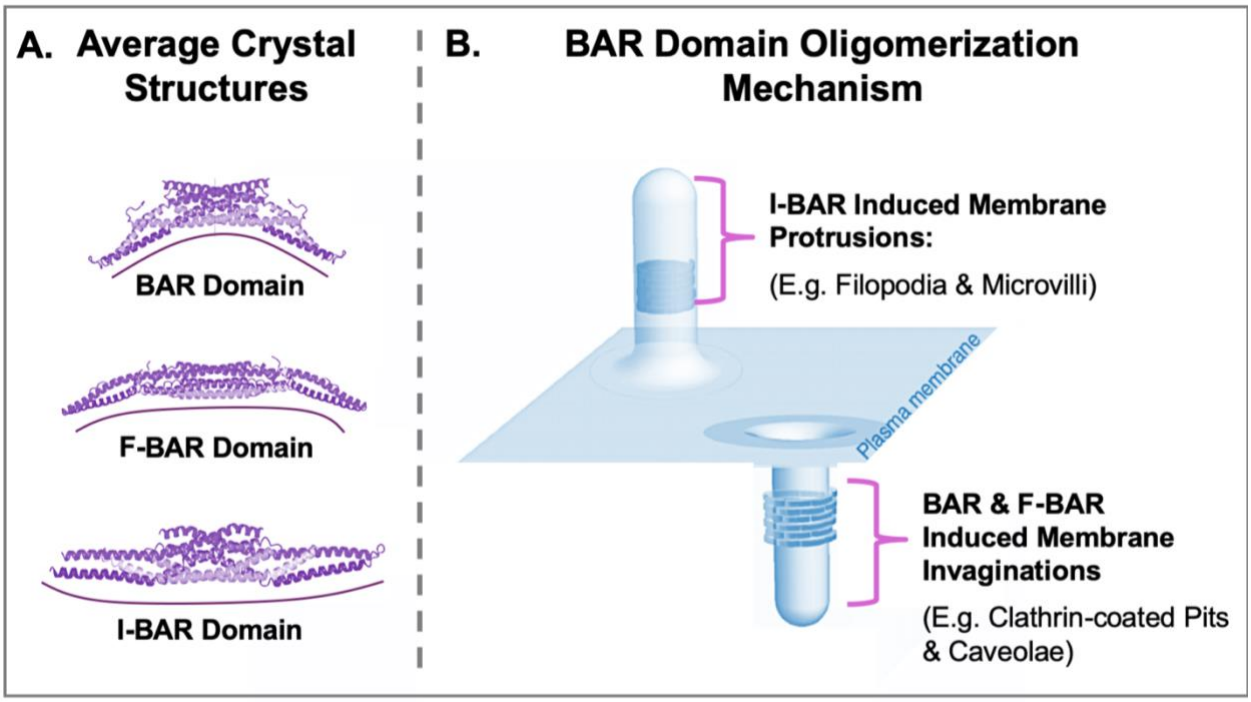

Figure 1-5: BAR domain structure and protein function. Schematic representation of **(A)** averaged crystal structures from the three BAR domain subfamilies, and **(B)** how the BAR domains dimerize/ oligomerize to generate membrane invaginations (BAR and F-BAR) and membrane protrusions (I-BAR). Adapted from (Suetsugu et al., 2010).

All BAR domains are made of three extended helix bundles between 200 and 300 amino acids in length that fold in an antiparallel fashion (Peter et al., 2004) (Fig. 1-5). The characteristic curved, crescent-shaped BAR structure is generated when the folded alpha helices dimerize with other BAR domains. Members of the BAR domain family often do not possess any sequence similarity outside of their BAR domains and thus a lot of

functional variability exists within the large superfamily of proteins. Additional structural variability exists within the BAR domains themselves, and the family is subdivided into three categories depending on the direction and degree of curvature the BAR domains encompass. They can also be subdivided further depending on whether they possess a membrane insertion domain, which is usually an amphipathic helix or loop. The three main categories are the BAR, F-BAR (Fer-Cip4 homology domain) and I-BAR (Inverse BAR). BAR domains bind to areas of high positive curvature while F-BAR domains are slightly more extended and possess a lower degree of curvature. However, both BAR and F-BARs associate with areas of positively curved membrane, such as endocytosing vesicles. I-BAR domains on the other hand possess negative curvature and associate with membranes protruding out of a cell, such as filopodial protrusions (Fig. 1-5).

I-BAR domain-containing proteins

I-BAR domain proteins are the smallest subfamily of the BAR domain-containing proteins, consisting of only five known members (Mattila et al., 2007). The I-BAR domain-containing proteins can be split into two separate groups based on similarity; though all five produce outward membrane protrusions. MIM (missing-in-metastasis) and ABBA (actin-bundling protein with BAIAP2 homology) are more similar in identity and are both involved in brain specific processes, such as neurite outgrowth. These two have C-terminal Wasp-homology-2 (WH2) domains, which are actin-binding domains, in addition to their N-terminal I-BAR domains. The other three I-BAR proteins, IRSp53 (insulin receptor tyrosine kinase substrate 53, BAIAP2), IRTKS (insulin receptor tyrosine kinase substrate, BAIAP2L1) and Pinkbar (BAIAP2L2) are involved in outward protrusions

elsewhere in the body and are the molecules involved in microvillar and filopodial protrusions (Postema et al., 2018; Pykalainen et al., 2011; Scita et al., 2008). These three I-BAR molecules have protein binding SH3 domains as well as C-terminal WH2 domains. The interactions formed through the SH3 domains are specific to the expression patterns of the different I-BARS and help determine their mode of action. In terms of linear, actin-based protrusions, the interactions are usually with actin regulatory proteins that influence their individual functions.

The I-BAR protein within the intestinal brush border is IRTKS, which was first identified in 1996 as a tyrosine phosphorylated insulin receptor substrate (Yeh et al., 1996) and then in 2004 found to contain an N-terminal I-BAR domain (Yamagishi et al., 2004). Work in 2007 found that IRTKS is similar in both structure and function to IRSp53 and that it induces the formation of microskpikes when overexpressed in Cos7 cells (Millard et al., 2007). IRTKS is also one of the mammalian host proteins hijacked by EHEC during pedestal formation. During an EHEC infection, the IRTKS SH3 domain binds with extremely high affinity to the EHEC effector $EspF_u$, leading to Arp2/3 recruitment and branched actin nucleation (Aitio et al., 2010; Aitio et al., 2012; Crepin et al., 2010; Vingadassalom et al., 2009). However, it was not until 2011 that IRTKS was found to be a member of the intestinal brush border through a proteomics screen performed by our lab (McConnell et al., 2011). It was subsequently found to help elongate brush border microvilli within the intestinal crypt domain, which will be examined in more detail in Chapter III (Postema et al., 2018).

F-BAR domain-containing proteins

Found in most eukaryotes except plants, F-BAR domains play large roles in endocytosis, especially clathrin-mediated vesicle formation and caveolae biogenesis, but also in cell division and migration. The first F-BAR domain was discovered in the Cdc42 Interacting Protein 4 (CIP4) (Aspenstrom, 1997) that was found to share a similar N-terminal structure as Fes, leading to the classification of the Fes/Cip4 Homology Domain (F-BAR). Since then, countless more F-BAR proteins have been discovered and found to play roles in many cellular processes that require membrane deformation. A few of these processes-endocytosis, migration, and contractile ring formation, will be discussed in more detail in later sections.

PACSIN2 is ubiquitously expressed throughout the body and is the main F-BAR domain-containing protein studied in the intestinal brush border (Grega-Larson et al., 2015; Postema et al., 2019). It is one of three PACSIN isoforms that all contain an N-terminal F-BAR domain that associates with negatively charged phospholipids and a C-terminal protein interacting SH3 domain. PACSIN proteins are known to be involved in several different cellular processes, such as clathrin-dependent endocytosis, caveolae formation, endosomal and vesicle trafficking, actin polymerization and dynamics, neuronal development, and cell migration (de Kreuk et al., 2011; Qualmann and Kelly, 2000; Qualmann et al., 2000; Senju et al., 2011). Through several of its SH3 domain binding partners, PACSIN2 can be linked to actin nucleation and vesicle scission in epithelial cells. One binding partner that has been implicated in microvillar assembly is the actin nucleator COBL, which is recruited the apical domain of enterocytes by PACSIN2 (Grega-Larson et al., 2015). Previous studies in a cell culture model showed a

significant reduction in the percent of cells able to form a brush border when PACSIN2 was knocked down, implicating it as necessary for microvillar assembly (Grega-Larson et al., 2015). A second SH3 domain binding partner linking PACSIN2 to actin nucleation is N-WASP, an adaptor protein that activates the branched actin nucleator ARP2/3 (Padrick and Rosen, 2010). N-WASP binding connects PACSIN2 to the actin cytoskeleton in processes like endocytosis and junctional actin assembly (Kessels and Qualmann, 2002). Another way that PACSIN2 has been linked to endocytosis is through binding to the large GTPase protein Dynamin2, which wraps around the neck of vesicles to help excise them from the membrane. PACSIN2 binds to Dynamin2 in clathrin-mediated endocytosis and in the formation of caveolae, where it has also been implicated in Dynamin2 recruitment (Kessels and Qualmann, 2006). Other studies have shown that PACSIN2 itself oligomerizes and binds around the neck of vesicles through its F-BAR domain to help stabilize vesicles on the membrane before they are excised (Senju and Suetsugu, 2015). Recent studies in our lab implicate PACSIN2 as a regulator of membrane tension within the enterocyte apical domain, which ultimately controls microvillar morphology (Postema et al., 2019). More details on this and the experiments performed will be further examined in Chapter IV.

Membrane binding and higher order assemblies of BAR domains

The first BAR domain crystal structure was obtained in 2004 of the Drosophila protein Amphiphysin (peter et al science 2004). Since then, over 20 additional crystal structures have been obtained that have helped shed light on the physical differences within the BAR subfamilies. The Amphiphysin structure was able to identify clusters of positively

charged amino acids at the tips and dispersed along the curved surface of the BAR dimer's crescent shape. Similar positive charges are seen on all BAR domains and are what associate with the negatively charged phospholipids within the membrane. Additionally, some BAR domains (called N-BAR) contain N-terminal sequences of approximately 26 amino acids that fold into amphipathic α helices (AH) that physically penetrate the lipid bilayer. The association of the AH into one side of the bilayer is thought to act like a wedge, displacing the lipids in its vicinity and helping the BAR domain generate curvature. The insertion of an AH is also speculated to help anchor the BAR domain at the membrane to reinforce its function (Gallop et al., 2006).

Interestingly, some BAR domains have also been shown to directly bind actin filaments through their positive charges associating with the negatively charged actin. Examples of this are the I-BAR protein IRSp53 and the F-BAR protein PACSIN2; both BAR domains have been shown to bind to low concentrations of actin *in vitro* (Kostan et al., 2014). However, the *in vivo* relevance of direct actin-binding is speculative as it involves the same interface as membrane binding, which is more likely to occur in cells. However, there is the possibility that both membrane binding and actin-binding occur synonymously within certain cellular processes. There are two proposed mechanisms that BAR domain-containing proteins utilize to bind the membrane, 1) through the physical rigidity of the BAR domain structure or 2) through higher order assembly, or oligomerization, of the proteins. It is generally thought that BAR domain proteins are very rigid structures and thus possess ability to shape the lipids within the membrane (Masuda and Mochizuki, 2010; Zimmerberg and Kozlov, 2006). Data supporting this comes from the BAR protein Amphiphysin where simulations performed on its BAR domain suggested

it was the actual rigidity of the structure that enabled membrane bending (Blood and Voth, 2006).

However, many BAR domains also possess the ability to oligomerize through their BAR domains as they can bind both tip-to-tip and side-by-side along the membrane (Jarin et al., 2019; Mim et al., 2012). This allows membrane coating in highly patterned arrays that often leads to the formation of stable membrane tubules (Simunovic et al., 2016; Sorre et al., 2012). This membrane tubulation ability was first discovered in a liposome binding assay with the BAR domain of Amphiphysin, where it was found that the isolated N-terminal 265 amino acids could tubulate lipids in vitro (Takei et al., 1999). Since then, many additional studies have been performed on the membrane tubulation ability of BAR domains. However, because the additional domains of BAR proteins help control their localization and function, membrane tubulation is not often seen in *in vivo* systems. It is likely an overexaggerated phenomenon related to the oligomerization of F-BAR domains around the neck of endocytosing vesicles. During cellular controlled endocytosis, other proteins function to remove the vesicle from the membrane before extreme membrane tubulation occurs. However, there are exceptions to this as overexpression of some F-BAR domain-containing proteins, such as FBP17 or CIP4, have been shown to cause membrane invagination and tubulation in cell culture models (Itoh et al., 2005; Tsujita et al., 2006). In contrast, the ability of BAR domains to self-assembly into patterned arrays does not always lead to membrane tubule formation. There are several F-BAR domain-containing proteins that have been shown to have no tubulation ability in *in vitro* assays and their oligomerization ability is limited to roles in membrane scaffolding (McDonald and Gould, 2016; McDonald et al., 2016).

Auxiliary domains and regulatory mechanisms of BAR proteins

The large degree of heterogeneity in the function of BAR domain proteins is due to the vast range of additional domains they contain, referred to herein as auxiliary domains. The most common auxiliary domain is the Src Homology 3 (SH3) domain, which is found in approximately 50 percent of all BAR proteins (Carman and Dominguez, 2018). SH3 domains are ~60 amino acids long and contain a hydrophobic pocket that associates with proline rich (PR) regions in binding partners. Most SH3 domain associations occur with actin regulatory proteins and GTPases, such as Dynamin. The actin regulatory proteins usually consist of nucleation promoting factors (NPFs), such as N-WASP and further activators of the ARP2/3 complex (Suetsugu and Gautreau, 2012), formins (Garabedian et al., 2018; Graziano et al., 2014; Willet et al., 2015; Yan et al., 2013), and Ena/VASP family members (Disanza et al., 2013; Krugmann et al., 2001; Vehlow et al., 2013).

Many BAR proteins contain PR regions themselves that enable intramolecular interactions with their SH3 domains leading to autoinhibition. These intramolecular interactions can control many aspects of the BAR proteins function, from their localization and membrane binding to their interactions with downstream membrane binding proteins (Rao et al., 2010). One well studied example of autoinhibition is through the I-BAR protein IRSp53 where its CRIB-PR domain binds to its SH3 domain (Kast et al., 2014; Krugmann et al., 2001). IRSp53 normally exists in an autoinhibited state and is only released when Cdc42 binds to its CRIB-PR, releasing the interaction with its SH3 domain (Kast et al., 2014); this occurs when IRSp53 is needed for membrane deformation in filopodial protrusions. Another example of SH3 facilitated autoinhibition occurs in the F-BAR protein PACSIN1 which has intramolecular interactions between its SH3 domain and BAR

domain. When PACSIN1 is needed for endocytic vesicle formation, binding of Dynamin1 to its SH3 domain releases the autoinhibition (Goh et al., 2012; Rao et al., 2010; Wang et al., 2009). An interesting case of autoinhibition is seen in the F-BAR protein Nervous wreck (Nwk) where binding of the SH3 domain to the F-BAR does not block its membrane-binding ability, but only increases the amount of phosphatidylinositol-4,5-bisphosphate ($PI(4,5)P_2$) required for the binding (Kelley et al., 2015).

The second most common auxiliary domain found in BAR proteins are Rho family GTPase binding domains. Approximately 35% of BAR proteins contain regions that bind to Rho GTPases to regulate their activities or are themselves regulated through the binding. Examples of proteins with GTPase binding sites are the F-bar proteins FBP17, Toca-1 and CIP4 (Aspenstrom, 2014). Other known BAR proteins with GTPase binding sites are the I-BAR protein IRSp53, which has cdc42 and Rac binding sites in its CRIB domain, and IRTKS, which possesses a Rac binding site in its I-BAR domain. It is thought that Rho family GTPases bind the BAR domain proteins to regulate their cellular localization and oligomerization ability, thus determining how they function in membrane remodeling. Autoinhibitory interactions can also occur through Rho GTPase binding domains in BAR proteins to prevent downstream signaling. Examples of this are found in ARHGAP45 where an intramolecular interaction between the BAR and RhoGAP domain inhibits the GAP activity (de Kreuk et al., 2013) and in GRAFs where an intramolecular interaction between the BAR and RhoGAP domains inhibits downregulation of Rho GTPase activity via the GAP domain (Eberth et al., 2009; Fauchereau et al., 2003).

Additional regulatory mechanisms of BAR domain proteins can occur through the membrane structure itself. There have been studies that suggest that localized

concentrations of phosphoinositides could be regulating BAR domain proteins through their electrostatic interactions. For example, high $PI(4,5)P_2$ concentrations could direct membrane binding of BAR proteins to areas of future membrane curvature. Another way that the membrane itself can help regulate BAR proteins is through its tension (Tsujita et al., 2015). In the BAR protein FBP17, high membrane tension inhibits its ability to bind to and invaginate the membrane. Additionally, studies on endocytosis show that increased membrane tension is necessary for the formation and scission of vesicles (Boulant et al., 2011). For instance, during caveolae biogenesis at the plasma membrane, tension differences cause Protein Kinase C to phosphorylate the F-BAR protein PACSIN2, which then triggers the removal of caveolae (Senju et al., 2015).

BAR domain curvature sensing vs. curvature generation

The ability of BAR domains to bind areas of membrane curvature and to generate membrane tubules is consistently observed *in vitro* and in cells; however, it is not yet fully understood whether BAR domains sense instances of membrane curvature or induce them (Fig. 1-6). This question is important because it can shed insight into the relationship hierarchy between BAR domain proteins and the actin cytoskeleton. If BAR domain proteins only sense curvature, then the actual BAR domain is only necessary for localization of the molecule with the additional domains playing the dominant role in downstream protein binding and actin regulation. For example, existing membrane curvature could need BAR proteins to localize and facilitate downstream pathways like GTPase signaling or actin polymerization. Curvature sensing is thought to occur because of the preference BAR domains have for curved membrane over flat, which is sometimes

dozens or even hundreds of times higher (Mim and Unger, 2012). Tested BAR domains from amphiphysin (Sorre et al., 2012), endophilin (Zhu et al., 2012), BIN1 (Wu et al., 2014), syndapin (Ramesh et al., 2013), and IRSp53 (Prevost et al., 2015) have all shown to exhibit preferential binding to membrane tubules. Alternatively, if BAR domains physically induce membrane curvature then they are likely cooperating with actin polymerization and additional protein domains.

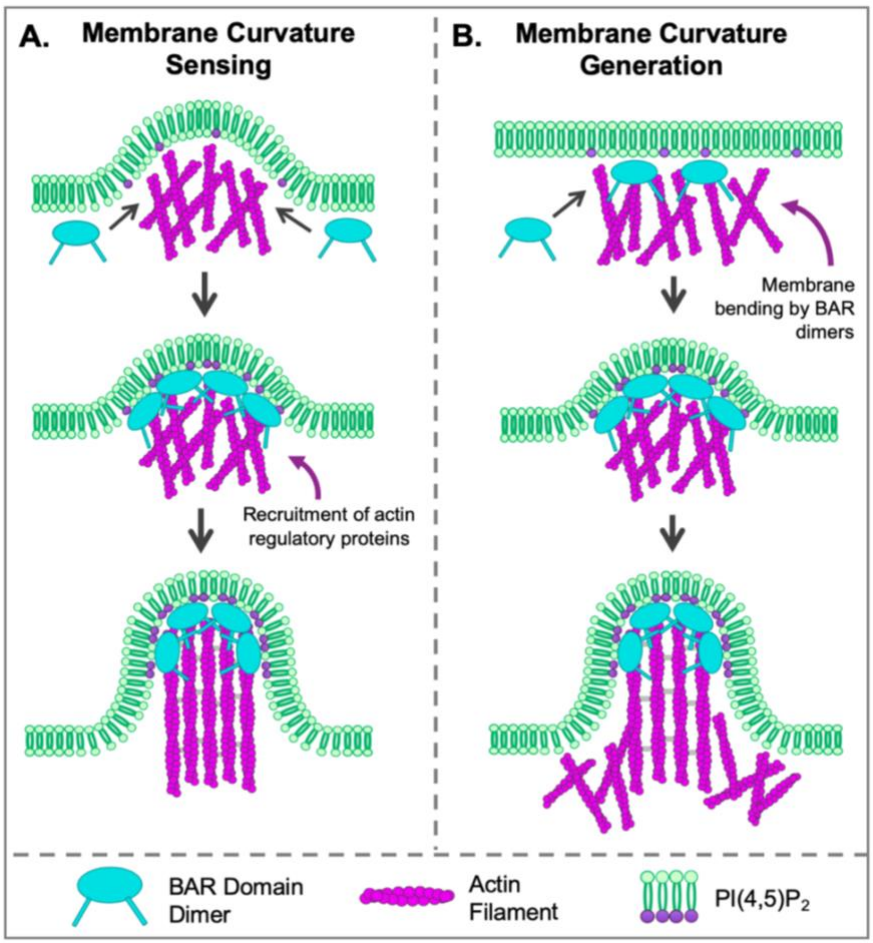

Figure 1-6: Membrane curvature sensing vs. generation. (A) Full-length BAR domain-containing proteins can localize to areas of membrane with existing curvature. **(B)** BAR domain proteins can also generate membrane curvature through the inherent shape of their BAR domains. Adapted from (Zhao et al., 2011).

Recent studies are bringing more light to this problem. The current theory is that both curvature sensing and generation occur in a concentration dependent manner, with low levels of BAR domains able to sense curvature and high levels able to induce it. The duel action of both curvature generation and sensing has also been proposed to exist in the form of a positive feedback loop, with the generation of curvature by a BAR domain causes more domains to sense and localize to the curvature. Recent studies show that salt bridge formation between positive amino acids within the upper side of I-BAR domains and the head groups of lipids increases the density of phospholipids within the region, which contributes to membrane bending (Takemura et al., 2017). Isolated I-BAR domains have also been shown to oligomerize and form membrane tubules that are not associated with the actin cytoskeleton, suggesting a scaffolding role for the domain (Zhao et al., 2011). It is most likely that both curvature generation and sensing take place within cells and that they are coupled processes. The initial curvature generation is caused by the binding of one BAR domain to the membrane that is then strengthened through the sensing of additional BAR domains. When BAR domains bind to membranes they can corral $PI(4,5)P_2$ together, even generating stable phosphoinositide containing microdomains in the membrane bilayer (Zhao et al., 2013).

Cellular Roles for BAR Domain Proteins

The variability in the sequence and auxiliary domains of BAR domain superfamily members leads to a high variability in cellular functions. A lot of these functions involve obvious areas of a cell with high degrees of membrane deformation, such as neurons and the intestinal brush border. Cellular functions that will be discussed in further sections are

cell migration and endocytosis, where both filopodial growth and vesicle generation contain high degrees of membrane curvature and thus necessitate the aid of BAR proteins. However, there are also instances of BAR protein cell involvement that does not involve distinct membrane deformation, such as cellular junction formation and cytokinesis in yeast. Furthermore, there are instances of BAR domain proteins being hijacked by pathogens to promote their colonization and infection, such as during EHEC pedestal formation. The following sections will highlight just a few of the many cellular roles that BAR domain-containing proteins participate, in concluding with an overview of IRTKS and PACSIN2 in microvillar protrusions (Fig. 1-7).

Cell Migration

Cell migration is the directed movement of cells due to chemical signals or mechanical stimuli, and is an important aspect of mammalian development and tissue formation. Most migration is facilitated through actin-based lamellipodia and filopodial protrusions. Lamellipodia are composed of ARP2/3 nucleated branched-actin networks and extend over the entire leading edge of a migrating cell, while filopodia are substrate attached linear-actin based protrusions that extend out from the lamellipodia. Because both filopodia and lamellipodia extend outward from a cell, they exhibit areas of negatively curved membrane at their tips, and thus they utilize I-BAR domain-containing proteins. The main I-BAR domain protein involved in migration is IRSp53, which has been shown to promote filopodial growth through its ability to induce membrane curvature (Lim et al., 2008; Mattila et al., 2007; Saarikangas et al., 2009). As I-BARS favor slightly negatively curved membranes, it is thought that binding of IRSp53 to areas of

premature filopodial and lamellipodial protrusions at the leading edge and can slightly deform the membrane, thus recruiting more IRSp53. Since I-BARs can also phase separate, it is likely that the signal seen along a filopodial shaft of IRSp53 is in two different phase separations of the protein, with a higher concentration at the tips and lower concentrations binding along the shaft after protrusion (Prevost et al., 2015). IRSp53 also contributes to cell migration and filopodial protrusion by binding to many actin regulatory proteins such as cdc42, Ena/VASP and EPS8 (Disanza et al., 2013; Disanza et al., 2006; Kast et al., 2014).

F-BAR domain-containing proteins have also been linked to cell migration, mainly through the ability to bind GTPases and actin-regulatory molecules. However, one interesting example of F-BAR proteins directly influencing filopodial formation are the F-BAR protein family slit-robo GTPase activating proteins (srGAPs) (Bacon et al., 2009; Chen et al., 2012; Wong et al., 2001). The srGAPs are three proteins that localize to neuronal cells and have been shown to generate membrane evaginations when dimerized, which is opposite from canonical F-BAR curvatures and resembles the outward bending of I-BAR domains (Guerrier et al., 2009; Zaidel-Bar et al., 2010). SrGAP2 specifically, has been shown to negatively influence the migration of neuronal cells through its ability to induce filopodial protrusions. These protrusions are generated directly through the action of its N-terminal F-BAR domain, are highly dynamic in Cos7 cells, and are filled with F-actin, entirely reminiscent of I-BAR induced protrusions. These are just a few examples of the roles of BAR domain proteins in cell migration.

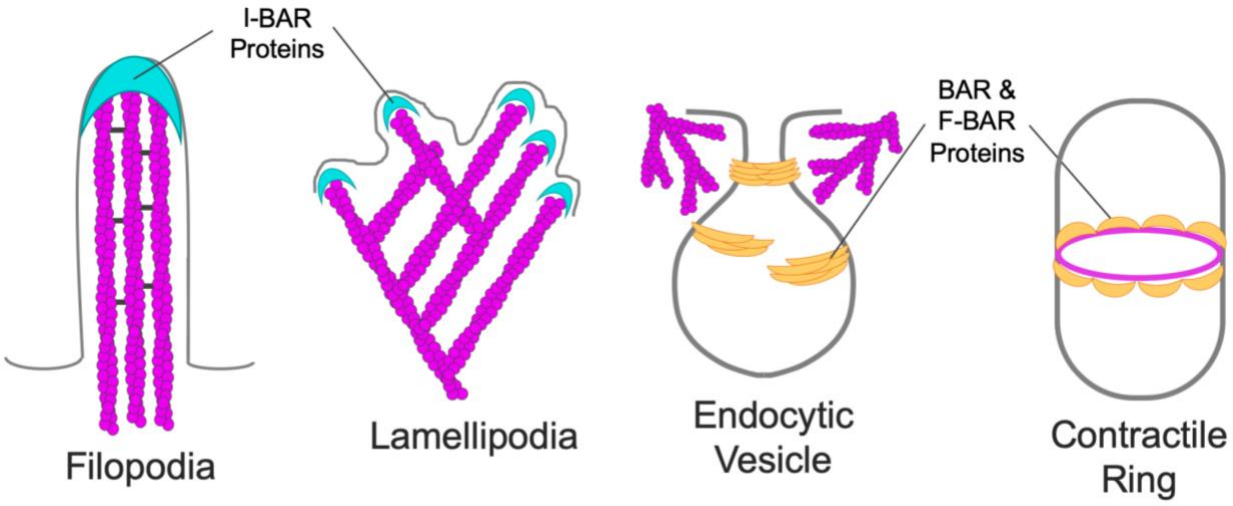

Figure 1-9: BAR domain proteins in common cellular structures. I-BAR proteins associate at the tips of filopodial and lamellipodial protrusions between the membrane and the actin cytoskeleton. BAR and F-BAR domain proteins bind to the membrane and F-actin in cellular processes with positive curvature, e.g. endocytic vesicles and *S. pombe* contractile ring formation.

Endocytosis

Endocytosis and the formation of vesicles is an important way for cells to uptake nutrients and molecules from the environment, and is critical to maintain cellular homeostasis. There are many different forms of endocytosis in cells from clathrin-dependent and independent to caveolae. However, all endocytosis involves the generation of membrane invaginations and thus utilize BAR domain-containing proteins to link the membrane curvature with the actin cytoskeleton. The roles for BAR domain proteins in vesicle formation during endocytosis also vary and involve budding and neck constriction, recruitment of scission proteins such as Dynamin, actin filament assembly, and recruitment of vesicle uncoating proteins (dTakei et al., 1999; Farsad et al., 2001; Yarar et al., 2007).

Several BAR domain-containing proteins, including amphiphysin, endophilin and SNX9, participate in clathrin-mediated endocytosis. Amphiphysin helps mediate endocytosis through its different protein interactions; it can bind to dynamin and N-WASP through its SH3 domain, and clathrin through a binding site between its BAR and SH3 domain. Clathrin binds to Amphiphysin first during vesicle formation and subsequent binding of Dynamin disrupts this interaction for vesicle fission (McMahon et al., 1997). Endophilin is also thought to play a role in clathrin mediated endocytosis, but at the later stage of vesicle uncoating. Endophilin wraps around the neck of the budding vesicle and binds to both Dynamin2 and Synaptojanin (Milosevic et al., 2011; Otsuki et al., 2003). It was not until a KO mouse of all three Endophilin A isoforms was studied that the molecule was shown to act during vesicle recycling where it binds to Synaptojanin, rather than vesicle scission through its Dynamin2 binding (Milosevic et al., 2011). The F-BAR protein PACSIN2 is also involved both in clathrin dependent and independent endocytosis as well as caveolae formation, as was discussed in earlier sections and in Chapter IV. Because it has a narrower F-BAR domain that more closely resembles a BAR domain, PACSIN2 also wraps around the neck of budding vesicles and binds to Dynamin2 (Senju and Suetsugu, 2015). Its lower membrane curvature is why PACSIN2 can associate around the neck of budding caveolae, which are smaller and thus have a thinner neck than clathrin- coated vesicles. Even though it binds to vesicles in a similar manner as Endophilin, PACSIN2 works at an earlier stage and assists with vesicle scission from the plasma membrane.

Contractile ring assembly

Cytokinesis is the last stage in cell division and is where a cell divides its contents into two daughter cells. This division is often accompanied by the formation of an actomyosin ring, called the contractile ring, below the plasma membrane that physically constricts to aid in division. Proper spatial and temporal assembly of the contractile ring is necessary to ensure cellular contents are distributed equally between the two daughter cells. The generation of a contractile ring during cytokinesis does not involve the characteristic membrane curvature normally associated with BAR domain proteins. However, several F-BAR proteins have been implicated in its assembly as a link between the actin cytoskeleton, the plasma membrane, and additional contractile ring proteins.

Many studies on the proteins involved in contractile ring formation have been performed in the fission yeast *Schizosaccharomyces pombe (S. pombe)*, where 3 different F-BAR proteins have been found to play a role, Cdc15 (Fankhauser et al., 1995), Imp2 (Demeter and Sazer, 1998), and Rga7 (Arasada and Pollard, 2011). Cdc15 is the most highly studied of these three S. pombe proteins during cytokinesis. It has been shown to localize to the site of contractile ring formation and oligomerize along the membrane forming a scaffold. Once on the membrane, Cdc15 can then bind to additional contractile ring proteins through the action of its SH3 domain to promote contractile ring assembly (McDonald et al., 2016). Additional studies on F-BAR proteins in the contractile ring have been completed in the budding yeast *Saccharomyces cerevisiae* (*S. cerevisiae*). Here, the F-BAR protein Hof1p was found to regulate contractile ring closure through its SH3 domain by binding to and controlling the symmetry of myo1p during ring constriction (Korinek et al., 2000; Oh et al., 2013; Vallen et al., 2000). Interestingly, in

Drosophila, PACSIN is another F-BAR protein that has been found to promote contractile ring formation. It was shown to associate with the PI(4,5)Ps in the membrane to link the cleavage furrow to the contractile ring. It provides this link by directly binding to the contractile ring component Anillin, thus acting as a scaffold to bind the contractile ring to the membrane (Takeda et al., 2013).

EHEC colonization

EHEC serotype O157:H7 is a non-invasive, highly pathogenic bacterium that colonizes the lower mammalian intestinal tract by hijacking the I-BAR domain protein IRTKS. During infection, EHEC releases Shiga toxin, which binds to the glycosphingolipid receptor Gb3 on systemic cells, leading to severe vascular damage (Robinson et al., 2006). Shiga toxin enters the blood stream through intestinal capillaries and damages the vascular endothelium throughout the body (Karch, 2001). This can result in major complications such as hemolytic colitis and hemolytic-uremic syndrome (HUS), which can lead to renal and cardiac failure (Kaplan et al., 1998; Thomas et al., 2005). More active Gb3 receptors reside on glomerular endothelial cells than anywhere else in the body, making the kidneys especially susceptible to EHEC infection (Noris and Remuzzi, 2005; Obrig, 2010). This is particularly hard on children and the elderly, with upwards of 10% of EHEC infections leading to diseases such as hemolytic-uremic syndrome, a leading cause of renal failure in infants and children (Kaplan et al., 1998; Thomas et al., 2005).

To promote infection, EHEC hijacks the actin cytoskeleton of enterocytes to form actin pedestals that adhere it to the apical surface (Griffin and Tauxe, 1991; Ho et al., 2013; Lai et al., 2013). EHEC is an example of an attaching/ effacing (A/E) pathogen, it

physically attaches to the intestinal wall to colonize the distal small intestine or proximal colon epithelium. The actin pedestals built by EHEC are lesions that rearrange underlying linear microvillar actin to form a branched actin case holding the bacterium onto the intestinal surface (Knutton et al., 1987; Moon et al., 1983). To build its actin pedestals, EHEC injects host cells with virulence factors that remodel the actin cytoskeleton (Jarvis and Kaper, 1996). To get its virulence factors into the host cell, EHEC utilizes a type 3 secretion system, (T3SS), which is a hollow protein transport tube that is syringe shaped and inserted into the host cell. These are used to insert bacterial proteins into a host cell to manipulate host proteins and signaling pathways to aid in the bacterial infection. T3SSs originally evolved from the flagellum are used by many different gram-negative bacterial species to translocate proteins in a trans-kingdom manner (Hueck, 1998; Macnab, 2003). T3SSs span the entire bacterial inner and outer membranes as well as the host cell membrane and are composed of more than 20 proteins (Deng et al., 2017).

Two effector proteins secreted by EHEC into the mammalian host cell through its T3SS are the Translocated Intimin Receptor (Tir) and $EspF_U$ (Fig. 1-8) (Campellone et al., 2004; Deibel et al., 1998). These are the main EHEC virulence factors that help reshape the mammalian actin cytoskeleton for pedestal formation. Once in the host cell, Tir inserts itself into the apical plasma membrane in a hairpin loop. In this confirmation, the central loop of Tir is exposed on the outside of the cell while the N- and C- termini are inside. Intimin, an EHEC outer membrane protein then binds to the central loop of TIr anchoring EHEC onto the epithelial apical surface (Campellone, 2010; Kenny et al., 1997). Large clusters of Tir at the apical surface of the host cell causes a signaling cascade to form

that reinforces the anchorage of the EHEC bacterium through the emergence of an actin pedestal.

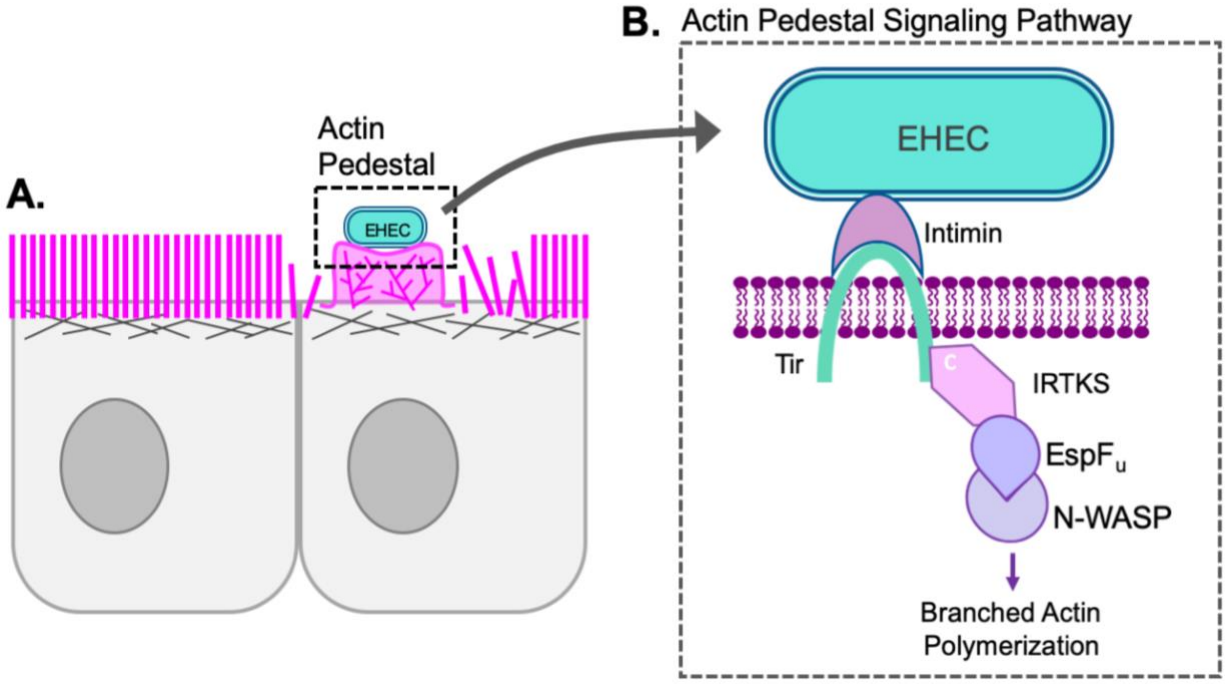

Figure 1-8: Mechanism of EHEC actin pedestal formation. Schematic depiction of **(A)** an enterocyte with a branched- actin filled pedestal anchoring an EHEC bacterium onto the apical surface on an enterocyte and **(B)** the pathway necessary for pedestal formation and EHEC infection. Intimin is in the bacterial outer membrane and TIR and EspF$_u$ are bacterial effectors secreted into the host cell. Adapted from (Aitio et al., 2012).

This actin pedestal signaling cascade is generated through the action of the I-BAR protein IRTKS, which binds to the C-terminus of Tir that remains inside the host cell. IRTKS also interacts with the other secreted virulence factor EspF$_u$ (Campellone et al., 2004), through tandem polyproline motifs that bind tightly to its SH3 domain (Aitio et al., 2010). This interaction is notable due to its high affinity (K_D ~500 nM) (Aitio et al., 2010). The resulting apically localized Tir-IRTKS-EspF$_u$ complex subsequently recruits N-WASP and Arp2/3, leading to a massive induction of actin assembly. Branched actin assembly by Arp2/3 ultimately leads to pedestal formation beneath adherent EHEC bacterium (Campellone et al., 2004; Vingadassalom et al., 2009). Therefore, without IRTKS, actin

pedestal formation does not occur (Crepin et al., 2010; Vingadassalom et al., 2009; Yi and Goldberg, 2009). This hijacking of the microvillar actin cytoskeleton to form pedestals indicates the importance of the specialized shape of enterocytes. When the normal actin-filled protrusion on the apical domain are rearranged into pedestals, the entire function of enterocytes is severely compromised.

Summary

The intestinal brush border is one of the most highly curved membranous organelles in the human body and is composed of vast amounts of linear F-actin. Since BAR domain-containing proteins link areas of membrane curvature to the actin cytoskeleton in many cellular processes, it's a logical assumption that these would exist within the brush border. However, it wasn't until recently that two proteins, the F-BAR protein PACSIN2 and the I-BAR protein IRTKS, were identified as necessary components of microvillar assembly. This highlights the significant gaps in our understanding of the molecules involved in brush border formation. Thus, the goal of this thesis is to shed insight into the molecular mechanisms of the two BAR domain proteins and how they physically link the actin cytoskeleton with the membrane in microvillar protrusion.

Our studies are the first to determine a role for the I-BAR domain-containing protein IRTKS in promoting microvillar elongation within differentiating enterocytes of the intestinal crypt. We show that IRTKS localizes to microvillar tips to promote protrusion through the action of its I-BAR domain, and subsequently helps elongate microvilli through its WH2 and SH3 domains. IRTKS also binds to and localizes the actin-regulatory protein EPS8 through its SH3 domain, which is another molecule necessary for microvillar

elongation. Beyond just understanding the mechanisms of brush border assembly, the localization of IRTKS at microvillar tips proposes a novel role for I-BAR domain-containing proteins within the intestinal brush border.

The F-BAR domain-containing protein PACSIN2 was first found to recruit COBL to the intestinal brush border for actin nucleation at the microvillar base (Grega-Larson et al., 2015). To better understand the role of PACSIN2 within the intestinal brush border, we characterized PACSIN2 KO mice using tissue staining and ultrastructural studies. It was found that loss of PACSIN2 leads to plasma membrane lifting from the base of microvillar actin cores leading to increased rootlet lengths. Moreover, Dynamin2 and other endocytic factors were lost from their normal localization near the intermicrovillar endocytic region, indicating that PACSIN2 helps promote vesicle scission at the enterocyte apical domain. A role linking the endocytosis between microvilli to the membrane forces that control microvillar morphology is a novel concept. This shows that PACSIN2 helps promote apical endocytosis and is a fundamental molecule for both microvillar growth and maintenance.

Overall, the studies performed over the course of this dissertation show how BAR domain-containing proteins use their inherent curvature and ability to bind to the plasma membrane to influence microvillar assembly. We were the first to identify and characterize the I-BAR protein IRTKS in the intestinal brush border. Furthermore, we determined a role for the F-BAR protein PACSIN2 in promoting microvillar membrane coverage through its ability to excise endocytic vesicles. Future studies will provide more mechanistic detail regarding how BAR domain proteins promote brush border assembly and maintenance, ideally in an *in vivo* context.

CHAPTER II

MATERIALS AND METHODS

Cell culture and organoids

Ls174T-W4 cells (female *Hs* colon epithelial cells) were cultured in DMEM with high glucose and 2 mM L-glutamine supplemented with 10% tetracycline-free fetal bovine serum (FBS), G418 (1 mg/ml), blasticidin (10 µg/ml), and phleomycin (20 µg/ml). The cell line was obtained from Dr. Hans Clevers (Utrecht University, Netherlands) and has not been additionally authenticated. B16F1 (Male *Mm* melanoma cells) and HeLa cells (female *Hs* cervix epithelial cells) were cultured in DMEM with high glucose and 2 mM L-glutamine supplemented with 10% FBS. Intestinal organoids were generated from P42-56 mice (C57BL/6, both genders). Organoids were suspended in 50 µl matrigel (BD Biosciences) and cultured in advanced DMEM/F12 (Invitrogen) supplemented with the following growth factors: 500 ng/ml EGF (Invitrogen), 100 ng/ml Noggin (R&D Systems), 500 ng/ml R-spondin 1 (R&D Systems), and 1mM N-Acetylcysteine (Sigma). All cells were grown at 37°C and 5% CO2.

Transfections and lentivirus production

All transfections were performed using Lipofectamine 2000 (Invitrogen) according to the manufacturer's instructions and the cells were allowed to recover overnight (ON). Lentivirus was generated by co-transfecting HEK293FT cells (Fetal *Hs* embryonic epithelial cells; T75 flasks at 80% confluency) with 6 µg of pLKO.1 shRNA KD plasmids

(Open Biosystems; IRTKS, TRCN0000005350; EPS8, TRCN0000061545; PACSIN2, TRCN0000037980), 4 µg of psPAX2 packaging plasmid, and 0.8 µg of pMD2.G envelope plasmid using FuGENE 6 (Promega). For efficient lentiviral production, cells were incubated for 48 hr, then lentivirus-containing media was collected and concentrated with Lenti-X concentrator (Clontech). To transduce W4 cells with lentivirus, the media was supplemented with 6 ug/ml polybrene (Sigma) and the lentiviral shRNAs. After a 24-hour incubation, the media was changed and resupplemented with 6 ug/ml polybrene and lentiviral shRNAs for an additional 24 hours. The cells were then seeded into plates or flasks and incubated ON in the absence or presence of 1 µg/ml doxycycline, and then prepared for immunofluorescence or SDS-PAGE. For rescue experiments, cells were transiently transfected 48 hours after the second lentiviral infection using Lipofectamine 2000 and induced with 1 ug/ml doxycycline ON. They were then fixed the following morning and immunofluorescent staining with respective antibodies (usually anti-mCherry and/ or anti-EGFP) was performed according to the protocol outlined in the immunofluorescence section below.

Cloning and constructs

pTOB7-IRTKS (Open Biosystems) corresponding to full-length human IRTKS was purchased and shuttled into a pEGFP-C1 vector (Clontech) adapted for Gateway cloning using the Gateway conversion kit (Invitrogen) to generate pEGFP-C1-IRTKS (aa 1-511) and verified by sequencing. IRTKSΔWH2 (aa 1-482), I-BAR alone (aa 1-249), ΔI-BAR (aa 250-511), WH2 alone (aa 473-511) constructs were generated by PCR and TOPO cloned into the pCR8 Gateway entry vector (Invitrogen). To generate the IRTKS-SH3*

construct, mutations W378K and W391K were introduced into pEGFP-IRTKS using site-directed mutagenesis. All entry vectors were verified by DNA sequencing and then shuttled into the destination vector pEGFP-C1 (Clontech) that was Gateway-adapted using the Gateway vector conversion kit (Invitrogen). pDONR221 EPS8 (Open Biosystems) was also purchased and shuttled into a pEGFP-C1 vector (Clontech) adapted for Gateway cloning using the Gateway conversion kit (Invitrogen) to generate pEGFP-C1-EPS8 (aa 1-822) and verified by sequencing. EPS8ΔPR1 (deleted aa 198-231) construct was generated by reverse PCR and TOPO cloned into the pCR8 Gateway entry vector. The mCherry-tagged UtrCH used for B16F1, HeLa, and W4 live-cell imaging was purchased from Addgene (26740, deposited by W. Bement). The TOM20-mCherry construct was generously provided by the Kaverina Lab (Vanderbilt), and the SH3 domain of IRTKS was fused to the C-terminus of mCherry. A non-targeting scramble control shRNA (Addgene; plasmid 1864), IRTKS KD shRNA, and EPS8 KD shRNA clones were expressed in pLKO.1, corresponding to TRC clones TRCN0000005350 and TRCN0000061545 (Sigma) respectively. To generate an IRTKS construct refractory to KD, three silent mutations were introduced into full-length IRTKS using site-directed mutagenesis. For the IRTKS shRNA, which targets nucleotides (nts) 1190–1211, nt 1190 (c→ a), nt 1192 (t → a), nt 1196 (a → t), nt 1197 (g→ c), and nt 1198 (t → g) were mutated. These silent mutations were also introduced into pEGFP-IRTKS SH3* and pEGFP-ΔWH2. For the EPS8 shRNA, which targets EPS8 nts 1712–1732, nt 1718 (c→ t), nt 1720 (g→ a), nt 1724 (t → a), nt 1725 (c→ g), and nt 1726 (t → c) were mutated. The same nts were mutated in the EGFP-EPS8ΔPR1 construct.

Immunofluorescence

For SIM imaging, cells were plated on glass coverslips and allowed to adhere for at least 6 hrs (W4 cells) or 3 hrs (HeLa cells). They were then washed with pre-warmed PBS and fixed with warm 4% paraformaldehyde/PBS for 15 min at 37°C. Cells were then washed three times with PBS and permeabilized with 0.1% Triton X-100/PBS for 15 min at room temperature. Cells were once again washed three times with PBS and blocked for 1 hr at 37°C in 5% bovine serum albumin (BSA)/PBS. Primary antibodies (listed below) were diluted in PBS and incubated with cells at 37°C for 1 hr, followed by four washes with PBS. Cells were then incubated for 1 hr with secondary antibodies (listed below) at room temperature. Coverslips were then washed four times with PBS and mounted on glass slides in ProLong Gold (P36930; Invitrogen).

Frozen tissue sections of WT and PACSIN2 KO intestinal tissue were washed in phosphate-buffered saline (PBS) three times and permeabilized for 10 min with 0.1% Triton X-100/PBS at RT. The tissue sections were then blocked with 10% bovine serum albumin (BSA) at 37°C for 2 hours and washed once with PBS. Primary antibodies (listed below) were diluted in 10% BSA/PBS and incubated with cells at 4°C O/N, followed by four washes with PBS. Tissue sections were then stained with phalloidin and secondary antibodies (listed below) in 1% BSA/PBS for 2 hrs at RT, washed three times with PBS and mounted with Prolong Gold Antifade mounting media (P36930; Invitrogen). Paraffin-embedded small intestinal tissue sections of WT and PACSIN2 KO were deparaffinized using Histo-clear solution (Fisher) and rehydrated in a descending graded ethanol series. Slides were then subject to an antigen retrieval step consisting of boiling for 1 hr in a solution of 10 mM Tris (pH 9.0) and 0.5 mM EGTA. Slides were then washed in PBS three

times and stained O/N at 4°C with primary antibodies (see below) in 10% BSA/PBS. After washing with PBS four times, samples were stained with secondary antibodies in 1% BSA/PBS for 2 hrs at RT. Slides were then washed four times with PBS and mounted in ProLong Gold Antifade mounting media. Organoids were processed in a similar manner as above with some exceptions. 1) Organoids were fixed with warm 4% paraformaldehyde/PBS for 40 min at 37°C and 2) organoids were permeabilized with 0.1% Triton X-100/PBS for 30 min.

For live cell confocal imaging of W4 cells, previously transfected cells were plated on glass-bottom dishes with 1 µg/ml of doxycycline and allowed to adhere for 6 hours. Images of single W4 cells were acquired every 5 seconds for 30 minutes or continuously for 4 minutes. For FRAP of scramble and IRTKS KD, images were acquired every 5 seconds with an initial acquisition of 15 sec followed by bleaching and an additional 10 minutes. Bleaching was performed within a 20 μm^2 ROI using 30% 405 laser power for a duration of 100 ms. For drug treatments, 80µM DMSO/ 80µM Dynasore (D7693; Sigma-Aldrich) or 30µM DMSO/ 30µM Pitstop 2 (SML1169; Sigma-Aldrich) were diluted into 1ml media and added to glass-bottom dish of W4s 10 minutes before acquisition. For live-cell TIRF imaging, previously transfected B16F1 cells were seeded onto 35 mm glass bottom dishes (Invitro Scientific, D35-20-1.5-N) that were coated with 25 µg/ml laminin (Sigma, L2020) in PBS. B16F1 cells were plated sparsely on the laminin-coated dishes, allowed to adhere for 2 to 3 hours, and images of single cells were acquired every 5 seconds for 15 minutes. All live cells were maintained in a humid environment at 37°C and 5% CO2 using a stage-top incubation system. Image acquisition was controlled with Nikon Elements software.

The following dilutions were used for primary antibodies for staining: anti-IRTKS (2 µg/ml, HPA021257; Sigma-Aldrich), anti-EPS8 (1 µg/ml Cat# 610143; BD Biosciences), anti-GFP (50 µg/ml, GFP-1020; Aves Labs), or anti-mCherry (1 µg/ml, Cat# M11217; Invitrogen); anti-PACSIN2 (2.5 µg/ml, HPA049854; Sigma-Aldrich), anti-COBL (1µg/ml, HPA 019033; Sigma-Aldrich), anti-Dynamin2 (4 µg/ml, NBP2-47477; Novus Biologicals), anti-villin (4µg/ml; Santa Cruz #sc-66022), anti-E-Cadherin (0.5 µg/ml; BD Biosciences #610182), anti-ZO-1 (5µg/ml, 61-7300; Thermo Fisher). The following dilutions were used for secondary antibodies and cell dyes for staining: goat anti-rabbit Alexa Fluor 488 F(ab')2 Fragment (2 µg/ml, A11070; Molecular Probes), goat anti-mouse Alexa Fluor 488 F(ab')2 Fragment (2 µg/ml, A11017; Molecular Probes), Alexa Fluor 568–phalloidin or Alexa Flour 647-phalloidin (1:200, A12380 and A22287 respectively; Invitrogen), or Wheat Germ Agglutin Oregon Green (WGA) (2µg/ml, W67-48; Life Technologies).

Frozen tissue preparation

Segments of WT and KO intestine were removed and flushed with PBS and pre-fixed for 10 minutes with 4% paraformaldehyde (PFA) to preserve the tissue structure. The tube was then cut along its length, sub dissected into 0.5μm^2 chunks, fixed for an additional 30min in 4% PFA at RT, and washed 3 times in PBS. Samples were then gently placed on top of a 30% sucrose solution in TBS and allowed to sink to the bottom overnight at 4°C. Specimens were then swirled in three separate blocks of embedding medium, oriented in a block filled with fresh embedding medium, and snap-frozen in dry ice-cooled acetone. Samples were cut in 10 µm sections and mounted on slides for staining.

Western blot analysis

IRTKS and EPS8 knockdown and scramble cells were seeded into T25 flasks and allowed to grow for at least 24 hr. Cells were harvested with a cell scraper into PBS, pelleted at low speed, and lysed using ice-cold RIPA buffer containing 2 mM ATP, cOmplete ULTRA tablets (Roche), and 1 mM Pefabloc (Roche). The resulting cell lysates were then centrifuged at 15,000 RPM for 20 min and the soluble material was diluted with Laemmli sample buffer and heated at 95°C for 5 min. Equal sample volumes were loaded on a 4–12% Nu-Page gradient gel (Invitrogen) and the proteins were transferred to nitrocellulose at 25V for 16 hr. The membrane blots were blocked for 1 h in 10% milk-PBS and incubated with primary antibodies diluted in PBS containing 0.1% Tween-20 (PBS-T) ON at 4°C. The primary antibodies used were anti-IRTKS (0.08 µg/ml, HPA021257; Sigma-Aldrich), anti-EPS8 (0.1 µg/ml, Cat# 610143; BD Biosciences) and anti-glyceraldehyde 3-phosphate dehydrogenase (0.5 µg/ml, Cat# 3907; Cell Signaling). The membranes were then washed four times with PBS-T and incubated with donkey anti-rabbit 800 IRdye (0.01 ug/ml, 926-32213; Li-Cor) or donkey anti-mouse 800 IRdye (0.01 µg/ml, 926-32212; Li-Cor) for 30 min at RT on a shaker. Membranes were washed with PBS-T an additional four times and imaged using a Li-Cor Odyssey infrared imaging system. The same protocol was used to generate EGFP-tagged IRTKS constructs for expression levels. Images of membranes were cropped and adjusted using ImageJ (NIH) and relative protein expression levels were quantified using the signal from GAPDH. The samples were normalized according to their detected protein concentrations during loading.

Pulldown assays

COS7 cells were grown in T75 flasks to 80% confluency and transfected with pull-down constructs using Lipofectamine 2000 according to the manufacturer's protocol. After 48 hr, cells were lysed using 1 ml of ice-cold Cellytic M buffer (Sigma) containing 2 mM ATP, 1mM Pefabloc (Roche), and cOmplete ULTRA tablets (Roche) and centrifuged at 15,000 RPM. The soluble material was recovered after centrifugation and incubated with a 30µl bed volume pre-equilibrated anti-FLAG M2 resin (Sigma) for 2 hr with continuous rocking at 4°C. Resin and bound material were pelleted at 300 RPM, washed four times using RIPA buffer supplemented with 2 mM ATP, 1 mM Pefabloc (Roche), and cOmplete ULTRA tablets (Roche), and eluted by boiling in SDS buffer to recover bound material. Resin-bound material was detected by western analysis with the following antibody dilutions: mouse anti-FLAG M2 (10 µg/ml; Sigma cat. #F3165) and chicken anti-EGFP (2 µg/ml; Aves Labs cat. #GFP-1020). The pull-down assays were repeated three times, and the results shown are representative.

Light microscopy

SIM of W4 and HeLa cells was performed using an Applied Precision DeltaVision OMX equipped with a 60X Plan-Apochromat N/1.42 NA oil immersion objective (Olympus) using softWorx software (GE Healthcare), or with a Nikon N-SIM with an Apo TIRF 100x/1.49 NA objective. Confocal microscopy was performed using a Nikon A1R laser-scanning confocal microscope. Live cell B16F1 imaging was performed on a Nikon TiE inverted light microscope equipped with 488 and 561 excitation LASERs, a 100x/1.49 NA TIRF objective, and an Andor Neo sCMOS detector. Imaging was performed using near-

TIRF illumination, where the incident angle of the LASER was adjusted to increase the depth of penetration of the excitation field. Live-cell imaging of W4 cells was performed on a Nikon Yokogawa CSU-X1 spinning disk confocal microscope. All images used for quantitative comparisons were prepared with equal treatment, acquired with identical parameters (e.g. pinhole diameter, detector gain), and processed in an identical manner. Richardson-Lucy deconvolution of image volumes (20 iterations) was performed using Nikon Elements software. Images were contrast enhanced and cropped using ImageJ software (NIH).

Electron microscopy

Segments of WT and KO intestine were placed into 0.1M HEPES (pH 7.3) and sub dissected into 2mm chunks at RT. Samples were placed into scintillation vials and incubated in RT fix buffer (4% PFA, 2.5% glutaraldehyde, 2mM $CaCl_2$ in 0.1M HEPES) for 1 hr and washed 3 times in HEPES buffer. Samples were incubated with 1% tannic acid/HEPES for 1 hr, washed 3 times with ddH_2O followed by incubation with 1% osmium tetroxide/ddH_2O for 1 hour. Samples were then washed 3 times with ddH_2O, incubated in 1% uranyl acetate/ddH_2O for 30 min then washed with ddH_2O. Samples were dehydrated in a graded ethanol series and then dried using critical point drying. Samples were then mounted on aluminum stubs and coated with gold/palladium using a sputter coater. Imaging was performed using a Quanta 250 Environmental SEM operated in high vacuum mode with an accelerating voltage of 5 kV. All SEM reagents were purchased from Electron Microscopy Sciences.

Image analysis

All image analysis was performed using FIJI or Nikon Elements software and all quantitative data are from at least three independent experiments. To perform line-scan analysis, a line was drawn along the axis of microvilli that were entirely in plane with a distinct tip and base visible. The intensity of the IRTKS or EPS8 signal was recorded and normalized with the lowest intensity set to 0 and the maximum set to 1. The microvillar length axis from individual scans was also normalized with the base set to 0 and the tip set to 1. Normalized line-scans were then plotted together and fit to a single Gaussian using nonlinear regression. For quantification of percentage of cells with BB, cells were scored as BB positive if they displayed polarized F-actin accumulation as visualized using a 40X objective on a Nikon A1R laser-scanning confocal microscope. Microvillar length measurements were performed on projected SIM images by tracing individual microvillar actin bundles using FIJI. For analyses in which individual microvilli were measured, at least 10 microvillar actin bundles were scored per cell and at least 25 cells measured per experiment.

In B16F1 melanoma cells, filopodia number was quantified in ImageJ by counting the number of actin protrusions on the outside of a cell. For measuring enrichment of EPS8 and at the distal tips of the BB in Ls174T-W4 cells, BB:cytosol enrichment was defined as the ratio of these two mean intensities. Percent BB and microvillar length data were analyzed with a D'Agostino and Pearson omnibus normality test to determine normal distribution. To perform intensity analyses, the BB and/ or cytosol were thresholded in villar confocal images using Nikon Elements software and the mean intensity numbers per villus were plotted; BB to cytosol enrichment was defined as the

ratio of these two mean intensities. Microvillar length measurements were performed on projected SIM images or on TEM images by tracing individual microvillar actin bundles using FIJI. For W4 cell microvillar length analysis, at least 10 microvillar actin bundles were scored per cell and at least 25 cells measured per experiment. Microvillar membrane coverage measurements were performed on projected W4 SIM images or on TEM images by dividing the length of a microvilli covered in membrane by the entire actin bundle from the rootlet to the tip. Nearest neighbor distance measurements were performed by thresholding microvilli in SEM images using Nikon Elements.

Statistical analysis

For all figures, error bars indicate SD and n values are reported in the figure legends. Normally distributed data were statistically analyzed to determine significance using the unpaired Student's *t* test. Statistical analyses performed are stated in the figure legends. All graphs were generated and statistical analyses performed using Prism (v.7, GraphPad).

Animal studies

Animal experiments were carried out in accordance with Vanderbilt University Medical Center Institutional Animal Care and Use Committee guidelines.

CHAPTER III

IRTKS ELONGATES EPITHELIAL MICROVILLI USING EPS8-DEPENDENT AND INDEPENDENT MECHANISMS

Originally published as:

Postema, M.M., Grega-Larson, N.E., Neininger, A. C., & Tyska, M.J. (2018) IRTKS (BAIAP2L1) elongates epithelial microvilli using EPS8- dependent and independent mechanisms. Current Biology *28*: 2876-2888.

Summary

Transporting epithelial cells like those that line the gut, build large arrays of actin-supported protrusions called microvilli, which extend from the apical surface into luminal spaces to increase functional surface area. Although critical for maintaining physiological homeostasis, mechanisms controlling the formation of microvilli remain poorly understood. Here we report that the I-BAR domain-containing protein insulin receptor tyrosine kinase substrate (IRTKS, also known as BAIAP2L1) promotes the growth of epithelial microvilli. Super-resolution microscopy and live imaging of differentiating epithelial cells revealed that IRTKS localizes to the distal tips of actively growing microvilli via a mechanism that requires its N-terminal I-BAR domain. At microvillar tips, IRTKS promotes elongation through a mechanism involving its C-terminal actin-binding WH2 domain. IRTKS can also drive microvillar elongation using its SH3 domain to recruit the bundling protein EPS8 to microvillar tips. These results provide new insight on

mechanisms that control microvillar growth during the differentiation of transporting epithelial cells, and help explain why IRTKS is targeted by enteric pathogens that disrupt microvillar structure during infection of the intestinal epithelium.

Introduction

Transporting epithelial cells line the luminal surface of many hollow organs where they promote solute uptake from the external environment. Transport is aided by actin-supported membrane protrusions called microvilli, which increase apical membrane surface area (Helander and Fandriks, 2014). A single microvillus contains a core bundle of parallel actin filaments with barbed ends oriented away from the cell and pointed ends embedded in an underlying terminal web (Mooseker and Tilney, 1975). Certain epithelial cell types, such as intestinal enterocytes, build hundreds of densely packed microvilli in an array known as the 'brush border' (BB) (Crawley et al., 2014b; Delacour et al., 2016). In addition to driving nutrient absorption, intestinal microvilli provide a barrier against luminal pathogens and toxins (Shifrin et al., 2012). In one example, infection with enterohemorrhagic *Escherichia coli* (EHEC) disrupts microvillar structure and packing and in turn leads to nutrient malabsorption and osmotic imbalances, which can prove life threatening (Vallance et al., 2002). Despite the critical physiological role of the BB, the molecules and mechanisms controlling microvillar growth remain poorly understood.

Microvillar growth occurs during enterocyte differentiation, which takes place in pit-like "crypts", sites that harbor intestinal stem cells (Friedman, 1945). Although crypt epithelial cells exhibit short, disorganized microvilli (Fath et al., 1990; Specian and Neutra, 1981), the apical domain undergoes a striking transition as nascent enterocytes migrate

out of crypts and onto the villus (Fath et al., 1990; van Dongen et al., 1976). Defining features of this transition include an increase in packing density (number of microvilli/cell) and an increase in microvillar length. Both of these changes increase apical membrane surface area and contribute to maximizing the absorptive capacity of mature enterocytes.

Although mechanisms that drive tight microvillar packing are beginning to emerge (Crawley et al., 2014b; Crawley et al., 2016; Li et al., 2016; Li et al., 2017; Weck et al., 2016; Yu et al., 2017), molecules responsible for elongation of microvilli during differentiation remain poorly understood. Previous studies implicated actin filament bundling proteins, including villin and espin, in elongation (Friederich et al., 1989; Loomis et al., 2003). Bundling proteins also play a role in the growth, elongation, and maintenance of other actin-supported protrusions including stereocilia (espin-1, plastin-1 and fascin-2) (Krey et al., 2016; Sekerkova et al., 2011; Shin et al., 2010) and filopodia (fascin-1) (Vignjevic et al., 2006), respectively. Remarkably, studies on KO mice lacking the three major microvillar actin bundlers (villin, espin, and plastin) revealed that BBs are still present (Revenu et al., 2012), suggesting the existence of alternate assembly pathways. Factors that target to the ends of core actin bundles would also be well positioned to exert control over bundle length. Indeed, cordon bleu targets near the pointed ends of microvillar actin cores and has been shown to promote their growth (Grega-Larson et al., 2015; Grega-Larson et al., 2016; Wayt and Bretscher, 2014).

Given the high outward membrane curvature generated during protrusion, another group of molecules likely to play important roles in microvillar elongation are I-BAR (Inverse-Bin-Amphiphysin-Rvs) proteins (Ahmed et al., 2010; Zhao et al., 2011). I-BAR domains are small membrane-binding, three helix bundles that dimerize and exhibit a

structural curvature that is well-matched to outward bending (Lee et al., 2007; Millard et al., 2005). Members of the I-BAR family (including IRSp53, IRTKS, Pinkbar, MIM, and ABBA) are comprised of an N-terminal BAR domain that interacts with acidic phospholipids, a central SH3 domain, and an actin-binding Wiskott-Aldrich syndrome protein homology 2 (WH2) motif at the C-terminus (Ahmed et al., 2010; Zhao et al., 2011). I-BAR proteins have been implicated in generating filopodia on the surface of motile cells (Lim et al., 2008; Yamagishi et al., 2004) and dendritic spines in neurons (Saarikangas et al., 2015), physiological scenarios that both require membrane protrusion.

A proteomic study by our laboratory identified insulin receptor tyrosine kinase substrate (IRTKS or brain-specific angiogenesis inhibitor 1-associated protein like 1 or BAIAP2L1) as the only I-BAR domain-containing protein in the intestinal BB (McConnell et al., 2011). IRTKS was first identified as a tyrosine phosphorylated insulin receptor substrate (Yeh et al., 1996) and subsequently predicted to be an I-BAR domain protein (Yamagishi et al., 2004). Later work showed that over-expression of IRTKS induced dramatic effects on the actin cytoskeleton in a WH2 domain-dependent manner (Millard et al., 2007). Studies on IRTKS KO mouse models implicate this molecule in insulin signaling and glucose homeostasis (Huang et al., 2013), as well as the formation of dorsal filopodia in embryonic fibroblasts (Sudhaharan et al., 2016). IRTKS is also hijacked by EHEC during its infection of the intestinal tract. Under these conditions, the IRTKS SH3 domain binds tightly to virulence factors that ultimately stimulate actin polymerization and adherent pedestal formation, which are required for survival of the microbe and continued infection (Aitio et al., 2010; Aitio et al., 2012; Crepin et al., 2010; Vingadassalom et al., 2009). The dependence of EHEC pathogenesis on IRTKS strongly implicates this

molecule as a resident of the enterocyte apical domain, the initial site of EHEC contact with the epithelium, yet how IRTKS contributes to normal BB function remains unknown.

Here we report that IRTKS plays an important role in elongating microvilli. Using super-resolution microscopy, we discovered that IRTKS exhibits striking localization to the distal tips of microvilli, where the growing ends of actin filaments are found. IRTKS targets to these sites of outward membrane curvature using its N-terminal I-BAR domain. Once at the tips, IRTKS serves to elongate microvilli via distinct mechanisms that require functional WH2 and SH3 domains. A role for the SH3 domain in elongation is in part explained by binding to EPS8, an established F-actin capping and bundling protein. We show that IRTKS controls the localization of EPS8 and promotes its targeting to microvillar tips. Thus, IRTKS functions in microvillar elongation directly using its WH2 domain, and indirectly using its SH3 domain to recruit EPS8, which also harbors its own elongation activity. Together these studies identify the first I-BAR protein in the epithelial apical domain, illuminate molecular mechanisms that promote microvillar growth during enterocyte differentiation, and provide an evolutionary rationale on the targeting of IRTKS during EHEC infection.

Results

IRTKS localizes to the tips of microvilli in differentiating epithelial cells

Using 2D-LC-MS/MS to define the mouse BB proteome, we previously identified IRTKS as one of 646 proteins enriched in BB fractions (McConnell et al., 2011). To examine the expression and localization of IRTKS, we stained mouse small intestinal organoids with an IRTKS specific antibody. Intestinal organoids are derived from isolated stem cell-

containing crypts; in culture, these structures reseal and differentiate through formation of new crypt domains budding from a shared villus domain that encapsulates a closed lumen (Fig. 3-1A) (Sato and Clevers, 2013a; Sato et al., 2009). The resulting primary cultures are highly amenable to whole mount imaging, which makes it easier to orient and capture full crypt-villus axes. Importantly, the accumulation of apical F-actin, which defines the crypt-villus transition, is recapitulated in this system (Fig. 3-1A). In these cultures, IRTKS is enriched at the apical surface in both crypt and villus domain cells. Interestingly, line scans orthogonal to the apex of crypt cells revealed peak IRTKS signal close to microvillar tips (0.78 ± 0.21, base = 0, tips = 1) (Fig. 3-1C). To define IRTKS localization at higher resolution, we examined Ls174T-W4 (W4) cells, an epithelial cell line that can be induced to form microvilli (Baas et al., 2004). W4 cells mimic the partially differentiated state of crypt cells and provide a model for studying IRTKS function in cells that have actively growing microvilli. Consistent with organoid staining, structured illumination microscopy (SIM) of endogenous IRTKS in W4 cells revealed puncta throughout the cytoplasm, as well as enrichment at microvillar tips (Fig. 3-1D, 3-1E). Thus, IRTKS is expressed in differentiating epithelial cells of the crypt and localizes to the tips of nascent microvilli.

IRTKS tracks the distal tips of growing microvilli

We next examined IRTKS dynamics in live W4 cells expressing EGFP-IRTKS and mCherry-Utrophin (UtrCH) to label F-actin (Fig. 3-3A). In kymographs created with lines along the microvillar axis, IRTKS tracked the tips of growing bundles, producing diagonal features with the slope indicating an elongation rate of ~0.75 μm/min (Fig. 3-3B).

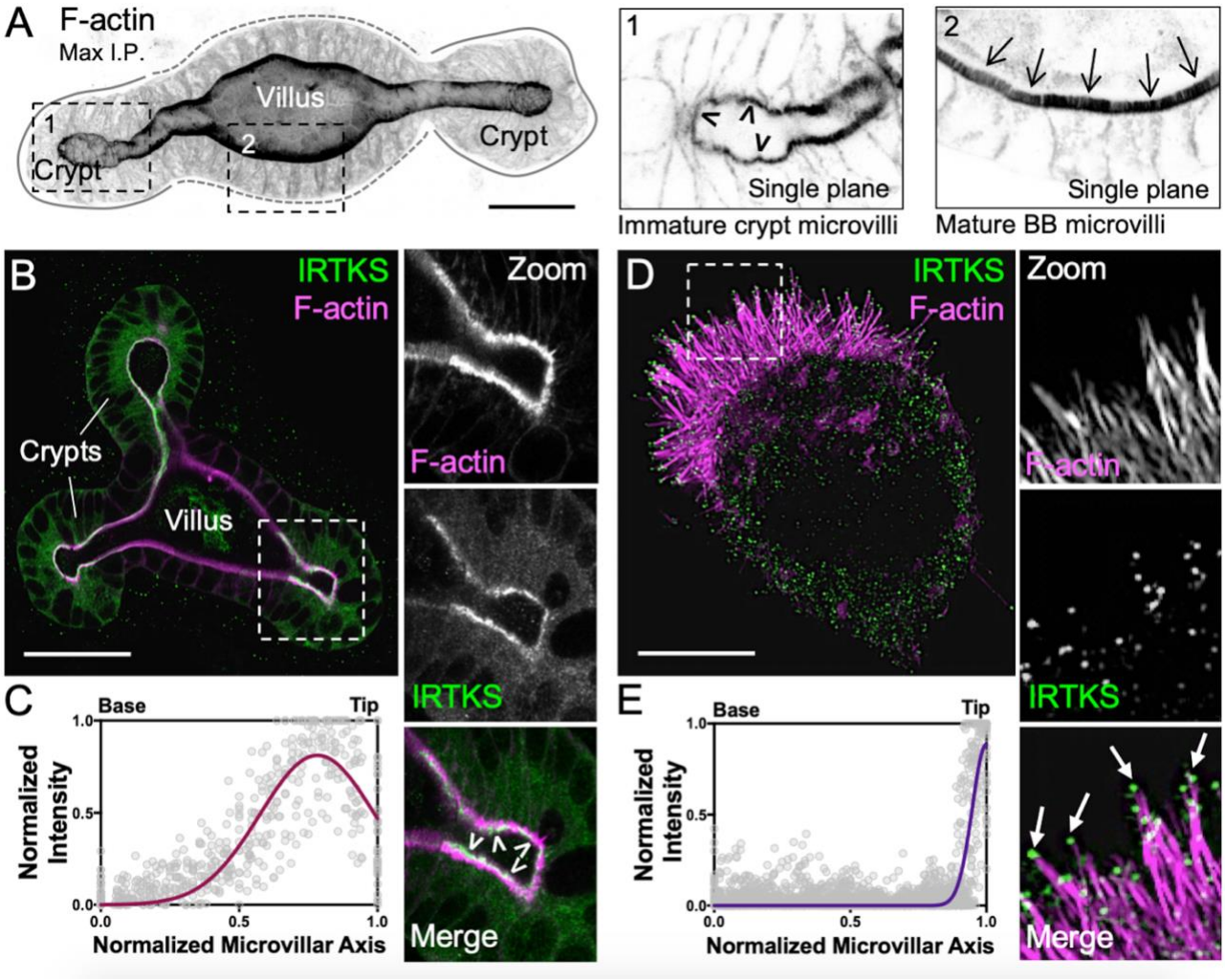

Figure 3-1: IRTKS localizes to the distal tips of epithelial microvilli. (**A**) Confocal maximum intensity projection of a mouse small intestinal organoid stained with phalloidin to label F-actin. Zooms indicate single plane images: 1) crypt cells, arrowheads highlight immature microvilli and 2) villar cells, arrows highlight mature microvilli. Scale bar, 25 µm. (**B**) Endogenous IRTKS (green) and phalloidin (magenta) labeling of an intestinal organoid. Dashed box indicates zoom of the crypt; arrowheads highlight IRTKS tip localization. Scale bar, 40 µm. (**C**) Line scans (n = 36 microvilli) of normalized endogenous IRTKS intensity parallel to the microvillar axis in organoid crypt domains. Length values are normalized such that 0 = base and 1 = tip. (**D**) SIM projection of a Ls174T-W4 (W4) cell showing endogenous IRTKS (green) and stained with phalloidin (magenta). Dashed box indicates zoom of the BB, arrows point to IRTKS puncta at the microvillar distal tips. Scale bar, 5 µm. (**E**) Line scans (n = 42 microvilli) of normalized endogenous IRTKS intensity parallel to the microvillar axis in W4 cells. Length values are normalized such that 0 = base and 1 = tip.

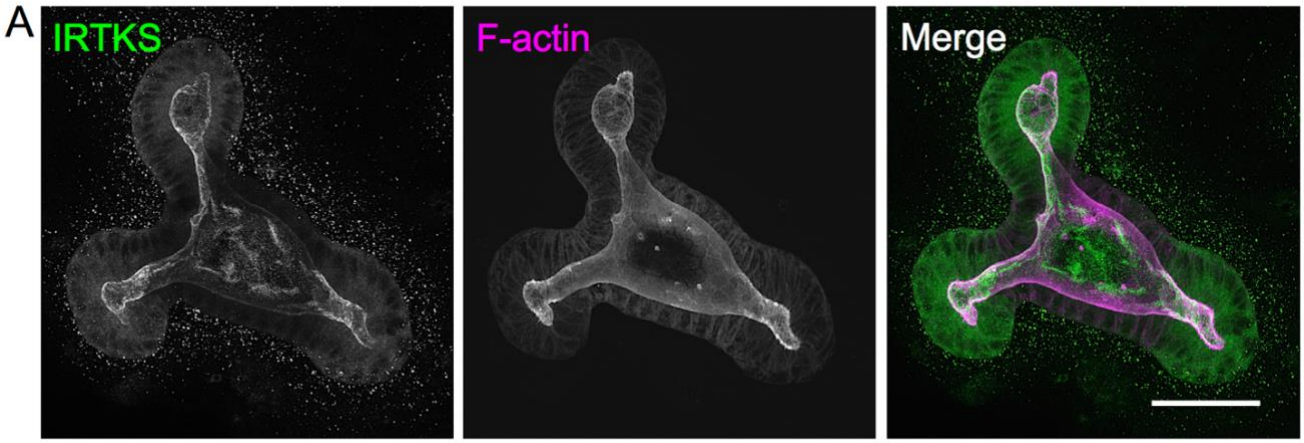

Figure 3-2: IRTKS is highly expressed in the intestinal crypt domain. (**A**) Maximum intensity projection of the IRTKS stained mouse intestinal organoid used in Fig. 1B. Scale bar, 40 µm.

Montages of individual microvilli also showed IRTKS puncta persistently tracking the tips of newly emerging protrusions (Fig. 3-3C). Of note, we were unable to detect clear examples of IRTKS tip tracking during microvillar retraction. This might suggest that IRTKS prefers the tips of growing bundles. However, we cannot rule out the possibility that retraction events may be obscured by the dynamic movements of microvilli during these time-lapse. To determine if tip targeting was specific to the parallel actin bundles in epithelial microvilli, we examined the localization of EGFP-tagged IRTKS in B16F1 melanoma cells. Time-lapse imaging showed strong localization to the tips of dynamic filopodia, as well as an increase in the total number of filopodia over control cells (Fig. 3-3D- 3-3G). Together, these results suggest that the IRTKS tip targeting mechanism senses general features of the distal tip compartment, such as outward membrane curvature and/or the actin filament barbed ends.

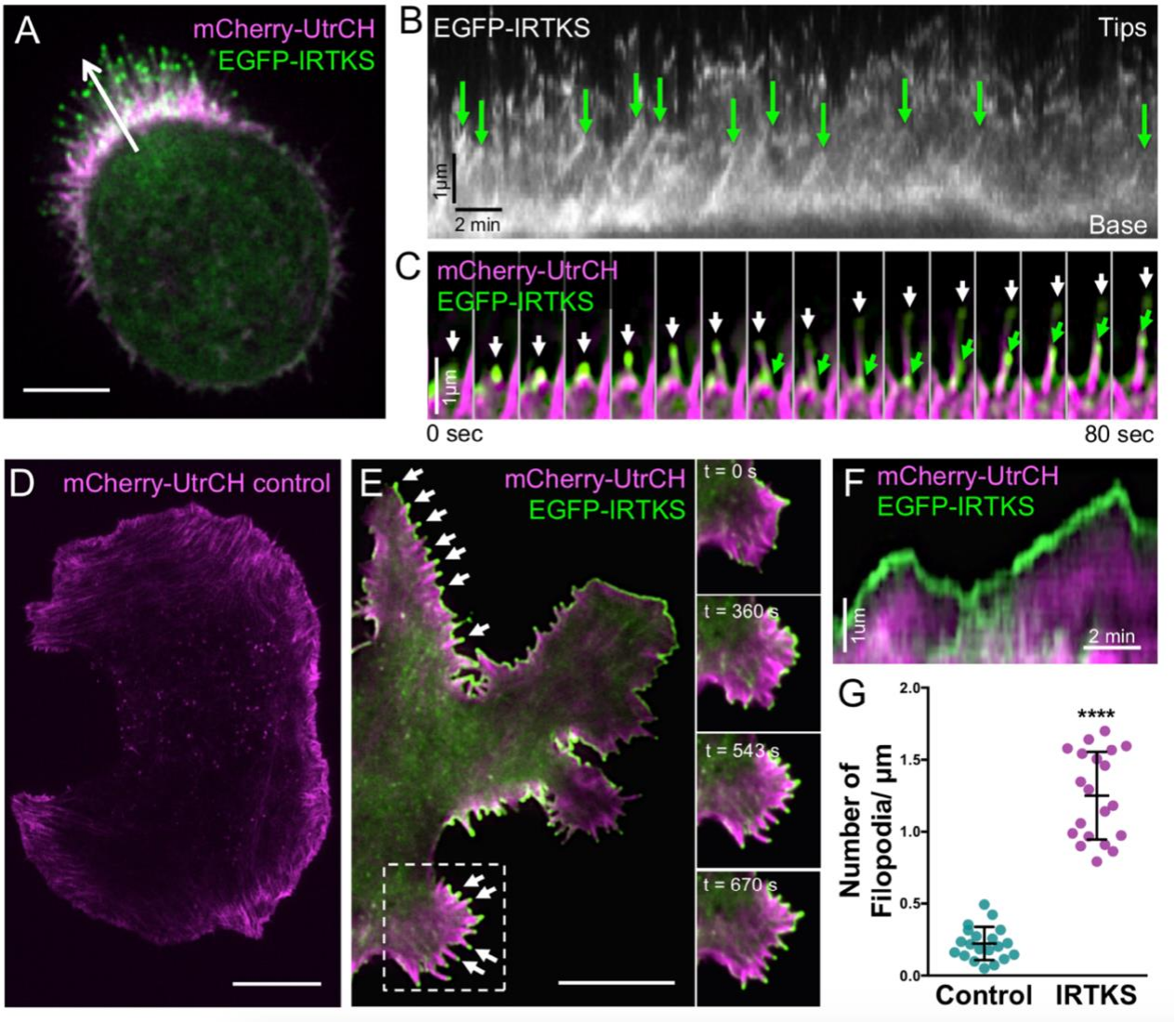

Figure 3-3: IRTKS tracks the tips of growing F-actin protrusions. (**A**) EGFP-IRTKS (green) targets to the tips of mCherry-Utrophin (UtrCH, magenta) labeled microvilli in live W4 cells. Scale bar, 5 μm. (**B**) Kymograph from the white arrow in A; RTKS puncta track the tips of protruding microvilli shown with arrows. **(C)** Montage of IRTKS tracking the tips of growing MV in a Ls174T-W4 cell expressing EGFP-IRTKS (green) and mCherry-UtrCH (magenta). White and green arrows indicate IRTKS at the tips of two distinct elongating microvillar bundles. (**D**) TIRF live-cell imaging of a control B16F1 melanoma cell expressing mCherry-UtrCH. Scale bar, 10 μm. (**I**) TIRF live-cell imaging of a B16F1 melanoma cell expressing EGFP-IRTKS (green) and mCherry-UtrCH (magenta); arrows point to individual filopodial protrusions with IRTKS enrichment at the distal tips. Dashed box indicates single movie frames with time in seconds. Scale bar, 10 μm. (**J**) Kymograph of a B16F1 cell filopodia. IRTKS (green) persists at the tips of filopodial actin bundles (magenta) during growth. (**K**) Quantitation of the number of filopodia per μm of cell perimeter in control and IRTKS expressing B16F1 melanoma cells; 20 cells/condition. Error bars indicate mean ± SD; p value calculated using a t test (****p<0.0001).

IRTKS tip targeting is driven by the N-terminal I-BAR domain

To define the mechanism of IRTKS tip targeting, we examined the impact of eliminating or mutating specific structural motifs (Fig. 3-4A). A full-length EGFP-IRTKS construct enriched at the tips of W4 microvilli similar to endogenous IRTKS (Fig. 3-4B, 3-5A). A construct containing loss-of-function mutations (W378K/W391K) in the SH3 domain (SH3*)(Tu et al., 2001) still displayed some tip targeting, but also accumulated near the base of microvilli (Fig. 3-4C, 3-5B). Deletion of the C-terminal WH2 domain (ΔWH2) had no impact on tip targeting (Fig. 3-4D, 3-5C), whereas deletion of the N-terminal I-BAR domain (ΔI-BAR) completely eliminated all membrane localization and tip targeting (Fig. 3-4E, 3-5D). The IRTKS I-BAR domain alone displayed targeting to the membrane and microvilli (Fig. 3-4F, 3-5E). Thus, IRTKS tip targeting is controlled primarily by the I-BAR domain, but is refined by the SH3 domain, likely through its interactions with binding partners.

IRTKS promotes microvillar elongation using its SH3 and WH2 domains

Our analysis of IRTKS targeting mechanisms revealed that overexpression of variants significantly impacted microvillar length (Fig. 3-4G). W4 cells overexpressing full-length IRTKS exhibited a minor increase in length over WT cells (2.7 ± 0.4 μm vs. 2.5 ± 0.4 μm, respectively). However, SH3* and ΔWH2 constructs significantly decreased length (1.8 ± 0.4 μm and 1.9 ± 0.4 μm, respectively), likely due to a dominant negative effect. Effects on length also scaled with expression level (Fig. 3-4H). Constructs lacking the I-BAR or with the I-BAR domain alone did not impact microvillar length (Fig. 3-4G).

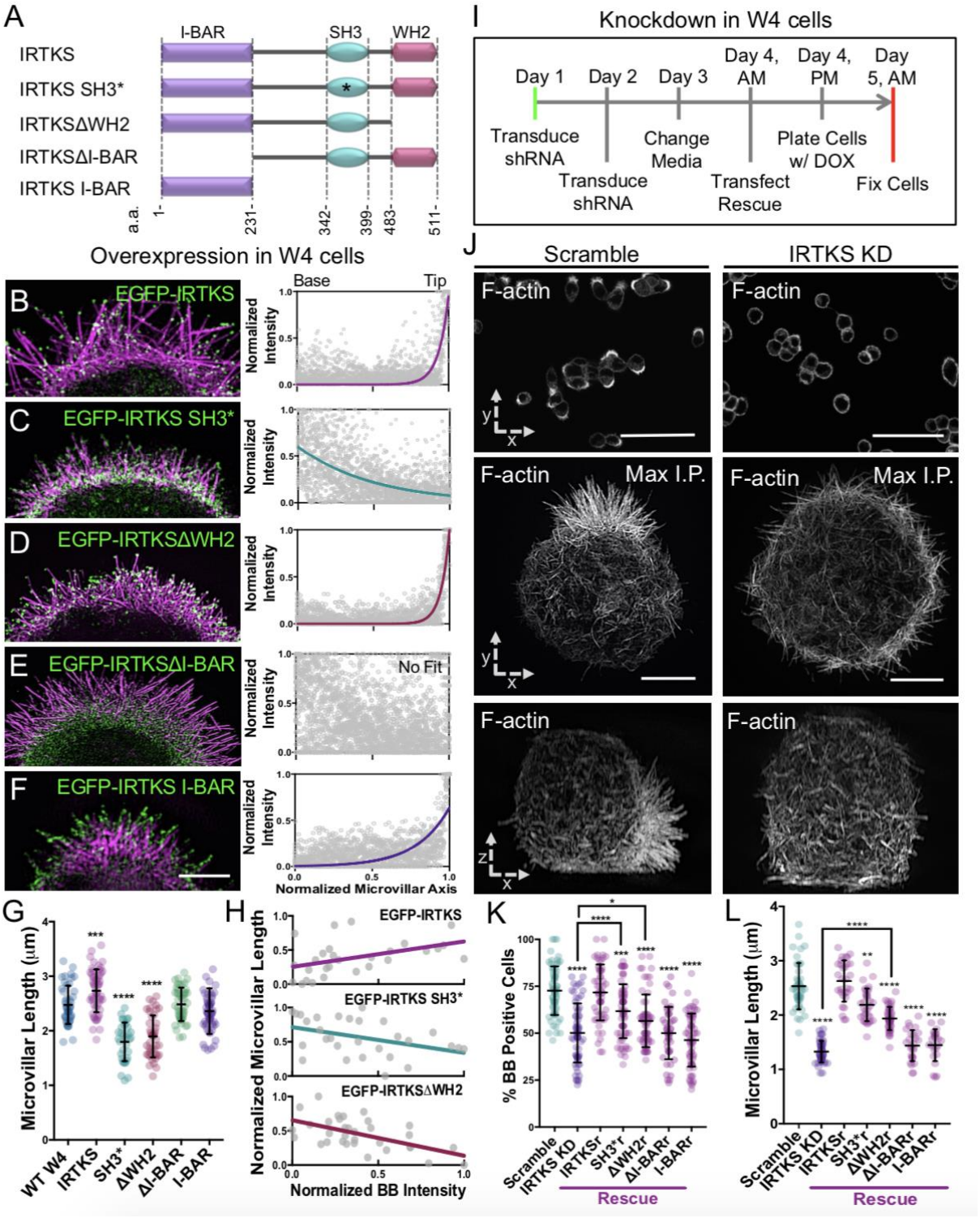

Figure 3-4: IRTKS promotes microvillar elongation. (**A**) Construct cartoons for the IRTKS variants used in this study. *refers to W378K/W391K point mutations within the SH3 domain; a.a. refers to the amino acid numbers of the indicated domain. (**B-F**) SIM projections of W4 cells expressing EGFP-IRTKS constructs (green) and stained with phalloidin (magenta). Line scans (n ≥ 32 microvilli for each construct) parallel to the

microvillar axis show the intensity distribution of each IRTKS construct; 0 = base, 1 = tip. Scale bar, 3.5 μm. (**G**) Quantitation of microvillar length from cells expressing IRTKS constructs; >34 cells/condition, >10 microvilli/cell. (**H**) Quantitation of total IRTKS fluorescent intensity within the BB versus averaged microvillar length for individual cells; >28 cells per condition, >10 microvilli averaged per cell. The slope of EGFP-IRTKS is significantly different from the slopes of EGFP-IRTKS SH3* and EGFP-IRTKSΔWH2 (**p<0.0021 and ****p<0.0001 respectively). The slopes of EGFP-IRTKS SH3* and EGFP-IRTKSΔWH2 are not significantly different (p<0.4957). (**I**) Schematic of KD/rescue experimental design. W4 cells are plated with doxycycline (DOX) to induce the formation of a BB (Baas et al., 2004). (**J**) Images of scramble or IRTKS KD W4 cells stained with phalloidin. Top panels: low magnification confocal images that were scored to generate "% BB positive cells" plots; scale bars, 40 μm. Middle panels: SIM whole cell maximum intensity projections (*en face*, x-y); scale bars, 5 μm. Bottom panels: SIM whole cell maximum intensity projections of the same cell as above (lateral, x-z). (**K,L**) Quantitation of IRTKS knockdown and rescue experiments in W4 cells. Percentage of BB positive cells; >200 cells/condition, individual points correspond to the percent of cells containing a BB for an individual 40x confocal image field. Microvillar length >28 cells/condition, >10 microvilli averaged/cell. All error bars indicate mean ± SD; all p values calculated using a t test (*p<0.033, **p<0.002, ***p<0.0002, ****p<0.0001).

Based on these data, we hypothesized that IRTKS plays a role in controlling microvillar length. To determine if IRTKS is required for microvillar growth, we used shRNA to knockdown (KD) IRTKS in W4 cells (Figs. 3-4J, 3-5G), and then examined the impact using confocal microscopy and SIM (Fig. 3-4J). IRTKS KD significantly reduced the fraction of cells able to grow a BB (72.7 ± 12.9% in scramble control vs. 50.1 ± 15.7% in KD) (Fig. 3-4K) and significantly decreased microvillar length (2.5 ± 0.5 μm control vs. 1.3 ± 0.2 μm KD) (Fig. 3-4L). These perturbations were specific to loss of IRTKS, as a construct refractory to KD (IRTKSr) rescued the fraction of cells able to grow microvilli (71.7 ± 14.9%) and microvillar length (2.7 ± 0.3 μm) (Fig. 3-4K, 3-4L, & 3-5J). Interestingly, expression of refractory SH3* and ΔWH2 constructs only partially rescued microvillar growth parameters, while refractory ΔI-BAR and I-BAR constructs had no effect on microvillar length (Fig. 3-4K, 3-4L, & 3-5K- 3-5N). These overexpression and KD/rescue

assays reveal that IRTKS is needed for normal microvillar elongation, which requires functional SH3 and actin-binding WH2 domains.

EPS8 colocalizes with IRTKS and interacts with its SH3 domain

Involvement of the IRTKS WH2 domain in microvillar elongation makes biological sense as this motif is known to bind actin directly (Millard et al., 2007). How the IRTKS SH3 domain contributes to microvillar length control is less clear. To develop our understanding of these observations, we sought to identify a binding partner for this domain. Previous studies identified the IRTKS SH3 domain as a high affinity-binding partner of the proline rich (PR) motifs in the EHEC virulence factor, $EspF_U$ (Aitio et al., 2010). Sequence analysis of $EspF_U$ PR motifs implicates several mammalian proteins as potential IRTKS binding partners under normal conditions. One candidate that stands out based on high sequence conservation is EPS8 (Fig. 3-6A), which exhibits actin bundling and capping activities through its C-terminal region (Fig.3-6B) (Disanza et al., 2004; Hertzog et al., 2010). Previous studies suggest that EPS8 targets to the tips of intestinal microvilli (Croce et al., 2004; Tocchetti et al., 2010), hair cell stereocilia (Behlouli et al., 2014; Manor et al., 2011; Zampini et al., 2011), and filopodia (Disanza et al., 2006) where it controls the length of these protrusions, although significant questions remain regarding its mechanism of targeting and action in these different contexts. In W4 cells, endogenous EPS8 was highly enriched at the tips of microvilli (Fig. 3-6C, 3-6D) and colocalized with endogenous IRTKS puncta at these sites (Fig. 3-6E- 3-6G). Whereas the majority of tip puncta contained both EPS8 and IRTKS, the stoichiometry of colocalization in the tip compartment was not fixed; this likely reflects structural variability inherent to the tips of

individual microvilli. Finally, using *in vitro* pull-downs, we found that FLAG-tagged EPS8 interacted with full length EGFP-tagged IRTKS; we also confirmed that the SH3 domain was sufficient for binding (Fig. 3-6H). Thus, using its SH3 domain, IRTKS holds the potential to interact with EPS8 at the tips of microvilli.

Interestingly, co-expressing IRTKS and EPS8 in W4 cells did not significantly elongate W4 cell microvilli (Fig. 3-7B). We suspect this is because a major fraction of cellular G-actin is incorporated into microvillar actin bundles upon induction with doxycycline. We tested this idea by co-expressing IRTKS and EPS8 in cells that do not normally build BBs: B16F1 melanoma and HeLa cells (Fig. 3-7C- 3-7F). In both cell types, dual expression dramatically increased the number of both dorsal and substrate-attached filopodia over control cells, indicating that IRTKS and EPS8 can work together to stimulate finger-like protrusion growth.

IRTKS promotes EPS8 enrichment at the tips of microvilli

To further elucidate the functional relationship between EPS8 and IRTKS at microvillar tips, we examined the impact of IRTKS KD on EPS8 localization. Although some EPS8 was still present in the shortened microvilli on the surface of IRTKS KD cells (Fig. 3-8A, 3-8B), we also found that cytosolic EPS8 levels were significantly increased relative to controls (Fig. 3-8A- 3-8C), suggesting that IRTKS promotes the tip targeting of EPS8 under normal conditions. To test this concept, we generated a variant of EPS8 lacking the predicted IRTKS interacting motif (EPS8ΔPR1, Fig. 3-6A, 3-6B). Strikingly, this variant localized in puncta throughout the cytoplasm (Fig. 3-8D), with significantly reduced tip targeting relative to EGFP-EPS8 (Fig. 3-8E). Using pulldowns, we also found that less

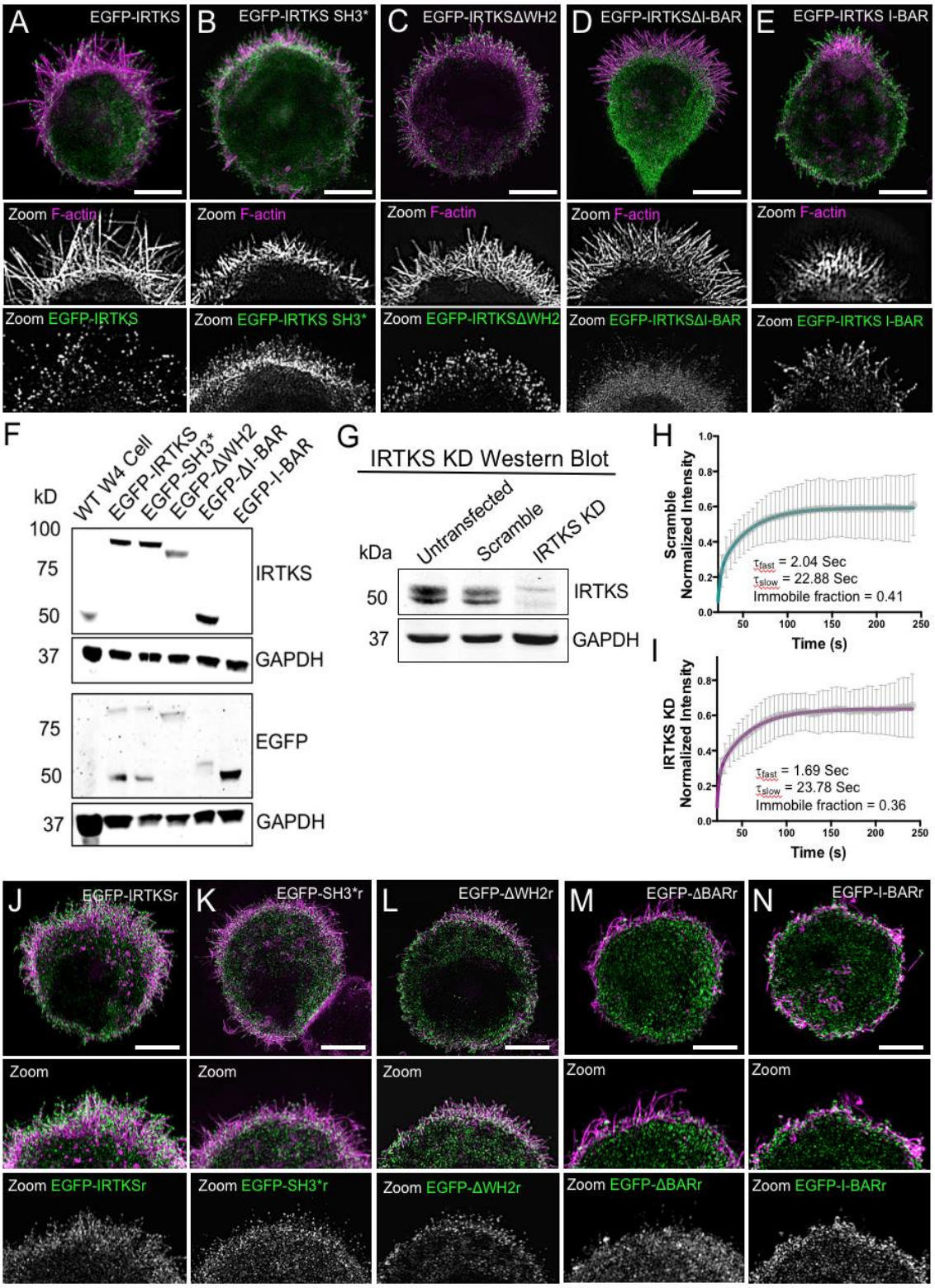

Figure 3-5: Split channel images of IRTKS overexpression and KD/rescue cells. (**A-E**) SIM projections of Ls174T-W4 cells expressing EGFP-IRTKS constructs (green) and stained with phalloidin (magenta); single channel zooms of the BB are below each image.

Scale bars, 5 μm. (**F**) Western blot analysis of expression levels of EGFP-IRTKS variants in lysates from Ls174T-W4 cells. Both IRTKS and EGFP antibodies were used because the IRTKS antibody is towards a peptide sequence within the SH3 domain, thus the EGFP-I-BAR alone construct will not be targeted. GAPDH was used as a loading control. (**G**) Western blot analysis of endogenous IRTKS levels in lysates from WT Ls174T-W4 cells, shRNA scramble control, and shRNA IRTKS KD. GAPDH was used as a loading control. (**H-I**) FRAP curves of shRNA scramble control and shRNA IRTKS KD in Ls174T-W4 cells. (**J-N**) SIM projections of IRTKS KD Ls174T-W4 cells expressing refractory EGFP-IRTKS constructs in rescue experiments. Zooms of the BB and single IRTKS channel below each image. Scale bars, 5 μm.

EGFP-EPS8ΔPR1 bound to a FLAG-tagged IRTKS SH3 bait relative to EGFP-EPS8 (Fig. 3-9A). To further determine if IRTKS is sufficient to control EPS8 localization, we fused its SH3 domain to TOM20, thus directing it to the surface of mitochondria. In cells expressing TOM20-mCherry-IRTKS-SH3, but not TOM20-mCherry alone, a large fraction of endogenous EPS8 was sequestered to mitochondria (Fig. 3-8F- 3-8G). Microvillar length was slightly decreased in these cells, likely due to the loss of EPS8 from the BB (Fig. 3-8I). Together, these results indicate that IRTKS can use its SH3 domain to promote the localization of EPS8 to microvillar tips.

EPS8 promotes microvillar elongation

Previous studies implicated EPS8 in controlling the length of actin bundle-supported protrusions (Croce et al., 2004; Manor et al., 2011), and we confirmed this in EPS8 depleted W4 cells (Fig. 3-10A, 3-10B & 3-9B). Interestingly, EPS8 KD phenocopied IRTKS KD (Fig. 3J-3L), by reducing the fraction of cells able to assemble BBs (71.9 ± 11.7% scramble control vs. 26.5 ± 10.7% EPS8 KD) (Fig. 3-10C) and decreasing microvilli length (2.5 ± 0.4 μm scramble control vs 1.6 ± 0.3 μm EPS8 KD) (Fig. 3-10D). Both microvillar growth parameters were rescued by expression of a refractory variant of

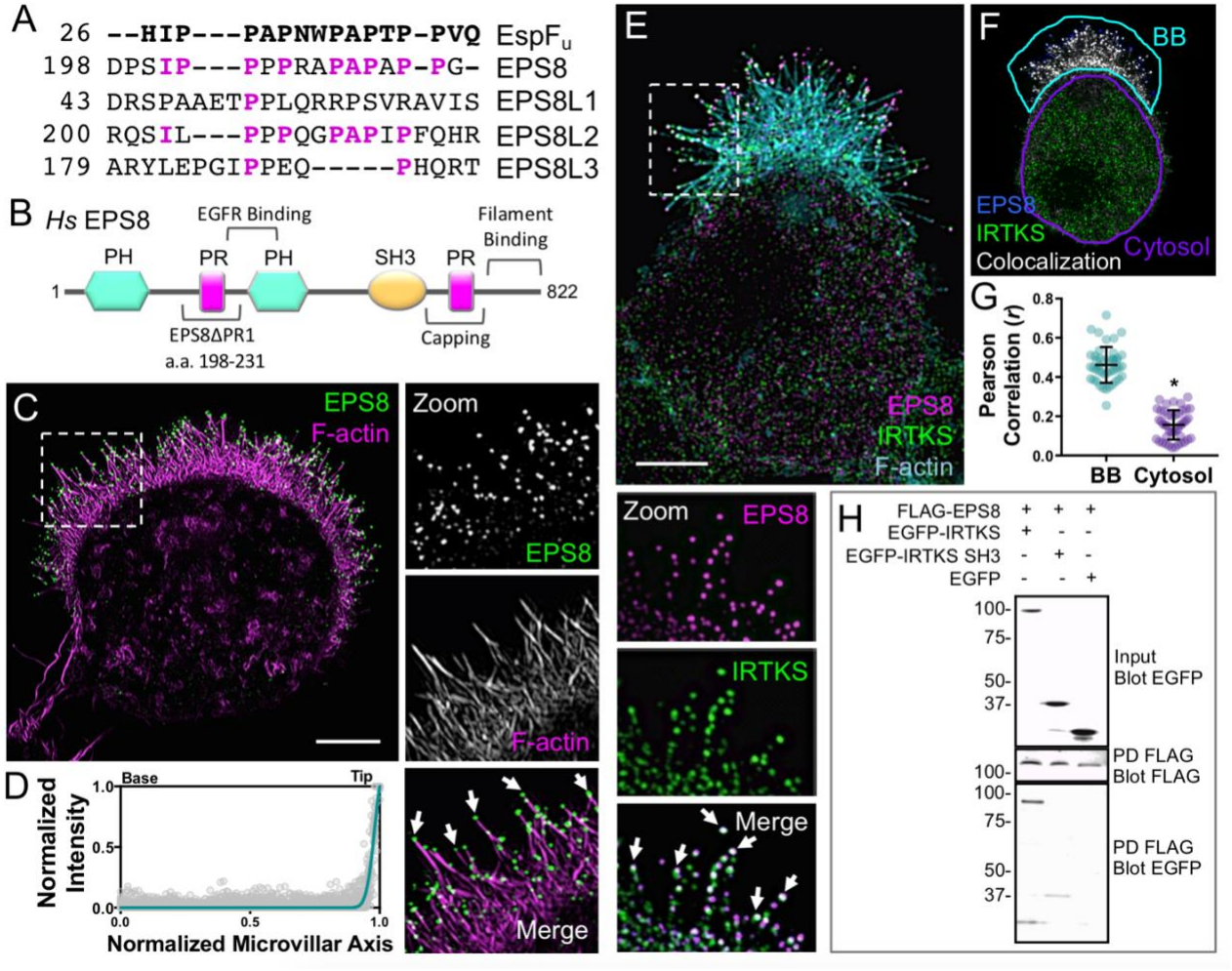

Figure 3-6: EPS8 colocalizes and interacts with IRTKS. (**A**) Sequence alignment of the proline rich (PR) motifs of $EspF_u$ and EPS8 isoforms. Magenta letters indicate EPS8 amino acids that align with the $EspF_u$ PR. (**B**) Domain organization of human EPS8. EPS8ΔPR1 refers to the construct used in Fig. 5 D, E; capping and filament binding refer to F-actin interactions. (**C**) SIM projection of an W4 cell stained for endogenous EPS8 (green) and phalloidin (magenta). Dashed box indicates zoom of the BB, arrows highlight EPS8 puncta at microvillar distal tips. Scale bar, 5 µm. (**D**) Line scans (n = 42) of endogenous EPS8 intensity parallel to the microvillar axis in W4 cells; 0 = base, 1 = tip. (**E**) SIM projection of an W4 cell stained for endogenous IRTKS (green), EPS8 (magenta), and phalloidin (blue). Dashed box indicates zoom of the BB (rotated 90° clockwise); arrows point to colocalized IRTKS and EPS8 puncta (white spots). Scale bar, 5 µm. (**F**) Colocalization of EPS8 and IRTKS; colocalized pixels (white), EPS8 pixels (blue), and IRTKS pixels (green). Teal outline designates the BB and purple outline designates the cytosol. (**G**) Pearson's Correlation analysis of IRTKS and EPS8 colocalization in the BB vs. cytosol (n = 44 cells). Error bars indicate mean ± SD; p value calculated using a t test (*p<0.0001). (**H**) Pulldown of FLAG-tagged EPS8 co-expressed with EGFP-tagged IRTKS variants reveals binding between EPS8 and the IRTKS SH3 domain.

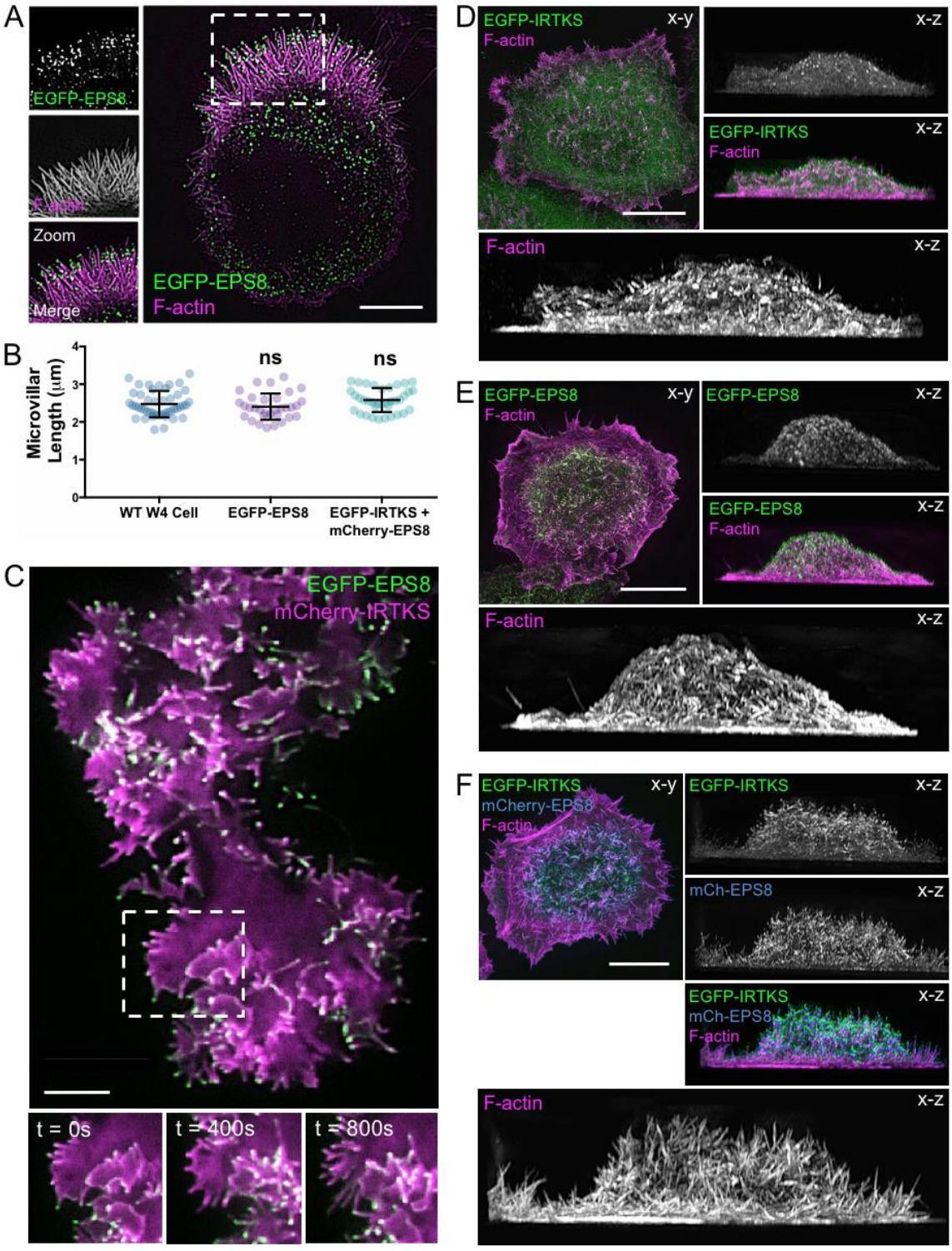

Figure 3-7: The impact of EPS8 and IRTKS co-expression on the formation of actin-based protrusions. (**A**) SIM projection of a Ls174T-W4 cell expressing EGFP-EPS8.

Dashed box indicates zoom; scale bar, 5 μm. (**B**) Quantitation of microvillar length comparing WT Ls174T-W4 cells, EGFP-EPS8 overexpression and EGFP-IRTKS and mCherry-EPS8 dual overexpression, which do not affect microvillar length. 25 cells/condition, 10 microvilli/cell; student's t test (*p<0.0001, ns, not significant) was used to determine the significance. (**C**) TIRF live-cell imaging of a B16F1 melanoma cell expressing EGFP-EPS8 (green) and mCherry-IRTKS (magenta). Dashed box indicates movie frames with time in seconds. Scale bar, 10 μm. (**D-F**) *En face* (x-y) and lateral (x-z) SIM projections of HeLa cells expressing either EGFP-IRTKS (D), EGFP-EPS8 (E), or EGFP-IRTKS and mCherry-EPS8 (F) and stained with phalloidin. Scale bars, 10 μm.

EGFP-EPS8, but only partially rescued with a refractory EGFP-EPS8ΔPR1 (Fig. 3-10C, 3-10D, 3-9B- 3-9D). Thus, EPS8 is also required for normal microvillar elongation though a mechanism requiring the PR1 motif**.**

IRTKS uses EPS8-dependent and independent mechanisms to elongate microvilli

Our results up to this point suggest a model where IRTKS promotes microvillar elongation using two distinct mechanisms: (1) a direct mechanism that involves its own actin-binding WH2 domain, and (2) an indirect mechanism that involves SH3 domain-dependent recruitment of EPS8, which in turn exerts its own elongation activity. As proposed, both mechanisms require functional IRTKS. If this model is accurate, EPS8 co-expression should rescue the shortening of microvilli observed in response to overexpression of IRTKSΔWH2, but not IRTKS SH3* (Fig. 3-4D, 3-4G). Indeed, EPS8 expression rescued microvillar length in cells expressing IRTKSΔWH2, but had no impact on the length reduction caused by IRTKS SH3* (Fig. 3-10E- 3-10H). A second prediction is that a functional SH3/PR1 interaction should be required for the increase in filopodia numbers observed with co-expression of EPS8 and IRTKS in B16 cells. Consistent with this proposal, co-expressing EPS8 with IRTKS SH3* or EPS8ΔPR1 on its own did not impact

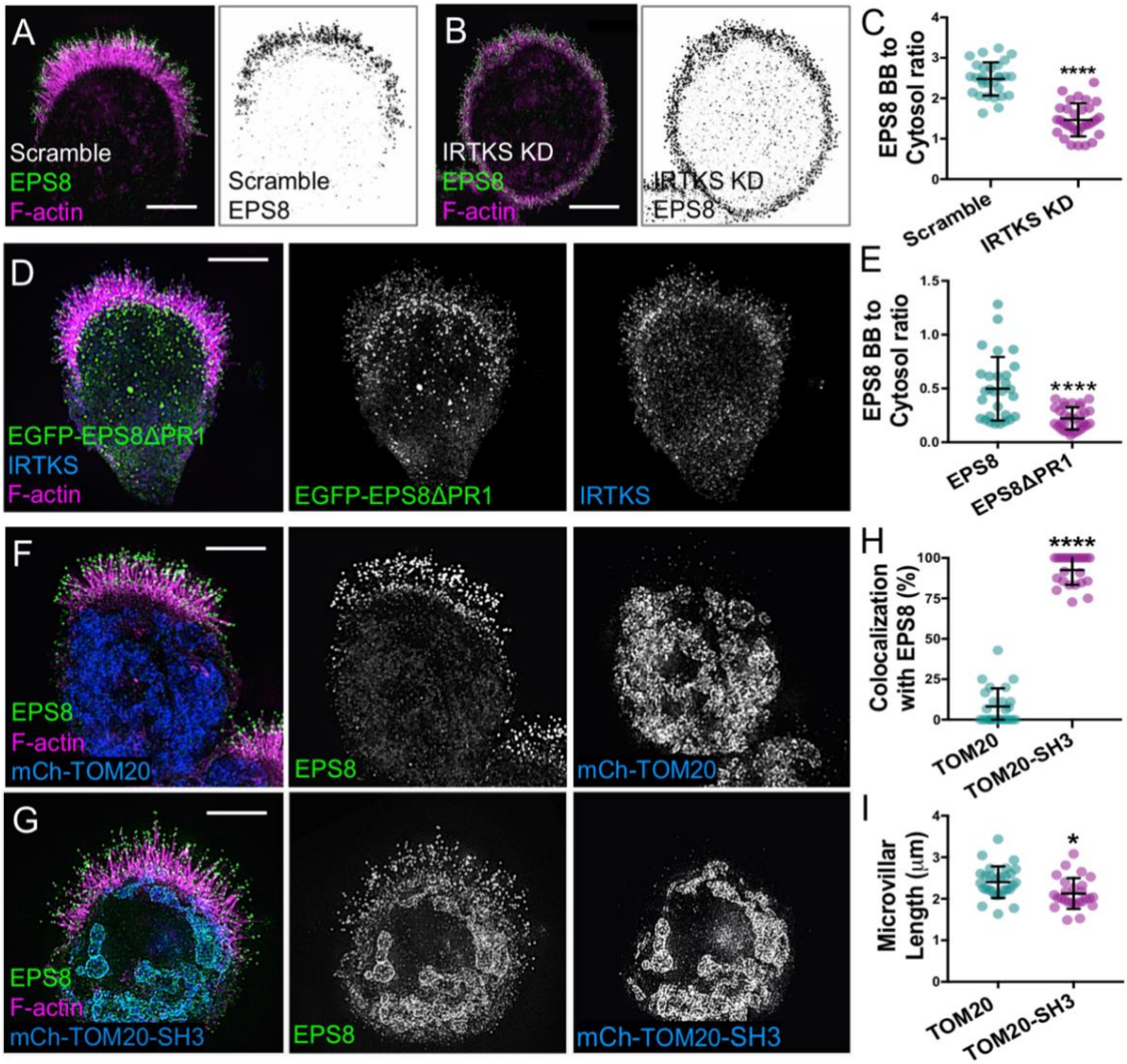

Figure 3-8: IRTKS recruits EPS8 using its SH3 domain. (**A,B**) SIM projections of scramble control and IRTKS KD W4 cells stained for EPS8 (green) and phalloidin (magenta). Inverted black and white images highlight the increased cytosolic localization of EPS8 in the IRTKS KD cells. Scale bars, 5 μm. (**C**) Quantitation of the ratio of endogenous EPS8 in the BB vs. cytosol for scramble and IRTKS KD W4 cells; scramble n = 29, IRTKS KD n = 31. (**D**) SIM projection of an W4 cell expressing EGFP-EPS8ΔPR1 (green) and stained with IRTKS (blue) and phalloidin (magenta). Scale bar, 5 μm. (**E**) Ratio of expressed EGFP-EPS8 and EGFP-EPS8ΔPR1 constructs in the BB vs. cytosol in W4 cells; EGFP-EPS8 n = 29, EGFP-EPS8ΔPR1 n = 33. (**F**) SIM projection of an W4 cell expressing mCherry-TOM20 (blue) and stained with EPS8 (green) and phalloidin (magenta) in control conditions. Scale bar, 5 μm. (**G**) SIM projection of an W4 cell expressing mCherry-TOM20 fused to the SH3 domain of IRTKS (blue) and stained with EPS8 (green) and phalloidin (magenta). The SH3 domain of IRTKS recruits EPS8 to the mitochondria. Scale bar, 5 μm. (**H**) Quantitation of the percentage of cells with EPS8 colocalized with mitochondria (n = 24). (**I**) Quantitation of microvillar length from cells expressing mCherry-TOM20 and mCherry-TOM20-SH3; >26 cells/condition, >10 microvilli averaged/cell**.** All error bars indicate mean ± SD; all p values calculated using t tests (*p<0.033, **p<0.002, ***p<0.0002, ****p<0.0001).

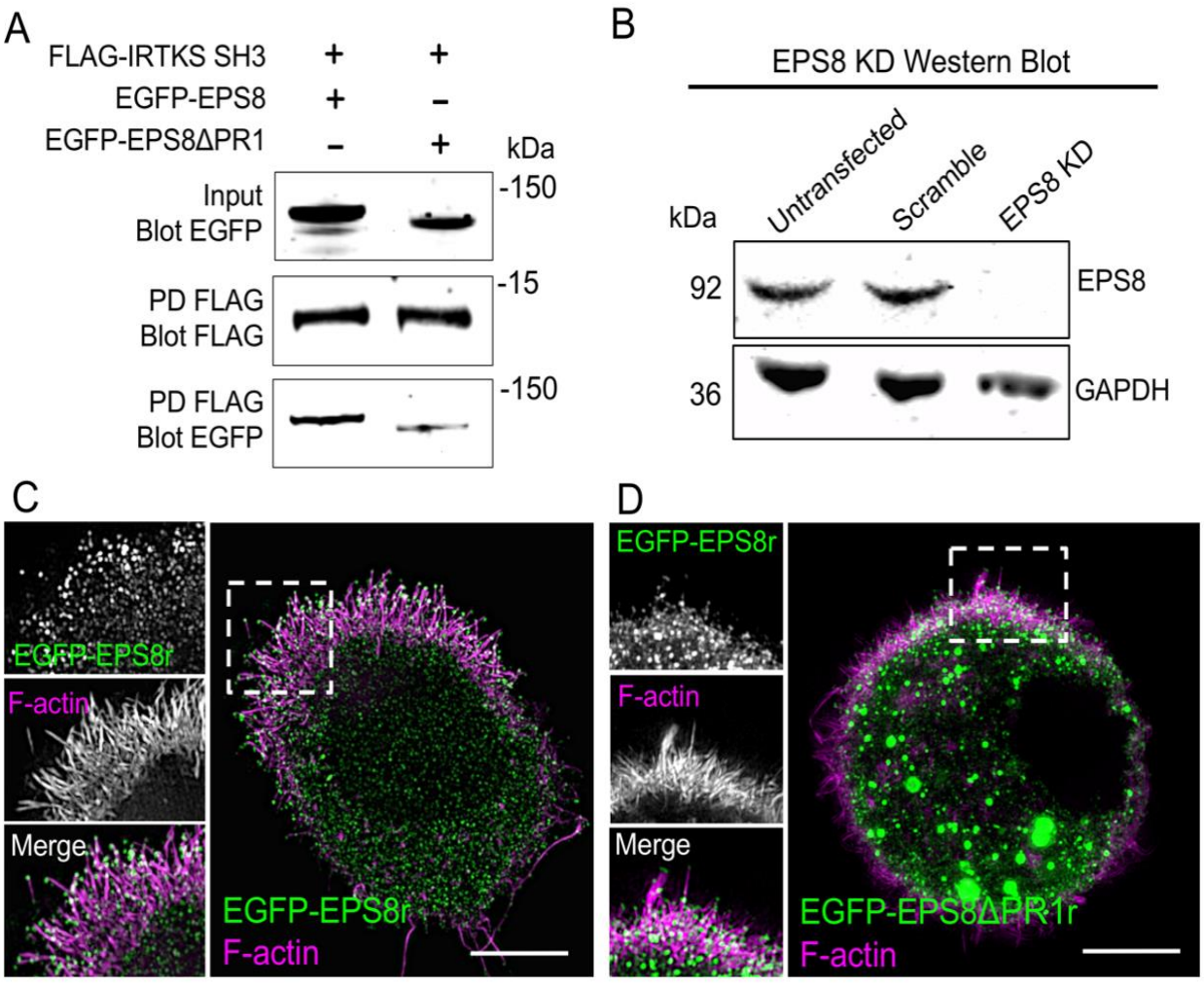

Figure 3-9: Images of EPS8 KD/ rescue Ls174T-W4 cells. (**A**) Pulldown of FLAG-tagged IRTKS SH3 domain co-expressed with EGFP-tagged EPS8 or EGFP-tagged EPS8ΔPR1 reveals binding between EPS8 and the IRTKS SH3 domain. (**B**) Western blot analysis of endogenous EPS8 levels in lysates from WT Ls174T-W4 cells (untransfected), shRNA scramble control, and shRNA EPS8 KD. GAPDH was used as a loading control. (**C**) SIM projection of an EPS8 KD Ls174T-W4 cell expressing refractory EGFP-EPS8 (EGFP-EPS8r) construct in rescue experiments; dashed box indicates zoom of the BB. Scale bar, 5 μm. (**D**) SIM projection of an EPS8 KD Ls174T-W4 cell expressing refractory EGFP-EPS8ΔPR1 (EGFP-EPS8ΔPR1r) construct in rescue experiments; dashed box indicates zoom of the BB. Scale bar, 5 μm.

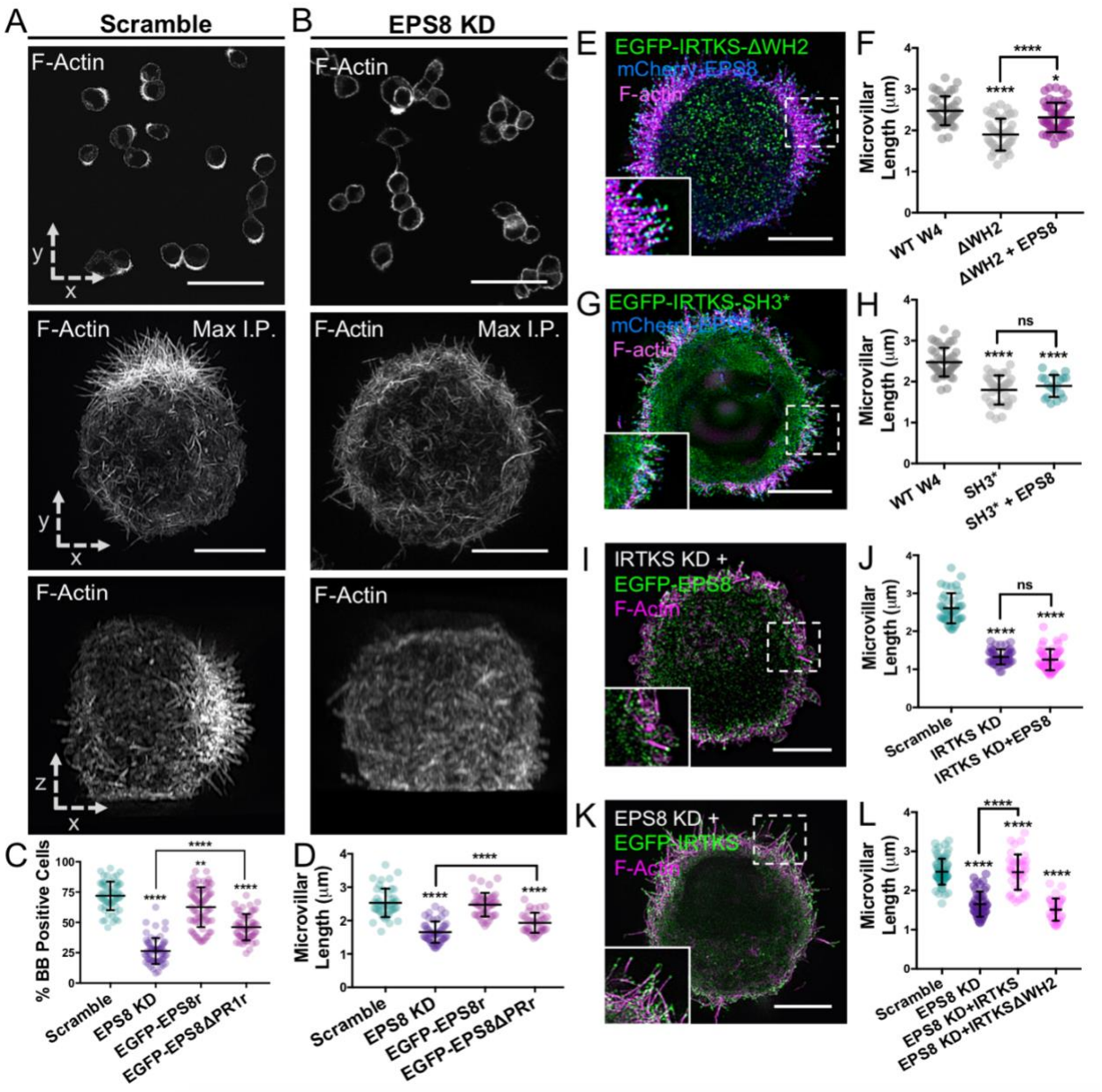

Figure 3-10: IRTKS elongates microvilli using EPS8 dependent and independent mechanisms. (**A,B**) Images of scramble and EPS8 KD W4 cells stained with phalloidin. Top panels: low magnification confocal images that were scored for "% BB positive cells" plots; scale bars, 40 μm. Middle panels: SIM whole cell maximum intensity projections (*en face*, x-y); scale bars, 5 μm. Bottom panels: SIM whole cell maximum intensity projections of the same cells as above (lateral, x-z). (**C**) Quantitation of the percentage of BB positive cells in EPS8 KD and rescue experiments; >200 cells/condition. Individual points correspond to the percent of cells containing a BB as scored in a 40x confocal image field. (**D**) Quantitation of microvillar length in EPS8 KD and rescue experiments; ≥41 cells/ condition, ≥10 microvilli averaged/cell. (**E,F**) SIM projection and quantitation of microvillar length in W4 cells expressing EGFP-IRTKSΔWH2 (green) and mCherry-EPS8

(blue) and stained with phalloidin (magenta). The WT W4 and ΔWH2 data (shaded gray tones) in this graph are replicated from Fig. 2G for a direct comparison. Scale bar, 5 μm; >30 cells, >10 microvilli/cell. (**G,H**) SIM projection and quantitation of microvillar length in W4 cells expressing EGFP-IRTKS SH3* (green) and mCherry-EPS8 (blue), and stained with phalloidin (magenta). The WT W4 and SH3* data (shaded gray tones) in this graph are replicated from Fig. 2G for a direct comparison. Scale bar, 5 μm; 18 cells, >10 microvilli/cell. (**I,J**) SIM projection and quantitation of microvillar length in IRTKS KD W4 cells expressing EGFP-EPS8. Scale bar, 5 μm; 45 cells/condition, >10 microvilli averaged/cell. (**K,L**) SIM projection and quantitation of microvillar length in EPS8 KD W4 cells expressing EGFP-IRTKS. Overexpressing IRTKS rescues microvillar length, whereas overexpressing IRTKSΔWH2 fails to rescue. Scale bar, 5 μm; ≥33 cells/condition, >10 microvilli averaged/cell. All error bars are mean ± SD; all p values calculated using a t test (*p<0.033, **p<0.002, ***p<0.0002, ****p<0.0001).

filopodia number over controls (Fig. 3-11A, 3-11D, 3-11E). However, co-expressing EPS8 with IRTKSΔWH2 significantly increased protrusion numbers (Fig 3-11B, 3-11E), likely because EPS8 can still localize through the intact IRTKS SH3 domain to induce filopodial growth. Similarly, expressing IRTKS with EPS8ΔPR1 significantly increased protrusion numbers (Fig 3-11C, 3-11E), likely because IRTKS is able to target without EPS8.

A third prediction based on our proposed model is that EPS8 overexpression should be unable to rescue the shortened microvilli observed with IRTKS KD (Fig. 3-4L). We confirmed this experimentally; EPS8 overexpression had no impact on microvillar length in cells lacking IRTKS (Fig. 3-10I, 3-10J). A fourth and final prediction states that IRTKS overexpression should rescue the shortening of microvilli observed with EPS8 KD (Fig. 3-10D), but this rescue would require the IRTKS WH2 domain. We found that microvillar shortening in EPS8 KD cells was in fact rescued by overexpression of IRTKS, but not IRTKSΔWH2 (Fig. 3-10K, 3-10L). Taken together, these findings indicate that IRTKS elongates microvilli using EPS8-dependent and independent mechanisms, which represent structurally distinct and thus experimentally separable activities.

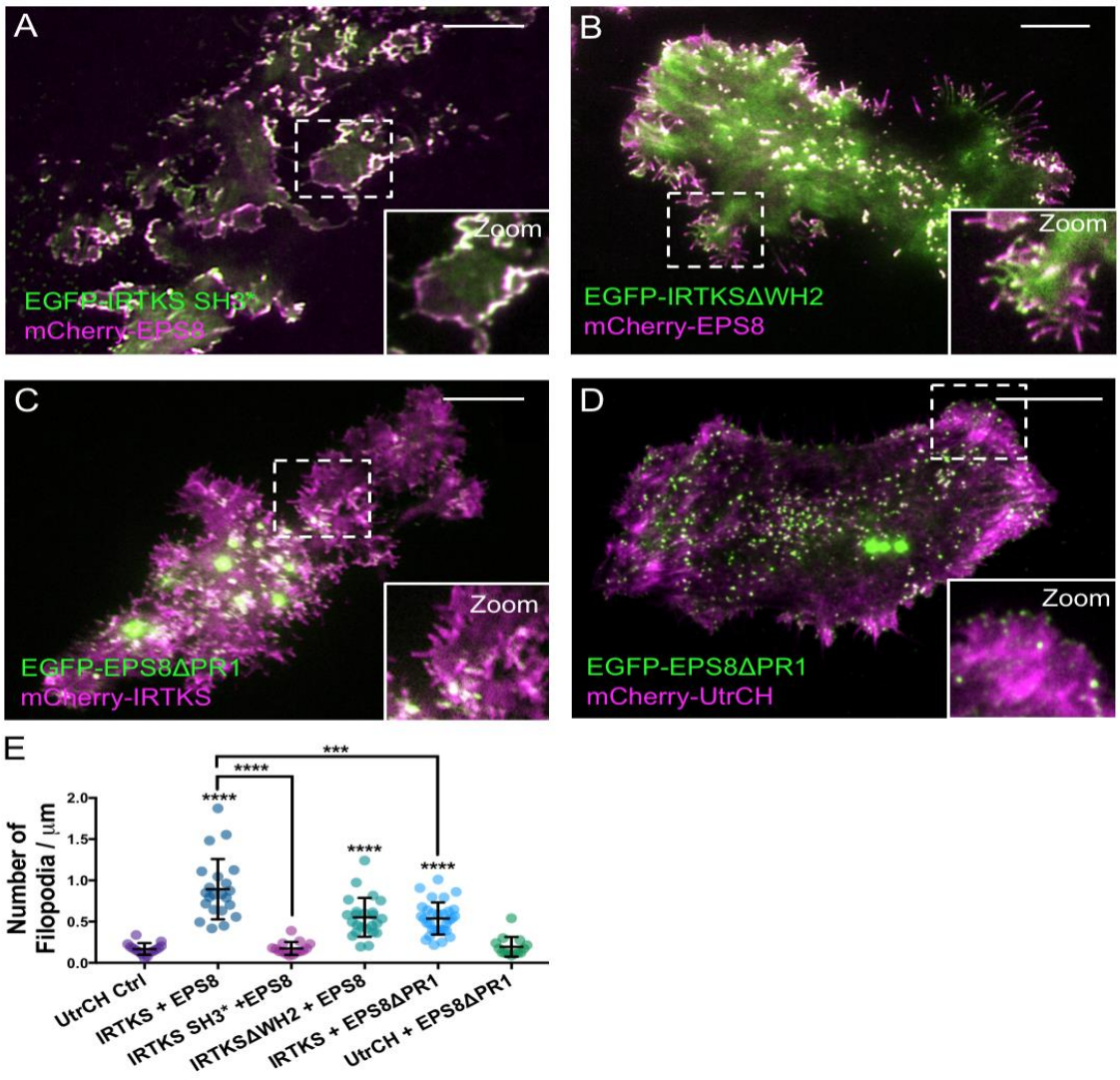

Figure 3-11: Additional characterization of the IRTKS/EPS8 complex in B16F1 Melanoma Cells. (**A-D**) TIRF live-cell imaging of B16F1 melanoma cells expressing either EGFP-IRTKS SH3* (green) and mCherry-EPS8 (magenta) (A), EGFP-IRTKSΔWH2 (green) and mCherry-EPS8 (magenta) (B), or EGFP-EPS8ΔPR1 (green) and mCherry-IRTKS (magenta) (C), and EGFP-EPS8ΔPR1 (green) and mCherry-UtrCH (magenta) (D). Dashed boxes indicate zooms. Scale bars, 10 µm. (**E**) Quantitation of the number of filopodia per µm of cell perimeter in B16F1 melanoma cells from C-E; at least 15 cells/condition. All error bars indicate mean ± SD; all p values calculated using a t test (*p<0.033, **p<0.002, ***p<0.0002, ****p<0.0001).

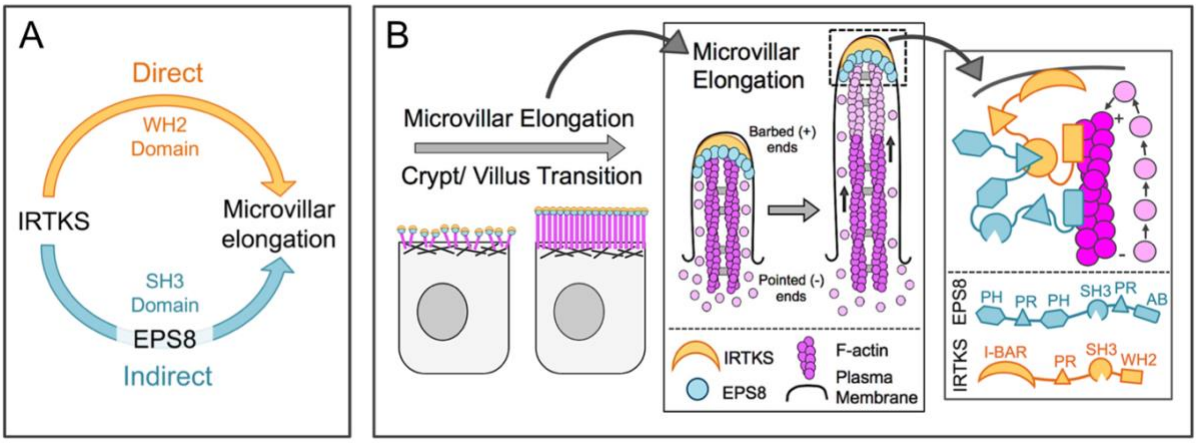

Figure 3-12: Models of IRTKS function in microvillar elongation. (**A**) Two distinct pathways for microvillar elongation: a direct pathway that requires the IRTKS WH2 domain, and a second indirect pathway that uses the IRTKS SH3 domain to recruit to EPS8. (**B**) IRTKS and EPS8 form a microvillar elongation complex at the tips of actively growing microvilli. AB= actin-binding domain. The EPS8 PR1 domain shown binding to the IRTKS SH3 domain is representative, as other PR domains may also have the ability to bind.

Discussion

IRTKS has been studied extensively as a target of EHEC virulence factors (Aitio et al., 2012; Crepin et al., 2010; de Groot et al., 2011; Yi and Goldberg, 2009). EHEC is a Shiga toxin-secreting attaching/effacing (A/E) pathogen (Ho et al., 2013) that colonizes distal small intestine or proximal colon epithelium by effacing microvilli and building adherent 'pedestals' on the apical surface (Licois et al., 1991). To build pedestals, EHEC injects host cells with virulence factors that remodel the actin cytoskeleton (Jarvis and Kaper, 1996). IRTKS is targeted by the virulence factor $EspF_u$ (Campellone et al., 2004), which uses tandem polyproline motifs to bind tightly to the SH3 domain (Aitio et al., 2010). This interaction is notable due to its high affinity (K_D ~500 nM) (Aitio et al., 2010). The resulting apically localized IRTKS-$EspF_u$ complex recruits N-WASP and Arp2/3, which leads to a massive induction of actin assembly and ultimately pedestal formation beneath adherent

EHEC organisms (Campellone et al., 2004; Vingadassalom et al., 2009). The current study may help explain why EHEC evolved to target IRTKS using $EspF_U$ in its pathogenic mechanism. Our findings reveal that, as a tip-targeted resident of apical microvilli, IRTKS is well-positioned and contains the appropriate domains and activities to influence apical actin assembly in response to microbial contact.

The studies presented here focused on elucidating the normal function of IRTKS in the apical domain. We found that IRTKS targets to and tracks the distal tips of growing microvilli (Fig. 3-3B, 3-3C), where the barbed ends of core actin filaments interface with highly curved plasma membrane. Combined with results from our overexpression and loss-of-function experiments, and the demonstrated physical association with the established protrusion elongation factor EPS8 (Croce et al., 2004; Tocchetti et al., 2010), our results indicate IRTKS plays an important role in elongating microvilli. Indeed, IRTKS KD eliminated BB formation in ~50% of the W4 cells assayed (Fig. 3-4K). In cells that were still able to form a BB, IRTKS KD significantly shortened microvilli compared to controls (Fig. 3-4L). Because short microvilli still form in KD cells, IRTKS-driven elongation may involve detection of outwardly curved regions of plasma membrane at some point *after* initiation of microvillar growth.

Our molecular dissection of IRTKS function revealed that the N-terminal I-BAR domain is the primary driver of tip targeting. Deletion of the I-BAR domain completely eliminated targeting to microvillar tips (Fig. 3-4E, 3-5D). The I-BAR domain alone was able to target to microvillar tips, but also exhibited more general plasma membrane labeling (Fig. 3-4F, 3-5E). This suggests that IRTKS probably requires additional motifs or interactions with other factors to focus its enrichment at the distal tips. Indeed, mutation

of the SH3 domain ligand-binding pocket disrupted localization, although some distal tip labeling persisted (Fig. 3-4C, 3-5B). Although it is tempting to speculate that involvement of the SH3 domain in targeting is related to EPS8 binding, IRTKS still localized to microvillar tips in cells lacking EPS8 (Fig. 3-10K).

Structure/function studies revealed that the IRTKS WH2 domain is critical for microvillar elongation. Whereas WH2 domain deletion had no impact on IRTKS localization, overexpression of IRTKSΔWH2 exerted a dominant negative effect on protrusion length (Fig. 3-4D, 3-4G, 3-4H), likely mediated by interactions with endogenous IRTKS. In addition, IRTKS KD phenotypes were only partially rescued by IRTKSΔWH2 (Fig. 3-4K, 3-4L). Exactly how the IRTKS WH2 domain contributes to elongation remains unclear, but WH2 domain-containing proteins in general have been implicated in actin filament nucleation and elongation (Dominguez, 2016). IRTKS is different from many of these other factors in two ways. Whereas most WH2 domain molecules contain multiple copies of this 17-20 amino acid motif arranged in tandem, IRTKS contains only a single WH2 motif at its C-terminus. Moreover, the IRTKS WH2 domain is divergent, containing ‘LRPT’ rather than the conserved ‘LKKV’ motif that typically contributes to monomer binding; IRTKS is also missing canonical hydrophobic residues upstream of this motif (Dominguez, 2016). Despite these distinctions, the IRTKS WH2 domain does bind actin and may prefer filaments over monomers (Millard et al., 2007). Interestingly, the WH2 domain of closely related IRSp53 binds strongly to G-actin despite containing an IRTKS-like ‘LKPT’ motif (Lee et al., 2007). Espin, which functions in the elongation of microvilli and stereocilia (Loomis et al., 2003; Sekerkova et al., 2011; Sekerkova et al., 2004; Zheng et al., 2000), also contains a WH2 domain characterized by ‘LKPT’ (Loomis et al., 2006).

The espin WH2 domain binds to G-actin and may function to increase local monomer concentration at the distal tips, which could promote elongation. Notably, espin-2B exerts its effects on microvillar length without significantly altering F-actin treadmilling rates in microvilli. This is consistent with our FRAP measurements on W4 cells expressing EGFP-β-actin, which revealed IRTKS KD had minimal impact on BB actin turnover (Fig. 3-5H, 3-5I).

Our findings suggest that the IRTKS SH3 domain also contributes to microvillar length control (Fig. 3-4C, 3-4G, & 3-4H), likely through its interaction with EPS8, an established elongation factor that enriches at the tips of protrusions in diverse systems (Croce et al., 2004; Manor et al., 2011; Roffers-Agarwal et al., 2005). Interaction with EPS8 was predicted in previous structural studies as its proline rich motifs are nearly identical to those found in EspF$_U$ peptides that bind IRTKS with high affinity (Aitio et al., 2010). Interestingly, higher cytoplasmic levels of EPS8 were seen with both the IRTKS KD and in cells expressing a variant of EPS8 lacking PR1, a predicted IRTKS binding motif (Fig. 3-8A- 3-8E). Forced targeting of the IRTKS SH3 domain to the mitochondrial surface also recruited EPS8 to these sites (Fig. 3-8F- 3-8G). Thus, we propose that IRTKS and EPS8 form a complex at the tips of microvilli, which stabilizes EPS8 in this compartment (Fig. 3-12). Once at the tips, both IRTKS and EPS8 hold the potential to contribute to core bundle elongation: IRTKS through its WH2 domain, and EPS8 through its actin bundling and capping activities (Disanza et al., 2004; Hertzog et al., 2010)**.** Our findings indicate these represent separable, parallel activities that both depend on IRTKS (Fig. 3-12).

Of note, overexpression of the I-BAR domain alone did not impact microvillar length (Fig. 3-4G). This might seem to contradict early reports suggesting I-BAR domains exhibit actin bundling activity (Bompard et al., 2005; Millard et al., 2007; Yamagishi et al., 2004). Yet our data are consistent with studies on IRSp53 and MIM, which indicate that membrane binding rather than actin filament bundling is the primary function of this domain in cells (Mattila et al., 2007). We note here that our results do not rule out the possibility that the IRTKS I-BAR domain exerts direct effects on membrane mechanical properties that facilitate microvillar elongation (Prevost et al., 2015).

Early models of microvillar growth emphasized the role of F-actin bundling proteins in protrusion assembly (Franck et al., 1990; Friederich et al., 1989). However, more recent studies on a mouse model lacking all three established bundling proteins, fimbrin, villin, and espin, revealed that microvilli still form (Revenu et al., 2012). Our studies highlight new mechanisms that also contribute to this biologically robust process. Future studies must focus on understanding how the IRTKS/EPS8 complex interfaces with known polarity pathways during enterocyte differentiation, and on defining the temporal sequence of molecular recruitment that drives microvillar growth.

Conclusion

Our studies highlight the role of the I-BAR domain-containing protein IRTKS in promoting microvillar elongation. Beyond just understanding the mechanisms of brush border assembly, the localization of IRTKS at microvillar tips during enterocyte differentiation implies that the molecule helps promote protrusion of microvilli. Because IRTKS binds to both PIPs in the membrane through its I-BAR domain and the actin cytoskeleton through

its WH2 domain, it could be a crucial molecule in completing the signaling pathways towards membrane protrusion. Additional studies are needed to determine the exact position of IRTKS in early steps of microvillar growth, and whether it binds and deforms the membrane with its I-BAR domain before or after actin polymerization begins. Moreover, the exact mechanism of EPS8 within this early protrusion pathway should also be determined to define its relationship with IRTKS further. Other future studies should focus on how IRTKS transitions to the base of the brush border in mature villar tissue and whether this is due to additional binding partners or autoinhibition between the PR motif and SH3 domain. Investigating the steps and molecular mechanisms of early microvillar protrusion will further our understanding of how the brush border develops and provide insight into how I-BAR proteins function.

CHAPTER IV

PACSIN2-DEPENDENT APICAL ENDOCYTOSIS REGULATES THE MORPHOLOGY OF EPITHELIAL MICROVILLI

Originally published as:

Postema, M.M., Grega-Larson, N.E., Meenderink, L.M., & Tyska, M.J. (2019) PACSIN2-dependent apical endocytosis regulates the morphology of epithelial microvilli. Molecular Biology of the Cell. *30:* 2515-2526.

Summary

Apical microvilli are critical for the homeostasis of transporting epithelia, yet mechanisms that control the assembly and morphology of these protrusions remain poorly understood. Previous studies in intestinal epithelial cell lines suggested a role for F-BAR domain protein PACSIN2 in normal microvillar assembly. Here we report the phenotype of PACSIN2 KO mice and provide evidence that through its role in promoting apical endocytosis, this molecule functions in controlling microvillar morphology. PACSIN2 KO enterocytes exhibit reduced numbers of microvilli and defects in microvillar ultrastructure, with membranes lifting away from rootlets of core bundles. Dynamin2, a PACSIN2 binding partner, and other endocytic factors were also lost from their normal localization near microvillar rootlets. To determine if loss of endocytic machinery could explain defects in microvillar morphology, we examined the impact of PACSIN2 KD and endocytosis inhibition on live intestinal epithelial cells. These assays revealed that when endocytic

vesicle scission fails, tubules are pulled into the cytoplasm and this, in turn, leads to a membrane lifting phenomenon reminiscent of that observed in PACSIN2 KO brush borders. These findings lead to a new model where inward forces generated by endocytic machinery on the plasma membrane control the membrane wrapping of cell surface protrusions.

Introduction

Apical specializations enable epithelial cells to carry out specific functions including solute uptake and mechano-sensation. In the context of transporting epithelia, the apical surface is occupied by actin bundle-supported microvilli: finger-like protrusions that serve to amplify membrane surface area and maximize solute uptake capacity (Helander and Fandriks, 2014). A well-studied example is found in the intestinal tract where enterocytes, the most abundant epithelial cell type in the gut, provide the sole site of nutrient absorption. Enterocytes build tightly-packed arrays of 1000s of microvilli, known as a brush borders. Microvillar growth and ordered packing take place as enterocytes differentiate, which occurs as they exit stem cell-containing crypt domains and move onto the villus surface (Fath et al., 1990; Specian and Neutra, 1981; van Dongen et al., 1976).

Microvillus formation requires coordination of a variety of activities, including actin filament nucleation, elongation, and bundling, which presumably all occur at the interface with the apical plasma membrane. Nucleation of the actin filaments that comprise core bundles is at least partially controlled by the WH2 domain protein cordon bleu (COBL), which is required for normal brush border assembly in intestinal epithelial cell lines (Grega-Larson et al., 2015; Grega-Larson et al., 2016; Wayt and Bretscher, 2014). COBL

overexpression drives microvillus elongation and also leads to protrusions that are straighter, with higher actin content (Grega-Larson et al., 2015). COBL localizes to microvillar rootlets, which are embedded in a dense sub-apical network of intermediate filaments known as the terminal web (Hirokawa et al., 1982). The actin bundling protein fimbrin also localizes to the terminal web and has been shown to link microvillar actin to keratin-19 in intermediate filament (Grimm-Gunter et al., 2009). Along with fimbrin, two other bundling proteins, villin and espin, stabilize the core bundle in a region-specific manner (Bartles et al., 1998; Bretscher and Weber, 1979, 1980; Mooseker et al., 1980) and may promote elongation by slowing disassembly at the pointed ends (Loomis et al., 2003). Later in differentiation, epithelial-specific protocadherins target to the tips of microvilli to promote their elongation and tight packing (Crawley et al., 2014b; Crawley et al., 2016; Li et al., 2016; Li et al., 2017; Weck et al., 2016; Yu et al., 2017). Such intermicrovillar adhesion allows cells to generate the maximum number of protrusions per unit apical surface area (Pinette et al., 2019).

Another recently identified factor that functions in microvillar growth is the I-BAR (inverse-Bin-Amphiphysin-Rvs) domain-containing protein, insulin receptor tyrosine kinase substrate (IRTKS) (Postema et al., 2018). BAR domains are small, three helix bundles that form curved dimers ~20 nm in length, which in turn form higher order oligomers capable of sensing and inducing membrane curvature (Peter et al., 2004). I-BAR domains exhibit a structural curvature that is well matched to membrane bending away from the cell (Millard et al., 2005), like that found at the distal tips of microvilli. Indeed, IRTKS targets to microvillar tips where it promotes elongation directly by interacting with the core actin bundle, and indirectly through its interactions with epidermal

growth factor receptor pathway substrate 8 (EPS8), another tip targeting factor implicated in the elongation of finger-like protrusions (Croce et al., 2004; Disanza et al., 2006; Manor et al., 2011; Postema et al., 2018; Zampini et al., 2011).

In contrast to the curvature preference of I-BAR domains, F-BAR (Fes-CIP4 homology Bin-amphiphysin-Rvs161/167) motifs prefer binding to membranes that curve in toward the cytoplasm (Frost et al., 2007; Henne et al., 2007; Itoh et al., 2005). Protein kinase C and casein kinase substrate in neurons (PACSIN) family members are F-BAR proteins that have been implicated in a variety of cellular processes, including clathrin-dependent and independent endocytosis, caveolae formation, vesicle trafficking, actin dynamics, and cell migration (Chandrasekaran et al., 2016; de Kreuk et al., 2012; de Kreuk et al., 2011; Hansen et al., 2011; Qualmann and Kelly, 2000; Qualmann et al., 2000; Senju et al., 2011). Although PACSIN2 is widely expressed (Ritter et al., 1999), PACSIN1 exhibits specificity for neural tissues (Plomann et al., 1998), whereas PACSIN3 is expressed in heart and skeletal muscle (Sumoy et al., 2001). All three PACSIN isoforms contain an N-terminal F-BAR domain, along with a C-terminal SH3 domain. Interestingly, previous studies in intestinal epithelial cells revealed that PACSIN2 localizes to the intermicrovillar region in the terminal web, which exhibits a high degree of inward bending and also serves as the site of endocytosis (Grega-Larson et al., 2015). Moreover, through its SH3 domain, PACSIN2 also interacts with several binding partners with roles in actin filament nucleation and endocytosis at the membrane-cytoskeleton interface (Fig 1A). One example is the actin nucleator COBL, which interacts with PACSIN2 in the terminal web. Loss-of-function studies in intestinal epithelial cell lines suggest that PACSIN2 serves to recruit or anchor COBL in this location (Grega-Larson et al., 2015). COBL in

turn uses its multiple WH2 domains to promote elongation of core actin bundles (Grega-Larson et al., 2016). In this context, PACSIN2 is critical for normal microvillar growth as knocking down the molecule in cell culture models leads to defects in brush border assembly (Grega-Larson et al., 2015).

A second SH3 binding partner that links PACSIN2 to actin assembly is N-WASP, a nucleation promoting factor and adaptor protein that activates the ubiquitous branched actin nucleator, ARP2/3 (Padrick and Rosen, 2010). N-WASP interactions with PACSIN2 are believed to physically link the actin cytoskeleton to membranes in processes such as endocytosis (Kessels and Qualmann, 2002, 2006). Yet another link between PACSIN2 and endocytosis is mediated by SH3 domain binding to the large GTPase Dynamin2, which drives vesicle excision from the plasma membrane. PACSIN2 binds to and recruits Dynamin2 in the context of clathrin-mediated endocytosis and the internalization of caveolae (Kessels et al., 2006). Other studies have shown that the F-BAR domain of PACSIN2 is capable of oligomerizing and coating the necks of newly forming vesicles, which likely stabilize these intermediates before excision (Senju and Suetsugu, 2015).

In the present study, we sought to develop our understanding of PACSIN2 function in the epithelial apical domain through the analysis of mice lacking PACSIN2 expression. Ultrastructural studies of tissues from KO animals revealed a plasma membrane lifting phenotype, where core actin bundles are no longer fully enveloped in membrane, and in some cases fuse with adjacent protrusions. Moreover, Dynamin2 and other endocytic factors were lost from their normal localization near the intermicrovillar endocytic region. To determine if the loss of endocytic machinery could explain defects in brush border morphology, we examined the impact of dynamin inhibition and PACSIN2 KD on live

intestinal epithelial cells. We found that when endocytic vesicle scission fails, tubules are pulled into the cytoplasm, and this leads directly to a membrane lifting phenomenon similar to that observed in PACSIN2 KO brush borders. Our findings illuminate a previously unrecognized link between endocytic function and the morphology of the epithelial apical domain, and also suggest that inward forces generated on the plasma membrane by endocytic machinery control the membrane in cell surface protrusions.

Results

PACSIN2 KO disrupts COBL localization

To explore how PACSIN2 contributes to enterocyte apical architecture and brush border assembly *in vivo*, we acquired mice expressing a PACSIN2$^{tm1b(EUCOMM)Hmgu}$ allele from the KOMP resource (Friedel et al., 2007). Tm1b mice are “CREed knockout first” and provide constitutive loss of expression in all tissues. KO of PACSIN2 was confirmed using western blot analysis (Fig. 4-1B). PACSIN2 KO mice did not exhibit gross level phenotypes or defects in growth. Analysis of hematoxylin- and eosin-stained swiss roll sections (Fig. 4-1C,D) and scanning electron microscopy (SEM) of duodenal tissue sections (Fig. 4-1E,F) revealed that PACSIN2 KO tissues were morphologically similar to WT. In frozen sections of WT tissue, PACSIN2 is strongly enriched at the base of the brush border in the terminal web (Fig. 4-1G). However, this labeling is completely lost in KO mice, further confirming loss of expression (Fig. 4-1H). As previous studies in intestinal epithelial cells lines suggest that this F-BAR protein functions in the recruitment of COBL, we next sought to determine if COBL was mislocalized in the absence of PACSIN2. As expected, COBL exhibits high level enrichment in the terminal web of WT tissues (Fig. 4-1I), but this

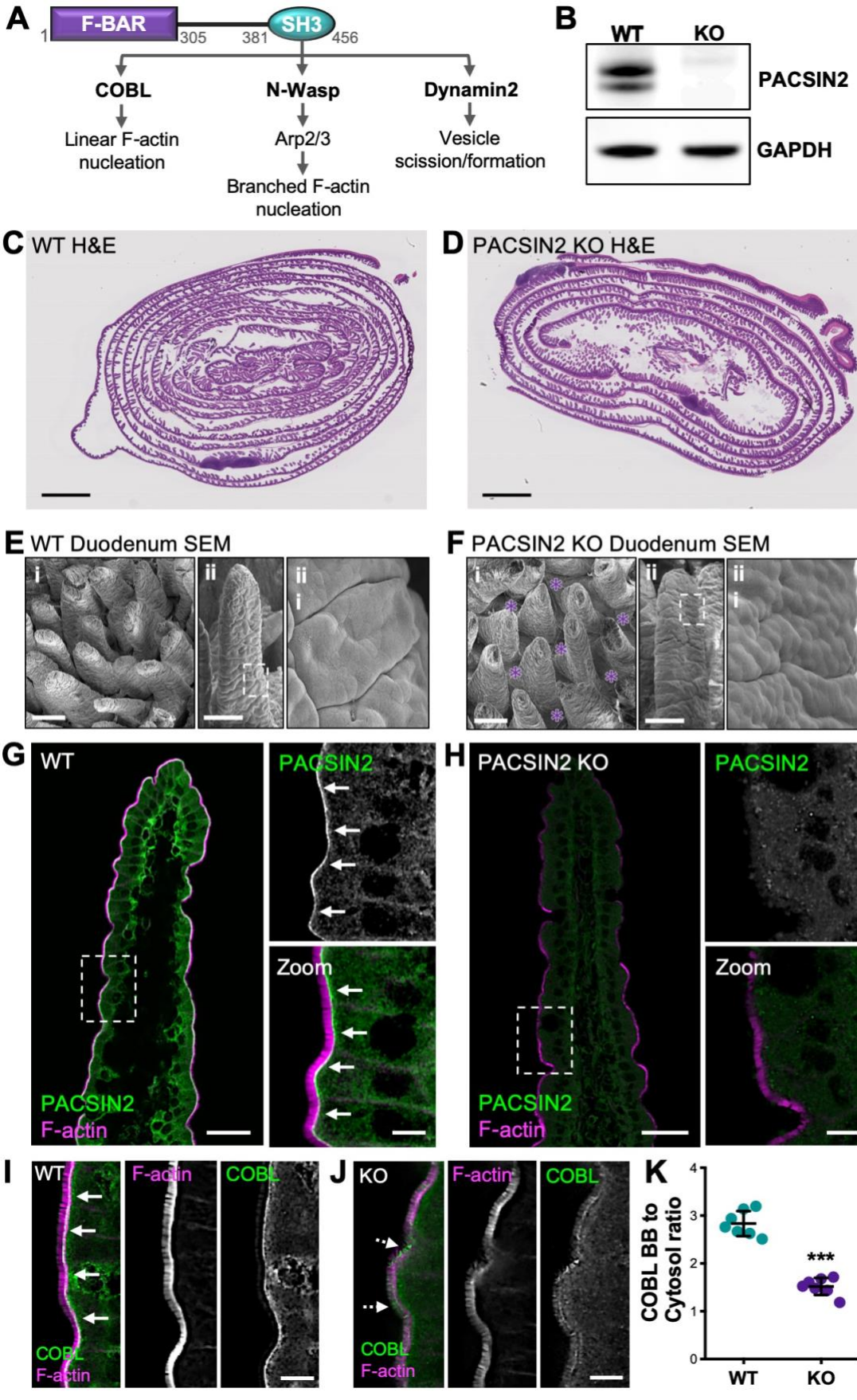
A
F-BAR
SH3
1
305
381
456
COBL
N-Wasp
Dynamin2
Linear F-actin nucleation
Arp2/3
Branched F-actin nucleation
Vesicle scission/formation
B
WT
KO
PACSIN2
GAPDH
C WT H&E
D PACSIN2 KO H&E
E WT Duodenum SEM
F PACSIN2 KO Duodenum SEM
G
WT
PACSIN2
Zoom
PACSIN2
F-actin
H
PACSIN2 KO
PACSIN2
Zoom
PACSIN2
F-actin
I
WT
F-actin
COBL
COBL
F-actin
J
KO
F-actin
COBL
COBL
F-actin
K
COBL BB to Cytosol ratio
***
WT
KO

Figure 4-1: PACSIN2 KO disrupts COBL localization. (A) PACSIN2 domain diagram depicting SH3 binding partners and prospective functions. (B) Western blot of WT and PACSIN2 KO tissue with GAPDH as a loading control. (C, D) H&E-stained swiss roll sections of paraffin-embedded small intestine from WT and PACSIN2 KO mice. Scale bars, 2mm. (E, F) Scanning EM images of intestinal tissue samples from WT (E) and PACSIN2 KO (F) mice. Scale bars, 100 μm for *i*, 100 μm for *ii*, and 10 μm for *iii*; purple asterisks in KO *Bi* indicate bare spaces in the epithelium between adjacent villi. (G, H) Endogenous PACSIN2 (green) and phalloidin (F-actin, magenta) labelling of WT and PACSIN2 KO frozen tissue sections. Arrows highlight PACSIN2 signal at the base of the brush border in WT tissue (G). Scale bars, 50 μm for main panels, 10 μm for zooms. (I, J) Endogenous COBL (green) and phalloidin (magenta) labelling of WT and PACSIN2 KO frozen tissue sections. Solid arrows highlight COBL signal at the base of the brush border in WT tissue (I), dashed arrows highlight mislocalization of COBL signal in KO tissue (J). Scale bars, 10 μm. (K) Quantification of the ratio of COBL brush border (BB) to cytosol signal intensity between the WT and PACSIN2 KO tissue; n = 7 tissue sections per condition. Error bars indicate ± SD; p value was calculated using a t test (***p<0.001).

labeling is significantly perturbed in KO samples (Fig. 4-1J). This point was also confirmed with quantification of brush border to cytosol intensity ratios, which were markedly reduced in KO samples (2.83 ± 0.26 WT vs. 1.52 ± 0.18 KO; Fig. 4-1K). Interestingly, in KO tissues COBL signal also appears redistributed along the microvillar axis (dashed arrows, Fig. 4-1J), suggesting a role for PACSIN2 in anchoring COBL near microvillar rootlets. These results confirm the loss of PACSIN2 in the KO intestinal tissue and are consistent with previous studies indicating that PACSIN2 is needed for efficient targeting of COBL to the apical domain.

Loss of PACSIN2 decreases apical and basolateral F-actin levels

Given that PACSIN2 and its binding partners have been implicated in actin network assembly (Kessels and Qualmann, 2004; Qualmann et al., 2000), we next sought to determine if KO tissues exhibited perturbations in the actin cytoskeleton. Indeed, our initial staining of KO frozen tissue sections (Fig. 4-1H) suggested that apical F-actin levels

(assessed with phalloidin staining) were reduced, especially in the distal regions of villi. To examine this in greater detail, we performed volumetric imaging of whole mounted segments of intestinal tissue stained for F-actin. 3D reconstructions of individual villi revealed several striking defects in KO samples (Fig. 4-2A,B). Levels of F-actin appeared reduced throughout the apical domain, both in the brush border and at the lateral margins of cells (Fig. 4-2A,B). We also noted that the apical surfaces of individual cells exhibited a domed appearance, curving outward towards the lumen (Fig. 4-2B). This phenotype was even more evident when we examined the apical surface of KO tissues using SEM (Fig. 4-1E,F). In higher-resolution tilted 3D projections, KO brush borders demonstrated an apparent thinning of the F-actin signal, with certain regions exhibiting significantly reduced microvillar density relative to WT controls (Fig. 4-2C,E). Line-scans drawn through the single plane images (Fig. 4-2C,E, bottom panels) showed an almost 2-fold decrease in the PACSIN2 KO F-actin signal with several gaps throughout (maximum F-actin peak signal of 4095 for WT vs. 2156 for KO; Fig. 4-2D,F). Further quantification using thresholding on multiple tissue sections also indicated a marked decrease in brush border F-actin intensity in PACSIN2 KO tissues (mean intensity units 1912 $\pm$ 323 for WT vs. 1123 $\pm$ 239 for KO; Fig. 4-2G-I). Together these data indicate that in the absence of PACSIN2, actin polymerization at the apical surface is compromised.

Given the striking reduction of apical F-actin signal observed in PACSIN2 KO brush borders, we also examined F-actin levels in actin networks in other parts of the cell (Fig. 4-2G,H). Mean F-actin intensity values, measured using a threshold that included all cellular structures basolateral to the brush border, were also markedly reduced (127.2

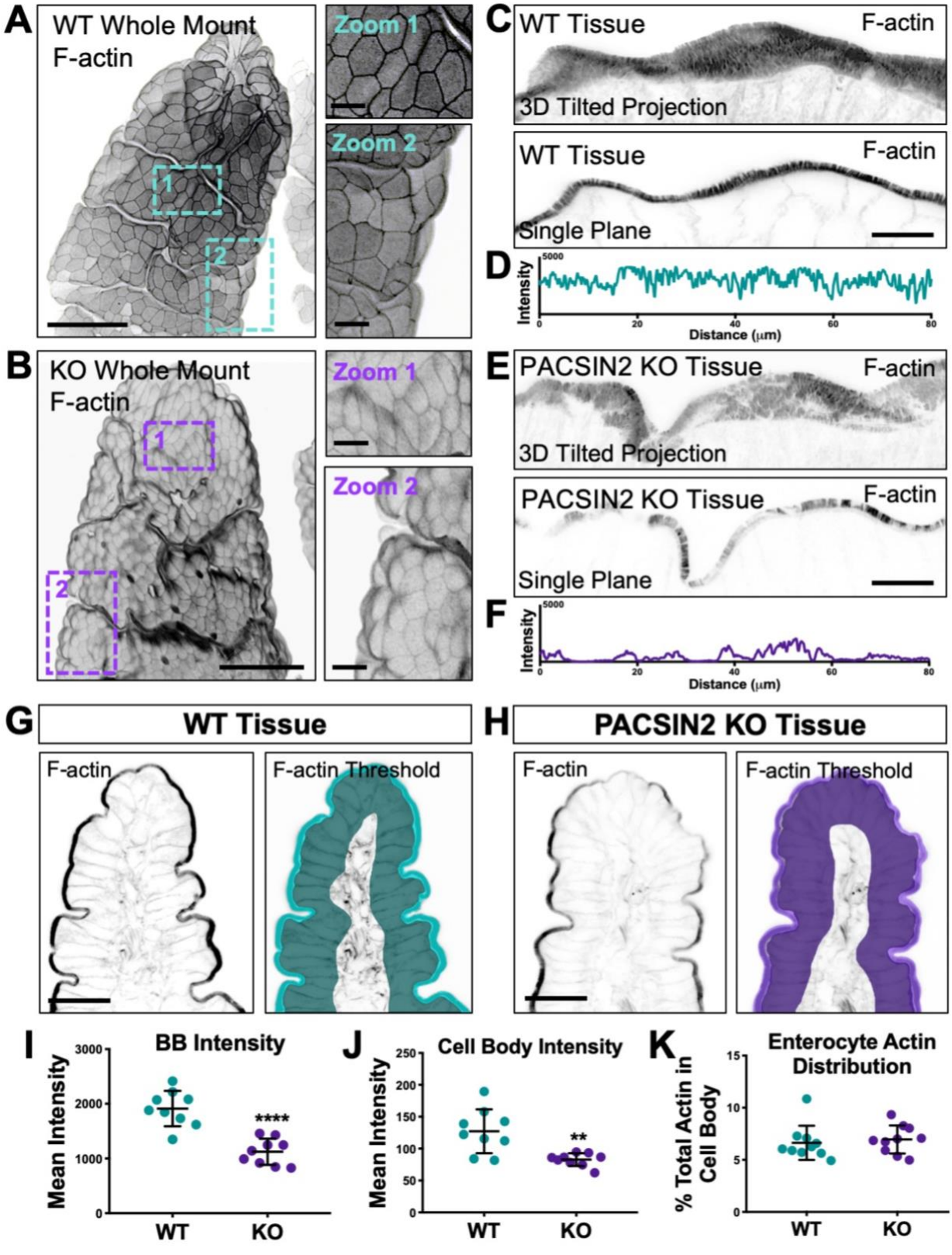
A
WT Whole Mount
F-actin
Zoom 1
Zoom 2
1
2
B
KO Whole Mount
F-actin
Zoom 1
Zoom 2
1
2
C
WT Tissue
F-actin
3D Tilted Projection
WT Tissue
F-actin
Single Plane
D
Intensity
5000
0
20
40
60
80
Distance (μm)
E
PACSIN2 KO Tissue
F-actin
3D Tilted Projection
PACSIN2 KO Tissue
F-actin
Single Plane
F
Intensity
5000
0
20
40
60
80
Distance (μm)
G
WT Tissue
F-actin
F-actin Threshold
H
PACSIN2 KO Tissue
F-actin
F-actin Threshold
I
BB Intensity
Mean Intensity
3000
2000
1000
0
****
WT
KO
J
Cell Body Intensity
Mean Intensity
250
200
150
100
50
0
**
WT
KO
K
Enterocyte Actin Distribution
% Total Actin in Cell Body
15
10
5
0
WT
KO

Figure 4-2: Loss of PACSIN2 decreases apical and basolateral F-actin levels. (A, B) 3D projections of 50 μm sections of WT (A) and PACSIN2 KO (B) whole mount tissue. Zooms highlight differences in cell surface morphology and actin intensity between WT and KO. Actin signal is inverted to simplify visualization; Scale bars, 50 μm for main panels, 10 μm for zooms. **(C, E)** 3D reconstructed volumes of 8 μm sections (top) and single image planes (bottom) of phalloidin stained WT and PASCIN2 KO frozen tissue sections. Scale bars, 25 μm. **(D, F)** Plots of raw 8-bit intensity data from an 80 μm line drawn through the brush border of the single plane images. PACSIN2 KO tissue has ~2-fold decrease in brush border actin intensity. **(G, H)** Phalloidin labelling of WT and PACSIN2 KO frozen tissue sections. Right panels show representative thresholding of brush border and cell body used in quantification (I-K). Scale bars, 50 μm. **(I)** Quantification of brush border (BB) actin intensity between WT and PACSIN2 KO tissue; 9 tissue sections per condition. **(J)** Quantification of cell body actin intensity of WT and PACSIN2 KO tissue; 9 tissue sections per condition. **(K)** Quantification of the percent of actin in the cell body to total actin between WT and PACSIN2 KO; 9 tissue sections per condition. Error bars indicate ± SD; p values were calculated using a t test (**p<0.01, ****p<0.0001).

± 34.5 WT vs. 82.7 ± 10.0 KO; Fig. 4-2J). Interestingly, ratios of brush border/cell body F-actin intensities were unchanged in KO relative to WT samples (Fig. 4-2K), suggesting that the overall distribution of actin polymer was similar. Further analysis of the cell body F-actin signal revealed that most of the intensity is derived from the basolateral margins, at sites of cell-cell contact (Fig. 4-3E-J). Linescan analysis through multiple cells revealed that junctional F-actin levels were also significantly reduced at these sites (Fig. 4-3G,J). Consistent with this, we also noted defects in the localization of tight and adherens junction markers, ZO-1 and E-cadherin; both probes exhibited significantly lower levels of junctional enrichment relative to WT tissue sections (Fig. 4-3K-M). These data indicate that in addition to promoting the growth of microvilli on the apical surface, PACSIN2 also drives the accumulation of F-actin at cell margins, where it promotes accumulation of factors that contribute to cell-cell adhesion.

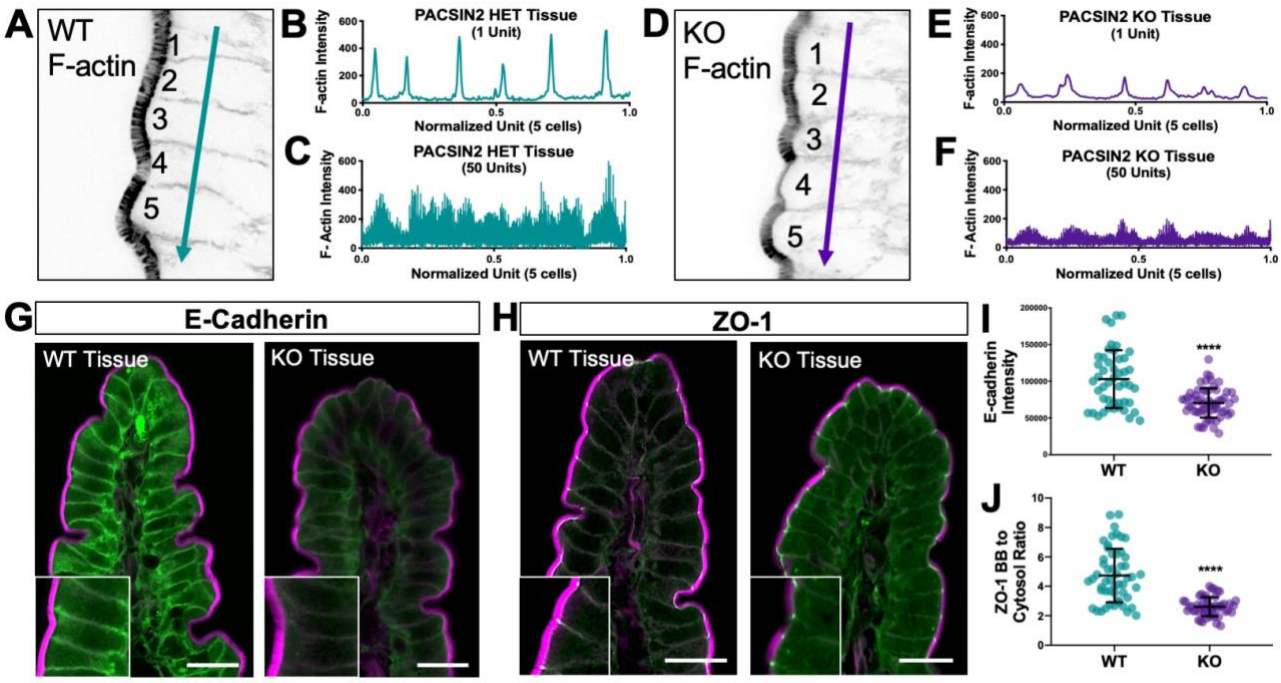

Figure 4-3: Loss of PACSIN2 leads to junctional instability. (A, D) Representative images used in quantification in D, E, G, H; phalloidin stained. **(B, C)** Top, raw intensity data of a line (depicted by teal arrow in C) through 5 total cells in WT tissue, peaks indicate the actin junctional intensity. Bottom, raw intensity data of lines through 5 cells in 50 WT tissue sections, lines have been smoothed for ease of viewing. **(E, F)** Top, raw intensity data of a line (depicted by purple arrow in F) through 5 cells in PACSIN2 KO tissue, peaks indicate the actin junctional intensity. Bottom, raw intensity data of lines through 5 total cells in 50 KO tissue sections, lines have been smoothed for ease of viewing. **(G)** Endogenous E-Cadherin (green) and phalloidin (F-actin, magenta) labelling of WT and PACSIN2 KO frozen tissue sections. Scale bars, 20 μm. **(H)** Endogenous ZO-1 (green) and phalloidin (F-actin, magenta) labelling of WT and PACSIN2 KO frozen tissue sections. Scale bars, 20 μm. **(I)** Quantification of E-Cadherin signal intensity between WT (n = 47 measurements) and PACSIN2 KO (n = 60 measurements). **(J)** Quantification of the ratio of ZO-1 BB to cytosol ratio between WT (n = 52 measurements) and PACSIN2 KO (n = 50 measurements). Error bars indicate ± SD; p value was calculated using a t test (****p<0.0001).

Endocytic machinery is mislocalized in the absence of PACSIN2

In addition to scaffolding factors such as COBL and N-WASP, which promote actin polymerization in the apical and basolateral compartments, PACSIN2 has also been implicated in endocytic function in epithelial cells. Therefore, we sought to determine if

the sub-apical endocytic compartment in the terminal web was disrupted in the absence of PACSIN2. Under normal conditions, Dynamin2 is highly enriched at the base of microvilli in the terminal web, the site of endocytic vesicle formation and fission (Fig. 4-4A). However, upon KO of PACSIN2, this striking band of enrichment is lost (Fig. 4-4B), which is also reflected in a significant decrease of the brush border to cytosol ratio for this signal (2.04 $\pm$ 0.76 WT vs. 1.20 $\pm$ 0.25 KO; Fig. 4-4C). We also stained sections for VAMP4 (vesicle associated membrane protein 4), which has established roles in endo- and exocytosis (Nicholson-Fish et al., 2015; Steegmaier et al., 1999). Similar to Dynamin2, VAMP4 exhibits striking enrichment at the base of the brush border in WT samples (Fig. 4-4D), but marked loss from this region in KO tissues (Fig. 4-4E); brush border to cytosol ratios confirmed the redistribution of VAMP4 in the absence of PACSIN2 (1.86 $\pm$ 0.52 WT vs. 1.31 $\pm$ 0.45 KO; Fig. 4-4F). We also examined the localization of RAB14, another factor implicated in endocytic trafficking at the apical membrane of polarized epithelial cells (Kitt et al., 2008). Once again, this marker demonstrated decreased apical localization in the PACSIN2 KO tissue and a decreased brush border to cytosol ratio (Fig. 4-5). Thus, in addition to disrupting F-actin assembly throughout the enterocyte, these results show that loss of PACSIN2 disrupts the normal enrichment of endocytic machinery including Dynamin2, VAMP4, and RAB14, in the region adjacent to the sub-apical terminal web.

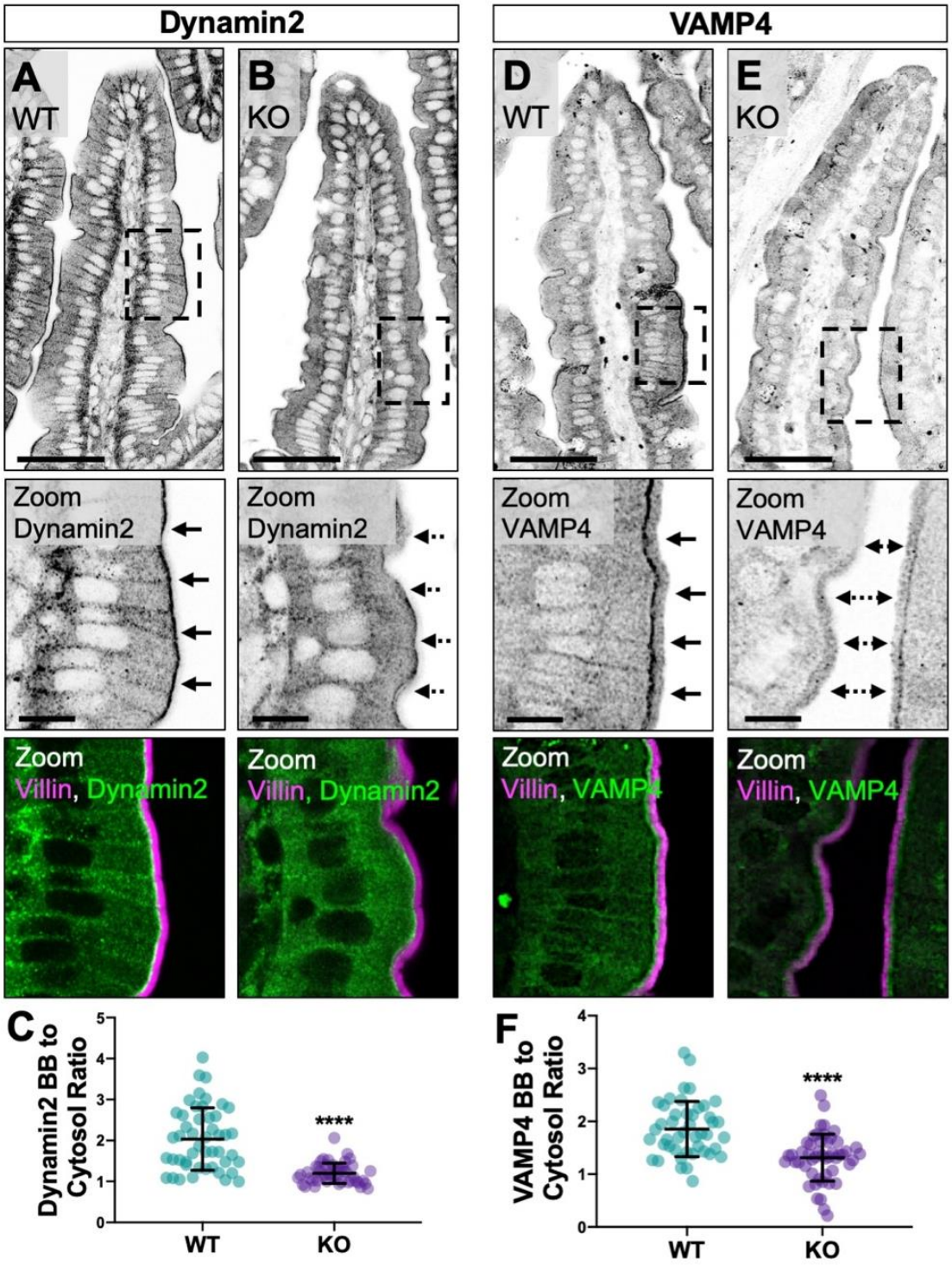

Figure 4-4: Endocytic machinery is mislocalized in the absence of PACSIN2. (A, B) Single confocal image planes of WT and PACSIN2 KO paraffin-embedded tissue sections stained with anti-Villin (magenta) to highlight the brush border and anti-Dynamin2 (green). Solid arrows in zoom panels highlight Dynamin2 signal at the base of the brush border in WT tissue (A), dashed arrows highlight mislocalization of Dynamin2 signal in KO tissue (B); Scale bars, 50 μm for main panel, 10 μm for zoom. **(C)** Quantification of the ratio of

Dynamin2 brush border (BB) to cytosol signal intensity between WT and PACSIN2 KO (n = 48 measurements). **(D, E)** Single confocal image planes of WT and PACSIN2 KO paraffin-embedded tissue sections stained with anti-Villin (magenta) and anti-VAMP4 (green). Solid arrows in zoom panels highlight VAMP4 signal at the base of the brush border in WT tissue (D), dashed arrows highlight mislocalization of VAMP4 signal in KO tissue (E); Scale bars, 50 μm for main panel, 10 μm for zoom. **(F)** Quantification of the ratio of VAMP4 brush border (BB) to cytosol signal intensity between WT (n = 45 measurements) and PACSIN2 KO (n = 50 measurements). Error bars indicate ± SD; p values were calculated using a t test (****p<0.0001).

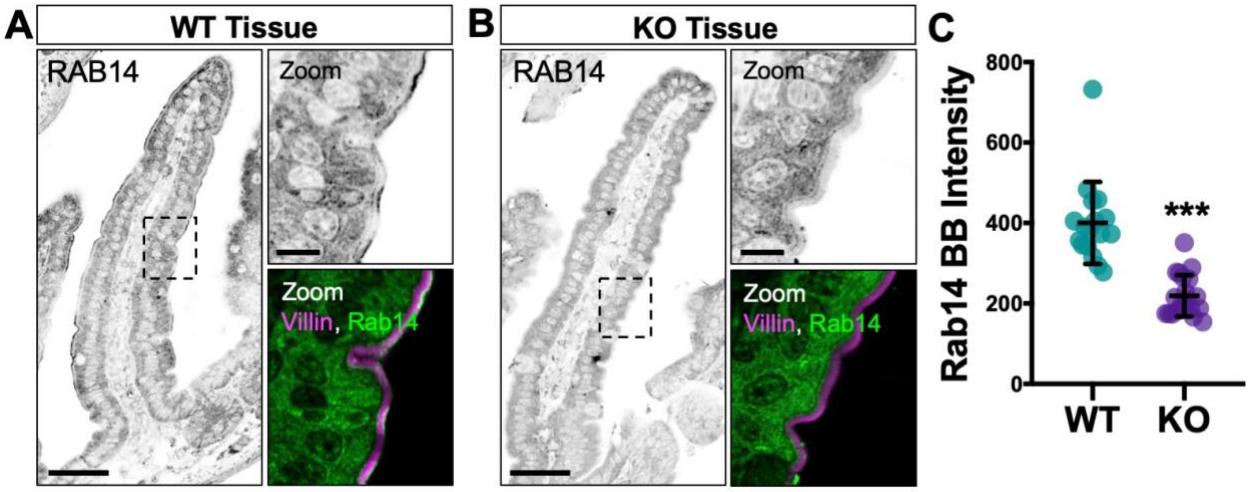

Figure 4-5: Endocytosis marker Rab14 is mislocalized in the KO mouse. (A, B) Single confocal image planes of WT and PACSIN2 KO paraffin-embedded tissue stained with anti-Villin (magenta) to highlight the brush border and anti-Rab14 (green). Signal is inverted for ease of viewing; scale bars, 50 μm in main panels, 10 μm in zoom. **(C)** Quantification of Rab14 signal intensity between WT (n = 17 measurements) and PACSIN2 KO (n = 20 measurements). Error bars indicate ± SD; p value was calculated using a t test (***p<0.001).

Loss of PACSIN2 disrupts microvillar ultrastructure and organization

To understand how loss of PACSIN2 impacts brush border architecture, we employed transmission electron microscopy (TEM) to visualize WT and PACSIN2 KO tissues at the ultrastructural level (Fig. 4-6A,B). TEM imaging of sections parallel to the microvillar axis allowed us to perform detailed morphometry. Strikingly, microvilli in PACSIN2 KO brush

borders were significantly shorter relative to WT (1.93 ± 0.35 μm WT vs. 1.08 ± 0.31 μm KO; Fig. 4-6C). We also found that the extent of membrane coverage, calculated as the percent of core actin bundle enveloped in membrane, was significantly reduced in KO brush borders (80.22 ± 3.16% WT vs. 66.34 ± 7.10% KO; Fig. 4-6B,D). Reduced membrane coverage was also linked to longer rootlets (0.47 ± 0.12 μm WT vs. 0.54 ± 0.15 μm KO; Fig. 6E). In addition, we noted a much more irregular membrane profile in the intermicrovillar region (Fig. 4-6F,G). In KO enterocytes, the straightness of this profile was significantly reduced compared to WT controls (0.87 ± 0.08 μm WT vs. 0.72 ± 0.11 μm KO; Fig. 4-6H). Upon closer inspection of the PACSIN2 KO terminal web, we found an increased number of membrane invaginations, most likely stalled endocytic intermediates, extending into the cytoplasm (1.98 ± 1.07 WT vs. 4.25 ± 1.87 KO; Fig. 4I). Combined with our staining data, these results indicate that loss of PACSIN2 disrupts endocytosis, which is associated with profound effects on microvillar morphology and the extent of membrane coverage.

To further analyze the organization of PACSIN2 KO brush borders, we performed SEM to visualize the apical surface. *En face* images immediately revealed perturbations in microvillar packing, with more apparent free space between adjacent protrusions (Fig. 4-7). We also examined inter-microvillar spacing by calculating nearest neighbor distances (NND) for large numbers of protrusions. KO brush borders exhibited greater NND values with higher variability relative to WT controls (116.9 ± 14.6 nm WT vs. 131.8 ± 18.4 nm KO; Fig. 4-7C). To examine the impact of this increase in NND on the organization of microvilli, we calculated fast Fourier transforms (FFTs) as previously

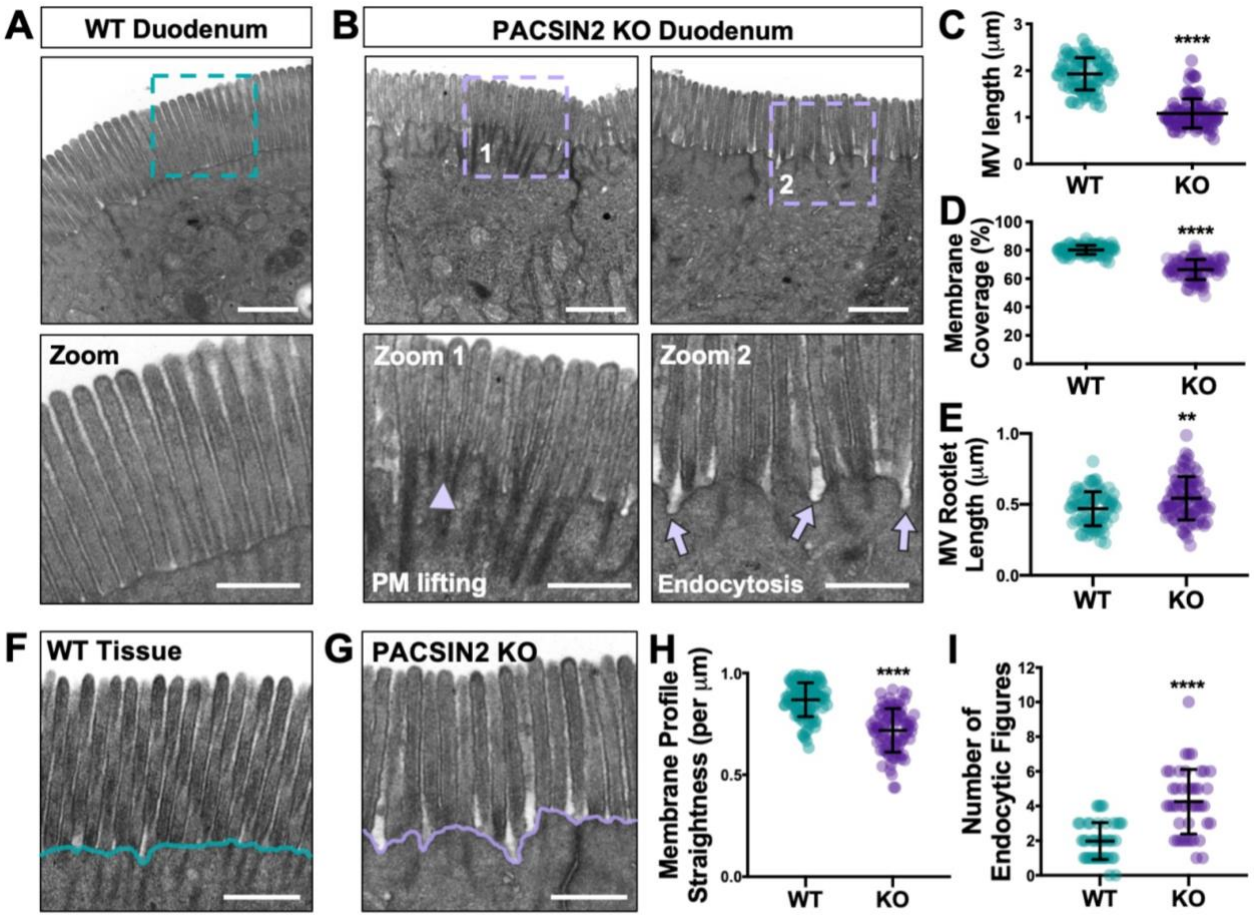

Figure 4-6: Loss of PACSIN2 disrupts microvillar ultrastructure and organization. **(A)** TEM image of a WT brush border in a plane parallel to the microvillar axis; teal dashed box indicates region highlighted in zoom panel below. Scale bar, 1 μm. **(B)** TEM images of PACSIN2 KO brush borders in a plane parallel to the microvillar axis; purple dashed boxes indicate region highlighted in zoom panels below. Arrowhead in zoom 1 highlights membrane lifting, arrows in zoom 2 highlight endocytic events. Scale bars, 1 μm. **(C)** Quantification of microvillar length in WT (n = 82) and KO (n = 102); measurements were selected so that only protrusions with actin cores fully visible along their length were scored. **(D)** Quantification of membrane coverage, the percentage of an actin core wrapped in membrane, in WT (n = 83) and KO (n = 102) microvilli. **(E)** Quantification of microvillar rootlet length in WT (n = 83) and KO (n = 102) microvilli. **(F, G)** Representative images of WT (F) and KO (G) tissue used in the quantification of membrane profile straightness (H); scale bars, 0.5 μm. Teal and purple lines highlight the decreased membrane straightness in KO. **(H)** Quantification of plasma membrane profile straightness at the base of WT (n = 102) and KO (n = 88) microvilli; total membrane length was measured over 1 μm units**. (I)** Quantification of the number of endocytic events, or structures that resemble stalled endocytic intermediates, at the plasma membrane of WT (n = 44 image fields) and KO (n = 44 image fields) brush borders. Error bars indicate ± SD; p values were calculated using a t test (**p<0.01, ****p<0.0001).

described (Pinette et al., 2019). FFTs generated by WT brush borders exhibited the expected hexagonal pattern with six prominent first order spots (Fig. 4-7D). However, FFTs generated from KO brush borders produced a pattern that lacked first order spots, indicating a loss of ordered packing (Fig. 4-7E). These data reveal that microvilli in the PACSIN2 KO brush borders are less densely packed and no longer organized in the hexagonal arrays that are a defining feature of normal enterocyte brush borders.

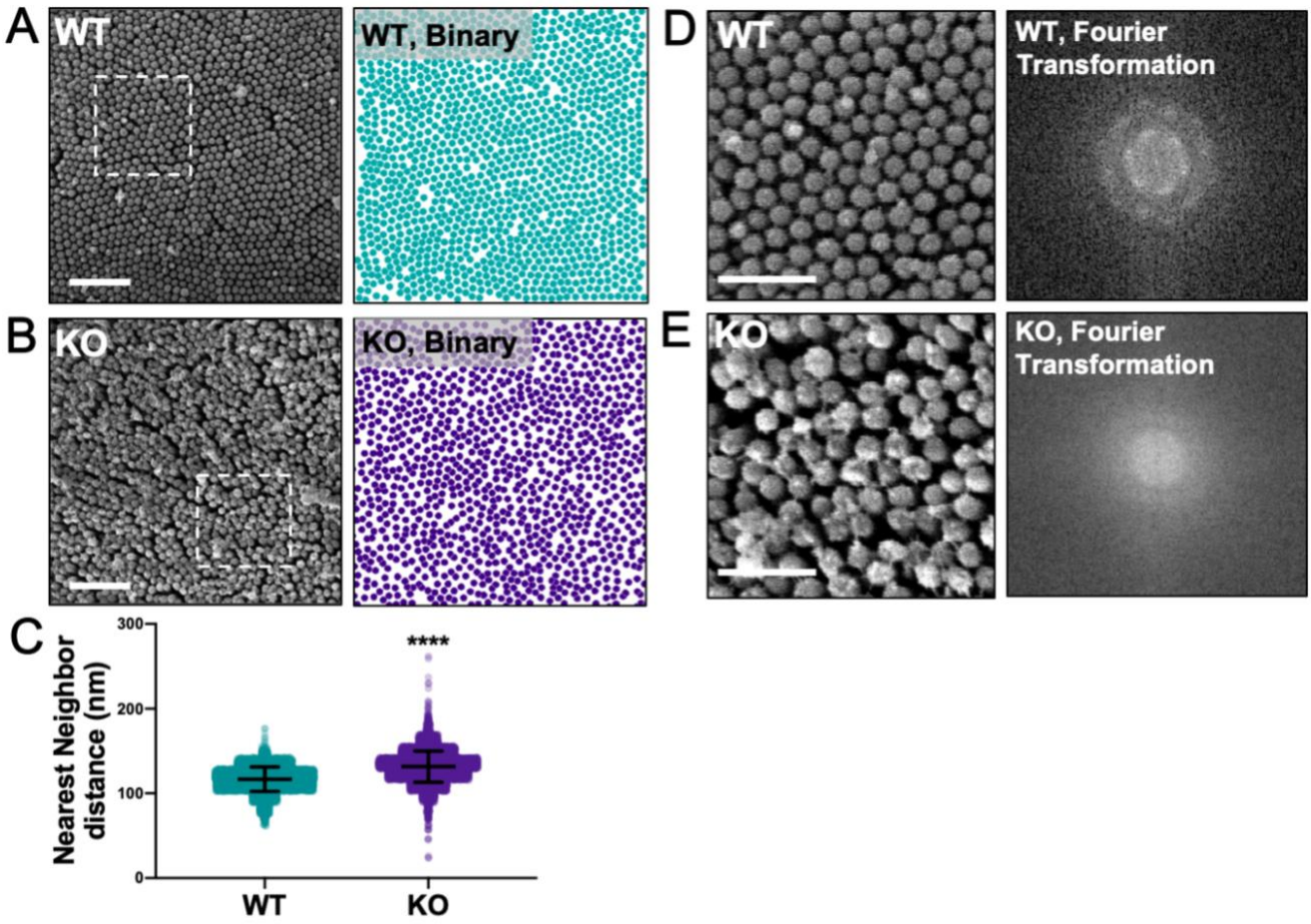

Figure 4-7: Microvillar packing is decreased in the PACSIN2 KO mouse. (A, B) SEM of WT and KO BBs reveal microvillar packing defects. Binary images were used to determine the nearest neighbor distances. **(C)** Quantification of nearest neighbor distance. The mean center to center distance between MV was calculated**;** 6 fields of microvilli per condition. Error bars indicate ± SD; p value was calculated using a t test (****p<0.0001). **(D, E)** 1.5 μm_2 images showing differences in microvillar packing and FFTs from samples.

Inhibition of endocytosis reduces microvillar membrane coverage

Our measurements indicate that under normal conditions, the distal ~80% of a microvillus actin core bundle is enveloped in apical plasma membrane (Fig. 4-6D). In the absence of PACSIN2, membrane coverage is significantly reduced with values that are much more variable across a population of protrusions (Fig. 4-6D). By promoting endocytic activity and/or anchoring the intermicrovillar membrane to the actin cytoskeleton, PACSIN2 could play a direct role in controlling the extent of microvillar membrane coverage. Because mechanisms that control microvillar membrane coverage remain poorly defined, we sought to test this hypothesis using the Ls174T-W4 (W4) intestinal epithelial cell culture model, which has been engineered to form microvilli upon exposure to doxycycline (Baas et al., 2004). Similar to WT intestinal tissue, W4 cells demonstrate localization of PACSIN2 and Dynamin2 in the terminal web (Fig. 4-9A,B).

We first sought to determine if PACSIN2 KD in W4 cells generated a phenotype similar to what we observed with PACSIN2 KO mouse intestinal tissues. W4 cells transduced with scramble control shRNA or shRNA targeting PACSIN2 were fixed and stained to label the plasma membrane and underlying actin cytoskeleton, and then imaged using super-resolution structured illumination microscopy (SIM). KD of PACSIN2 significantly decreased microvillar membrane coverage relative to scramble controls ($78.3 \pm 8.6\%$ KD vs. $89.1 \pm 6.2\%$ SCR; Fig. 4-8A-C). We also imaged PACSIN2 KD W4 cells live using spinning disk confocal microscopy (SDCM). Remarkably, time-lapse acquisitions revealed the formation of long aberrant membrane tubules,

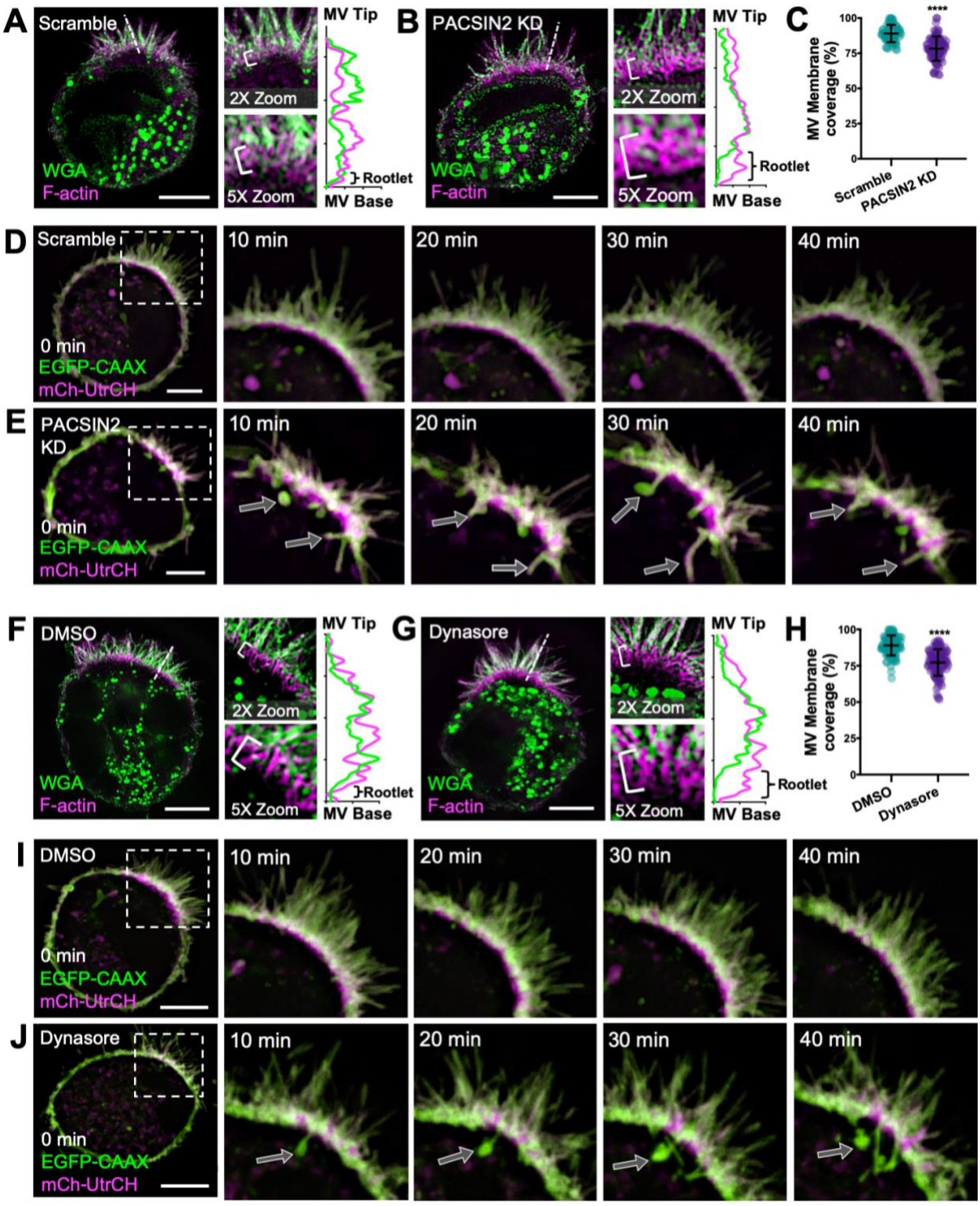

Figure 4-8: Inhibition of endocytosis reduces microvillar membrane coverage. (A, B) SIM projections of scramble control (A) and PACSIN2 KD (B) W4 cells stained for WGA (membrane, green) and phalloidin (magenta). Brackets in zoom panels indicate

actin rootlet lengths. Dashed lines denote where line scans were drawn through a single microvillus to show increased actin rootlet length; membrane (green), actin (magenta). Scale bars, 5 μm. **(C)** Quantification of microvillar membrane coverage; scramble n = 77 microvilli from 10 cells; PACSIN2 KD n = 88 microvilli from 11 cells. **(D, E)** Montages of scramble control and PACSIN2 KD W4 cells expressing EGFP-CAAX box (last 10aa of the GTPase HRas; membrane, green) and mCherry-UtrCH (F-actin, magenta). Arrows in the PACSIN2 KD cell (E) indicate membrane tubules forming into the cytosol. Scale bars, 5 μm. **(F, G)** SIM projections of DMSO control (F) and 80 μM Dynasore (G) treated W4 cells stained for WGA (membrane, green) and phalloidin (magenta). Brackets in zoom panels indicate actin rootlet lengths. Dashed lines denote where line scans were drawn to show increased actin rootlet length; membrane (green), actin (magenta). Scale bars, 5 μm. **(H)** Quantification of microvillar membrane coverage; DMSO n = 104 microvilli from 13 cells; Dynasore n = 105 microvilli from 12 cells. **(I, J)** Montages of DMSO control and 80 μM Dynasore treated W4 cells expressing EGFP-CAAX box (membrane, green) and mCherry-UtrCH (F-actin, magenta). Arrows in the Dynasore treated cell (J) indicate membrane tubules forming into the cytosol. Scale bars, 5 μm. Error bars indicate ± SD; p values were calculated using a t test (****p<0.0001).

presumably stalled endocytic intermediates, which originated in the intermicrovillar region (Fig. 4-8E). Coincident with the formation of these tubules, we noted significant apical membrane lifting, which exposed the rootlets of adjacent microvillar core actin bundles, in a manner that was strikingly reminiscent of membrane coverage perturbations observed in PACSIN2 KO brush borders (Fig. 4-6). Thus, in terms of the microvillar membrane coverage, PACSIN2 KD in W4 cells phenocopies the defects observed in brush borders from PACSIN2 KO mice.

We next set out to determine if the microvillar membrane coverage defects observed in PACSIN2 KO tissues and KD W4 cells were due specifically to perturbations in endocytic activity. For these experiments, we exposed differentiating W4 cells to Dynasore, a small molecule inhibitor of the GTPase domain of Dynamin2 that is expected to prevent the scission of endocytic vesicles from the apical membrane. Dynasore-treated W4 cells were fixed and stained to visualize the actin cytoskeleton and plasma

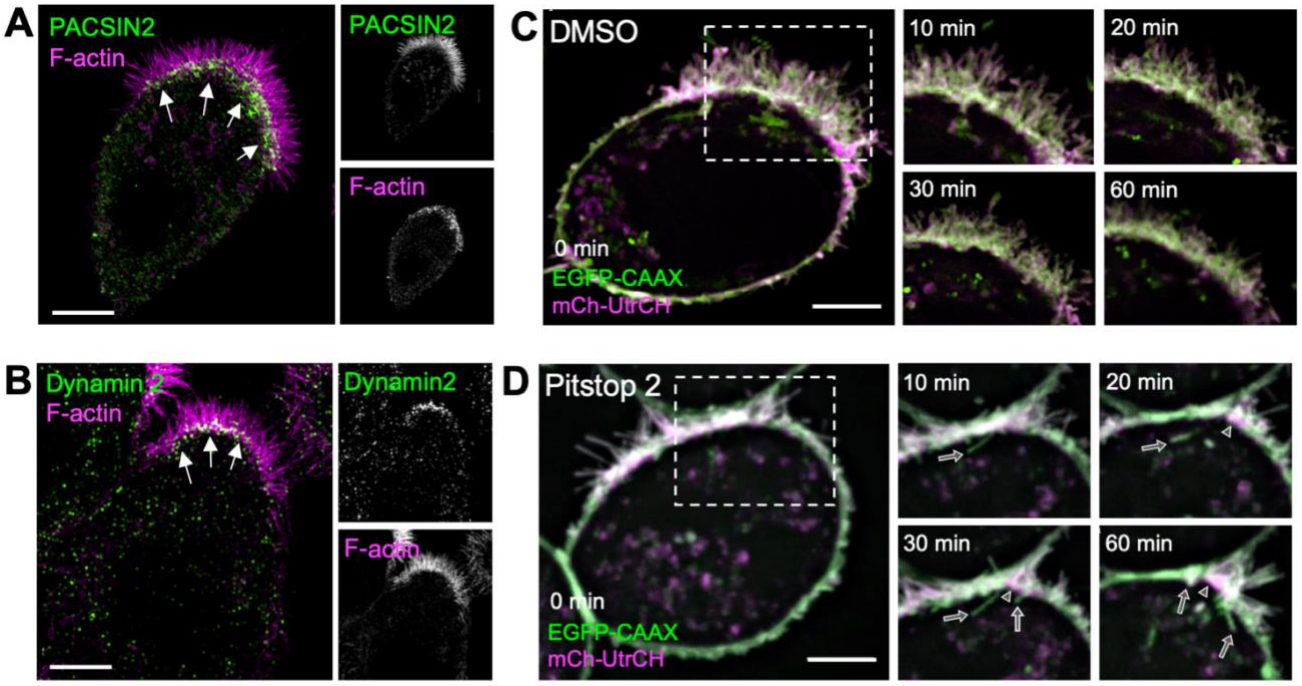

Figure 4-9: Pitstop2 inhibits endocytosis in W4 cells. (A) SIM projection of a W4 cell showing endogenous PACSIN2 (green) and stained with phalloidin (magenta). Arrows point to PACSIN2 puncta at the base of the brush border. **(B)** SIM projection of a W4 cell showing endogenous Dynamin2 (green) and stained with phalloidin (magenta). Arrows point to Dynamin2 puncta at the base of the brush border. **(C, D)** Montages of DMSO control and 30 μM Pitstop 2 treated W4 cell expressing EGFP-CAAX box (membrane, green) and mCherry-UtrCH (F-actin, magenta). Arrows in Pitstop 2 cell (D) indicate membrane tubules forming into the cytosol, arrowheads indicate membrane lifting. Scale bars, 5 μm.

membrane, and then imaged using SIM. Remarkably, exposure to Dynasore decreased microvillar membrane coverage significantly relative to control DMSO-treated cells (77.2 ± 9.1% Dynasore vs. 89.0 ± 6.9% DMSO; Fig. 4-8F-H). We also used SDCM to image the impact of Dynasore treatment on live W4 cells. Similar to that observed in PACSIN2 KD W4 cells, we noted the formation of long aberrant membrane tubules, which again originated in the intermicrovillar region (Fig. 4-8J). The formation of these tubules also coincided with significant membrane lifting and exposure of microvillar core bundle rootlets (Fig. 5J). We verified this effect using a second inhibitor of endocytosis, Pitstop

2, which generated similar aberrant tubule formation and membrane lifting (Fig. 4-9D). Together, these findings uncover a previously unrecognized link between PACSIN2-dependent endocytic activity and the extent of microvillar membrane coverage. These data further suggest that inward forces on the apical membrane, normally generated by endocytic machinery, serve to control microvillar morphology.

Discussion

PACSIN family proteins have long been implicated in the regulation of actin assembly in the context of membrane deformation during endocytosis and vesicle formation. Indeed, in the initial report, PACSIN1 (primarily expressed in neural tissues) co-immunoprecipitated with synaptic vesicle endocytic factors including dynamin, synaptojanin, and synapsin-1, as well as N-WASP, an actin nucleation promoting factor that activates the ARP2/3 complex (Qualmann et al., 1999). All of these interactions were mediated through the PACSIN1 C-terminal SH3 domain (Qualmann et al., 1999). During endocytosis, PACSINs are believed to recruit N-WASP, which in turn targets ARP2/3 to generate bursts of actin filament polymerization in the space between the plasma membrane and nascent budding vesicles. Combined with activity of the Dynamin GTPase, which constricts the necks of forming vesicles, these bursts of actin polymerization likely generate additional mechanical force for efficient vesicle scission (Kessels and Qualmann, 2002, 2004). Although PACSINs have been implicated in various forms of endocytosis, including activity dependent bulk endocytosis (ADBE) and clathrin-mediated endocytosis (Qualmann and Kelly, 2000), PACSIN2 has more recently been implicated in caveolar endocytosis, where it binds to the necks of nascent caveolae

and recruits Dynamin2 to promote vesicle scission (Hansen et al., 2011; Senju et al., 2011; Senju and Suetsugu, 2015). In support of an endocytic role in transporting epithelia, previous studies localized PACSIN2 to the sub-apical terminal web region of native enterocytes in the mouse small intestine and human W4 cells in culture (Grega-Larson et al., 2015). In the terminal web, endocytic vesicles are formed from the inwardly curving membrane found between neighboring microvilli (Michael Danielsen and Hansen, 2016). Indeed, SIM imaging of differentiated W4 cells revealed robust PACSIN2 localization in the intermicrovillar region, immediately between adjacent core actin bundles (Grega-Larson et al., 2015). In the present study, we found that markers of endocytosis which are normally enriched in the terminal web, including Dynamin2, VAMP4, and RAB14, were also lost from this region in the absence of PACSIN2. Together, all of these data establish a role for PACSIN2 in the normal targeting of endocytic machinery to the sub-apical compartment.

In addition to a role in apical endocytic vesicle formation, PACSIN2 was also found to play a role in recruiting the linear actin nucleator, COBL, to the terminal web. In the W4 cell culture model, COBL loss-of-function impairs brush border assembly, whereas overexpression promotes the formation of microvillar actin cores in a manner that depends on the number WH2 domains (Grega-Larson et al., 2015; Grega-Larson et al., 2016). COBL is also recruited to the apex of epithelial cells coincident with the earliest events in brush border assembly (Grega-Larson et al., 2015). Consistent with its role in targeting COBL to the terminal web, we found significantly lower levels of COBL at the base of the brush border in PACSIN2 KO tissues. PACSIN2 KO enterocytes also exhibited reduced apical actin levels as assessed with F-actin reporter, phalloidin (Fig. 4-

2). Confocal volume projections showed a clear thinning of brush border F-actin signal, with reduced microvillar density and regions that appeared to lack microvilli completely (Fig. 4-2C,E). In the ultrastructural analysis of KO tissues, we also noted a significant decrease in microvillar length (Fig. 4-6C). Together these findings suggest that KO of PACSIN2, and subsequent loss of COBL from the terminal web, impairs the production of actin filaments that form microvillar actin core bundles.

Remarkably, measurements of phalloidin intensity from other parts of PACSIN2 KO enterocytes revealed lower levels of F-actin, although the relative ratio of apical/cell body F-actin signal remained unchanged in response to PACSIN2 KO (Fig. 4-2K). Because most of the cell body signal derives from the basolateral margins, we propose that these perturbations are induced by loss of N-WASP stimulated ARP2/3 activity at the basolateral cortex. In support of this, previous studies showed that inactivation of ARP2, a component of the ARP2/3 complex, decreased actin polymerization and impairs the morphology and stability of epithelial adherens junctions (Tang and Brieher, 2012; Yamazaki et al., 2007). Inhibition of actin polymerization also impairs adherens junction reassembly and reduces E-cadherin enrichment (Ivanov et al., 2005a; Ivanov et al., 2005b; Kovacs et al., 2011). Interestingly, in our studies, the loss of junctional actin correlates with the loss of ZO-1 and E-Cadherin signal in the PACSIN2 KO mouse (Fig. 4-9), indicating a disruption in normal junctional stability and architecture.

Perhaps the most unexpected finding from the current investigation was the striking perturbation in microvillar ultrastructure in PACSIN2 KO brush borders. In PACSIN2 KO brush borders, we observed a significant decrease in microvillar length and the extent of membrane coverage, i.e. the fraction of core actin bundle encapsulated in

plasma membrane. These changes were also accompanied by a corresponding increase in the length of exposed rootlet. How does loss of PACSIN2 impact microvillar structure and membrane coverage? While it is known that membrane-cytoskeleton linkers, such as Myo1a and Ezrin, stabilize physical contact between the plasma membrane and the underlying actin core, factors that control the extent of membrane coverage are poorly understood. A clue to the mechanism might come from our observation of a higher frequency of membrane invaginations originating from the intermicrovillar region in PACSIN2 KO brush borders. Because PACSIN2 and its binding partners (e.g. Dynamin) normally stimulate vesicle scission at these sites, the elongated invaginations that extend through the terminal web are most likely stalled endocytic structures, an interpretation consistent with their tubular morphology. Indeed, PACSIN2 KD in cultured cells has been shown to generate elongated caveolae (Senju et al., 2011). If the entire apical membrane is composed of a single continuous surface, the formation of exaggerated tubules in the terminal web would directly reduce the amount of membrane material available for encapsulating microvilli and thus, compromise the extent of membrane coverage. To test this possibility more directly, we modeled the defects observed in PACSIN2 KO tissues in the W4 intestinal epithelial cell line. PACSIN2 KD in this context also lead to reduced membrane coverage of microvilli. Strikingly, we also observed that the inward pulling of exaggerated tubules temporally coincides with loss of membrane coverage on microvilli immediately adjacent to these sites. Because we were able to phenocopy these events with two distinct inhibitors of endocytosis, we conclude that the exaggerated tubules observed in PACSIN2 KO and PACSIN2 KD cells are in fact stalled endocytic

intermediates. Together our findings highlight a mechanistic link between sub-apical endocytic activity and the membrane coverage of apical microvilli.

Interestingly, a role for inward pulling forces on the apical plasma membrane in shaping finger-like protrusions has been highlighted in previous studies of the pointed-end directed motor, MYO6. MYO6 localizes to the terminal web where it interacts with endocytic machinery near the pointed-ends of microvillar core actin bundles, including DAB2, and GIPC (Tumbarello et al., 2013). In *Snell's Waltzer* mice, which lack functional MYO6, inner ear hair cells exhibit a membrane lifting phenotype similar what we observe in PACSIN2 KO brush borders (Self et al., 1999). These cells also manifest with fused or coalesced protrusions, where multiple core bundles appear to be enveloped in a single tubule of plasma membrane. Later studies with the same model system revealed similar phenomena in the enterocyte brush border, with marked decreases in the membrane coverage of core actin bundles and more general disorder in the terminal web (Hegan et al., 2012). In combination with the data we present here, these studies lead to a model whereby the formation and steady-state morphology of finger-like protrusions such as microvilli and stereocilia, are controlled by a balance of outward and inward mechanical forces that impinge on the plasma membrane. PACSIN2 likely limits these forces by promoting the budding and scission of endocytic vesicles from the intermicrovillar membrane. Whether PACSIN2 functions in the same pathway as MYO6 is not known, but functional links between these two factors should be the focus of future studies.

Conclusion

The studies here specify a role for the F-BAR domain-containing protein PACSIN2 in controlling the membrane coverage of enterocyte microvilli. Linking the endocytosis between microvilli to the membrane forces that control microvillar morphology is a novel concept. This shows that PACSIN2 is playing dual roles in the brush border, and that beyond its localization to the microvillar base and recruitment of COBL, PACSIN2 helps promote apical endocytosis. Because PACSIN2 binds to PIPs in the membrane through its F-BAR domain and both COBL and Dynamin2 through its SH3 domain, it is a crucial molecule in both microvillar growth and maintenance. Additional studies are needed to determine the type of endocytosis that PACSIN2 facilitates at the apical domain and whether it is clathrin-dependent, caveolae, or a mix of the two. As PACSIN2 has been shown to bind to Dynamin2 in multiple forms of endocytic vesicles, it is possible both of these two types of endocytosis occur in enterocytes. Other future studies should focus on the relationship between PACSIN2 and Dynamin2 at the apical domain and whether PACSIN2 is necessary to recruit in Dynamin2 directly, or if it is just necessary to stabilize the neck of budding vesicles for Dynamin2 to bind. Investigating the molecular mechanisms of PACSIN2 in endocytosis and how it controls the morphology of stable microvilli on the villar domain will further our understanding of brush border maintenance and the many roles of F-BAR domain-containing proteins.

CHAPTER V

FUTURE DIRECTIONS AND CONCLUSION

Function of IRTKS *in vivo*

IRTKS localizes to the tips of growing microvilli and, along with the actin regulatory protein EPS8, is required for microvillar growth and elongation in the intestinal crypt domain. Knocking down IRTKS in W4 cells led to a reduction in cells able to build a brush border (Fig. 3-4K) and reduced microvillar length (Fig. 3-4L); indicating that the molecule is necessary for complete brush border assembly. While these KD studies provided insight into what happens to microvilli when IRTKS is lost, the shRNA used only eliminated ~85% of total IRTKS protein expression. Thus, we do not know definitively if the presence of the reduced brush borders and shorter microvilli is due to compensatory pathways of other brush border proteins, or the result of low levels of IRTKS still present in the system. There was also an apparent mosaicism to the KD, with the amount of residual IRTKS expression in the W4 cells correlating to the degree of brush border formation. This made it hard to adequately determine the full effect of from losing IRTKS on microvillar growth. Also, as the W4 cells used in the study are thought to exist in a perpetually undifferentiated state, no insight into the effect loss of IRTKS has on mature brush borders could be gained from the data. Therefore, characterization of an IRTKS KO mouse will help us determine further roles for the molecule and whether it is a necessary component of brush border assembly *in vivo*.

Ultrastructural analysis of IRTKS KO tissue

Here, we provide preliminary characterization of mice that are homozygous KO for the IRTKS gene using scanning (SEM) and transmission electron microscopy (TEM). In SEM images of the IRTKS KO mice, the villi appear to be of a similar size and shape as the WT control villi (Fig. 5-1A, D), and there is no increased space between adjacent villi as has been observed in KO mice of other brush border molecules (Pinette et al., 2019; Postema et al., 2019). There also does not appear to be any extreme packing discrepancies in the knockout microvilli (Fig. 5-1C, F). However, there were areas around the base of KO villi where the microvilli appeared more disorganized than in WT tissue (Fig. 5-1I), which should be investigated further in future SEM tissue preps. Interestingly, one thing observed in many of the IRTKS KO images was increased vesicular structures at the tips of microvilli (5-1 G, H) which could result from abnormalities in microvillar actin cores. Thus, more data needs to be collected before a definitive conclusion can be made on whether or not the IRTKS microvilli have reduced packing.

TEM was performed on the IRTKS KO mouse for characterization of the microvillar actin cores. The TEM images did not reveal any organizational issues in the IRTKS KO microvilli when they were viewed in a plane parallel to the actin core (Fig. 5-2B). The KO microvilli did appear to be slightly shorter than WT and were quantified by measuring the length of membrane- bound actin cores (Fig. 5-2C). However, as only one round of tissue prep from 2 KO and 2 WT mice was performed, no statistical analysis can be completed on the data at present. Orthogonal cross sections through microvilli did appear to show differences in the number and packing (Fig. 5-2D-I), therefore fast Fourier transforms

(FFTs) were calculated as in Chapter IV (Fig. 4-7D, E) that suggest the KO microvilli are more disorganized than WT (Fig. 5-2F, I).

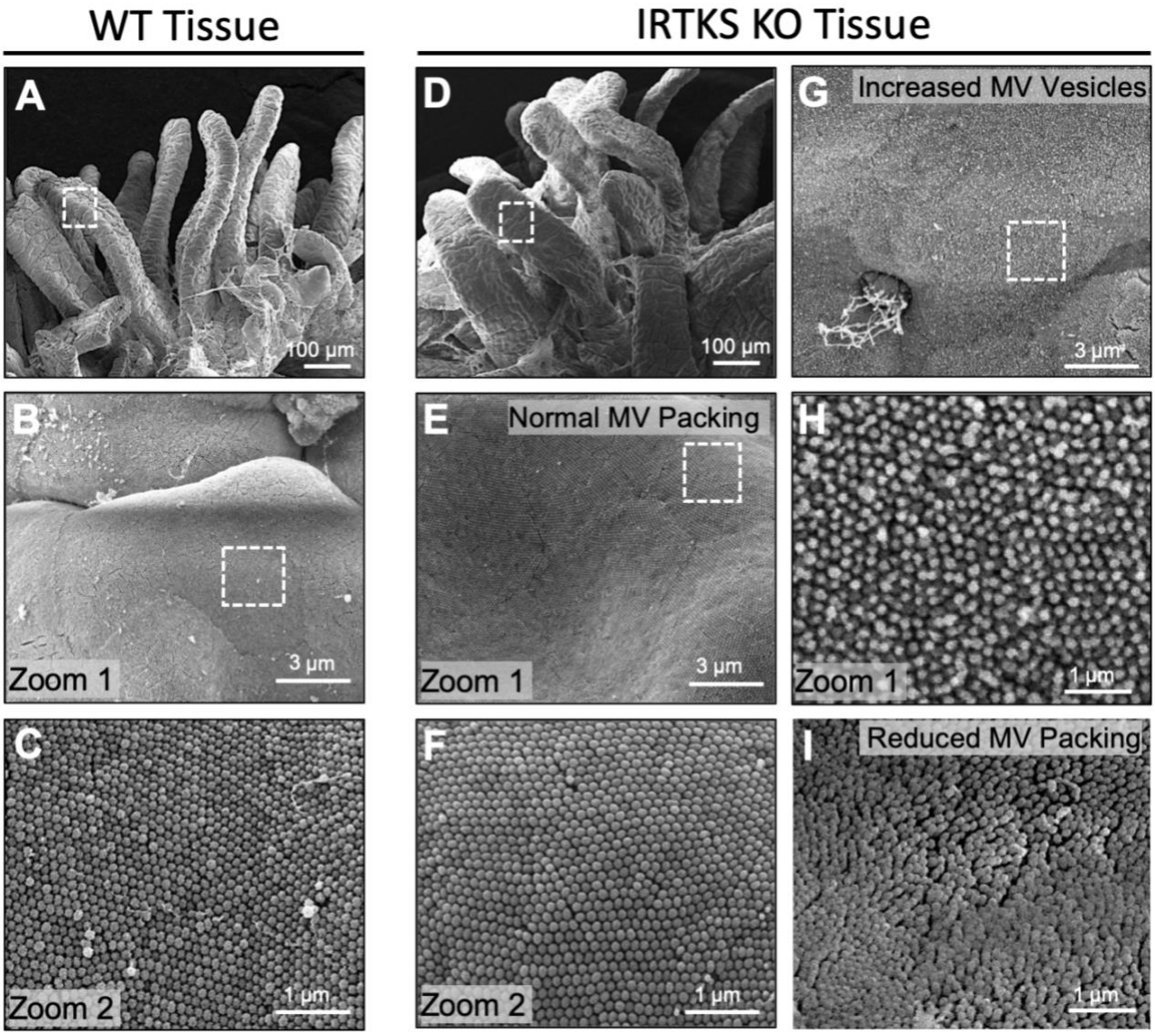

Figure 5-1: Preliminary SEM of the IRTKS KO mouse. (A-C) SEM images WT Intestinal duodenal tissue starting with whole villus sections (A) with increasing zooms of microvilli. **(D-F) S**EM images IRTKS KO Intestinal duodenal tissue starting with whole villus sections (D) with increasing brush border zooms. **(G, H)** IRTKS KO brush borders appear to have vesicular structures at the distal tips of individual microvilli. **(I)** Microvillar packing in the IRTKS KO tissue is decreased towards the base of villi.

The lack of an obvious phenotype in the KO SEM data could result from increased expression of other brush border proteins compensating for loss of IRTKS. To test for compensation, a candidate list of brush border proteins should be stained for in KO frozen tissue sections. If a molecule has increased expression to make up for loss of IRTKS, they would show increased staining in the KO tissue. Another way to examine compensation is by performing shotgun mass spectrometry on isolated IRTKS KO brush borders. This technique has previously been used by our laboratory on intestinal brush border samples (Benesh et al., 2010; McConnell et al., 2011), and would provide a direct comparison of the peptide levels of common brush border proteins between WT and KO mice. Any protein with increased peptide counts in the IRTKS KO samples would be a compensatory candidate. Additionally, mass spectrometry would provide information on molecules that could be down regulated in the absence of IRTKS, such as EPS8. Based on the reduced localization of EPS8 in the IRTKS KD W4 cells (Fig. 3-8C), it would be expected that EPS8 localization would also be reduced in KO tissue. However, with the differential localization of IRTKS between the crypt and villar domains (discussed in the next section), there is a chance that EPS8 would only be mislocalized within the crypt domain. If other proteins are controlling the tip localization of EPS8 on the intestinal villus, a loss of IRTKS might not affect its expression within this domain. More data needs to be collected before a definitive conclusion on the role of IRTKS *in vivo* can be made.

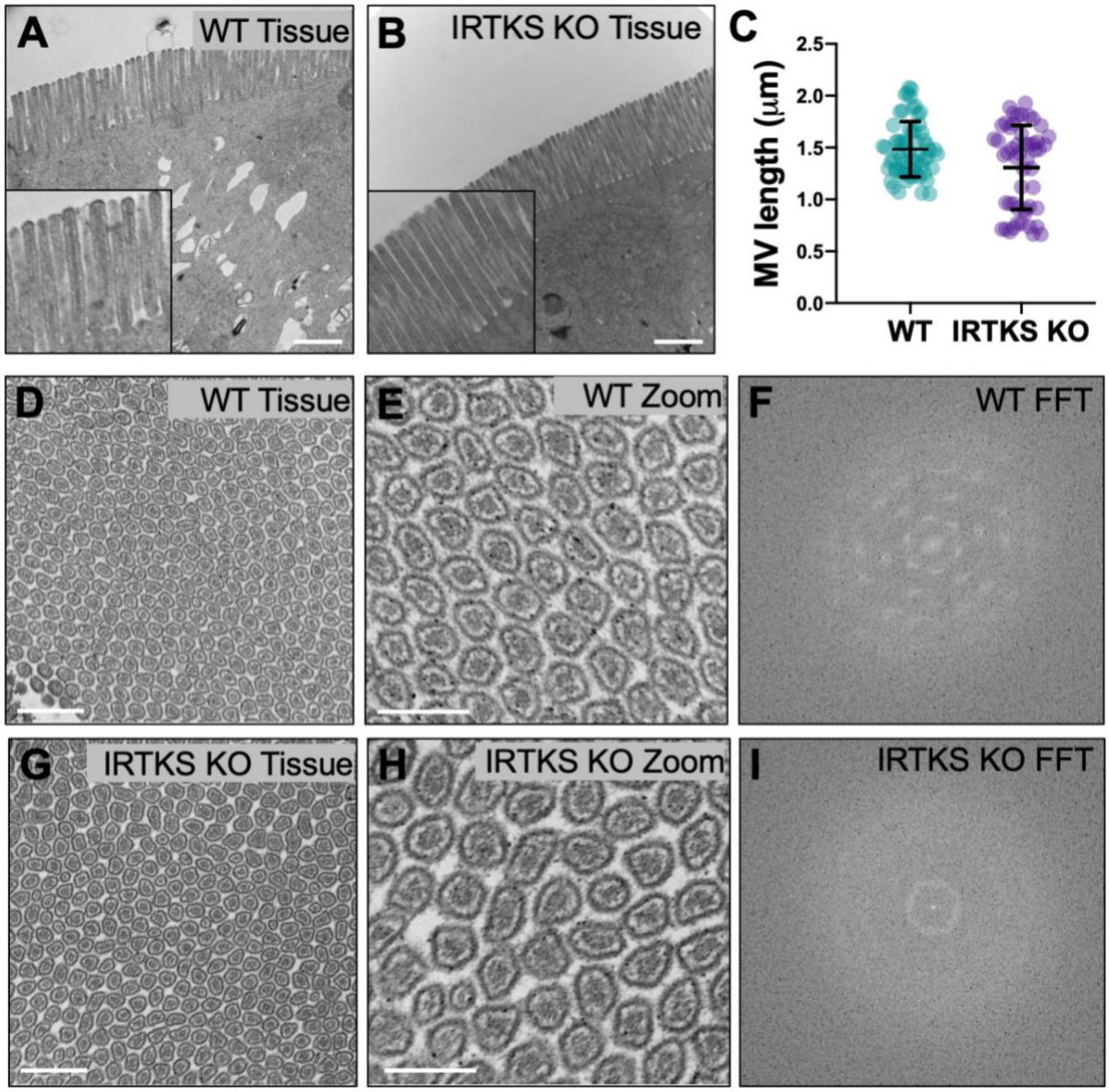

Figure 5-2: Loss of IRTKS disrupts microvillar ultrastructure. (A) TEM images of WT (A) and IRTKS KO (B) brush borders in planes parallel to the microvillar axis; scale bars, 1 μm. **(C)** Quantification of microvillar length in WT (n = 40) and IRTKS KO (n = 37). Measurements were selected so that only protrusions with actin cores fully visible along their length were scored. **(D, G)** TEM images of WT (D) and IRTKS KO (G) brush borders in planes orthogonal through the microvillar axis (*en face*); scale bars, 500 nm. **(E, H)** Zooms of D and G, showing individual actin filaments in the microvillar core; scale bars, 250 nm. **(F, I)** Fourier transformations (FFT) obtained from *en face* TEM images. The hexagonal pattern in F indicates normal microvillar packing, while the pattern in I shows loss of packing. TEM images were taken by Evan Krystofiak in the Vanderbilt EM core.

Utilizing IRTKS KO intestinal organoids to study BB assembly

Additional data on the role of IRKTS could come in the form of small intestinal organoids, which can be made from KO mouse tissue. Organoids are a powerful model system to study how differentiating epithelial cells form and maintain a brush border in an *in vivo* context. They are prepared by isolating stem cell containing crypts from mice, which reseal into “enterospheres” after being cultured in matrigel; over time, new crypt domains bud off from a shared villus. Similar to intestinal tissue, epithelial cells can then migrate from the crypt to the villar domain, with their apical BBs oriented into a central lumen (Sato and Clevers, 2013b; Sato et al., 2009; Stelzner et al., 2012). Organoids are a valuable model system because they can be fixed and stained as whole mount samples which allows us to dictate where in the sample we image, making it easier to visualize an entire crypt/villus axis in a single plane.

An organoid line from the IRTKS KO mouse will help determine how eliminating IRTKS impacts the time course and extent of BB maturation. Organoids are advantageous to use because they can be manipulated in a manner similar to cell culture lines, meaning they can be virally transduced to express proteins of interest. This means IRTKS truncation and mutant rescue constructs can be expressed in the KO organoids similar to the W4 KD/ rescue experiments in Chapter II. However, expressing the truncation and mutant constructs in a KO background will give better insight into the domains of IRTKS necessary to rescue brush border assembly as it eliminates the impact of endogenous protein dimerizing with the expression constructs. Stable fluorescent actin (or villin) expressing organoids can also be generated to visualize the enterocyte brush border during long-term imaging using spinning disk confocal microscopy. Overnight

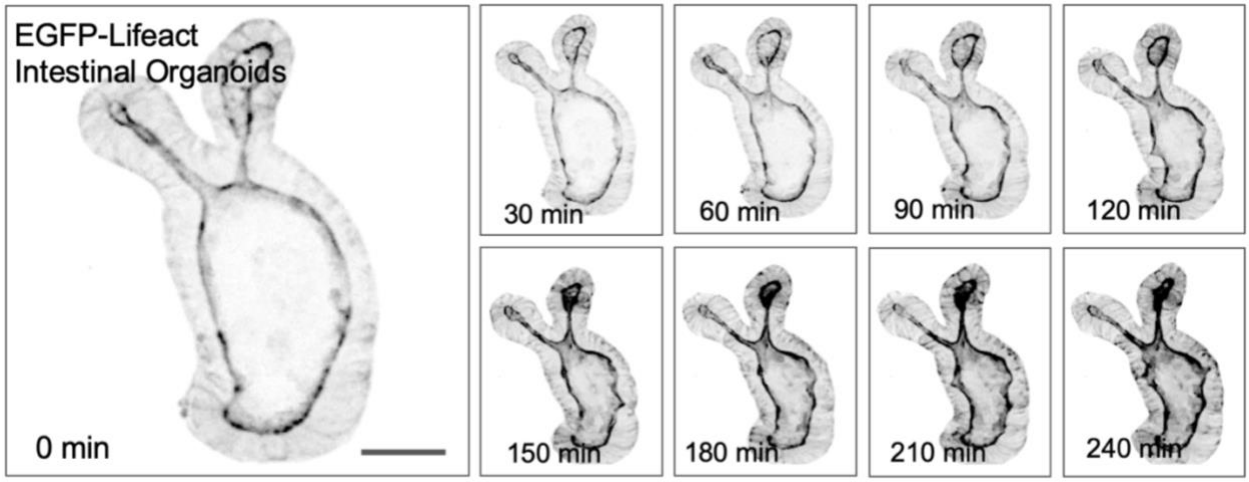

Figure 5-3: Live cell imaging of intestinal organoids. (A) Spinning disk confocal microscopy of EGFP-Lifeact expressing intestinal organoids. Imaging was performed overnight with 2-minute intervals and 30 μm Z-stacks; scale bar, 25 μm.

imaging of Myo5b KO intestinal organoids with 2-minute intervals and 30 μm Z-stacks has recently been performed in our lab with great success (Fig. 5-3). This means IRTKS KO organoids can be visualized with high temporal resolution to determine exactly how brush border assembly is affected without IRTKS as enterocytes mature.

Dissecting the Regulatory Mechanisms of IRTKS Targeting

Our initial studies on IRTKS show that it is expressed at the tips of microvillar protrusions in W4 cells and the tips of filopodial protrusions in B16F1 cells (Chapter III). However, in sections of native intestinal tissue, IRTKS surprisingly localizes at the base of brush border microvilli (Fig. 5-4). In both tissue and organoid staining, we saw that IRTKS was localized to the tips of the brush border in the crypt domain (white arrowheads in Fig. 5-4A and arrows in Fig. 5-4B), similar to the W4 cells. However, at the crypt/villus transition as seen in organoids, the IRTKS signal shifts to the base of the brush border (white

arrowheads in Fig. 5-4B), where it is localized in villar tissue sections. We believe the differences in the localization of IRTKS stems from the differences in the maturity of these cell types. For instance, W4 cells polarize after induction with doxycycline (Baas et al., 2003; Boudeau et al., 2003), leaving them in early stages of brush border formation characteristic of immature crypt enterocytes where microvilli are actively growing. Similarly, in B16F1 cells the filopodia are actively protruding and growing. However, the villus in native intestinal tissue contains mature enterocytes with more stable microvilli. Thus, the localization differences of IRTKS can be explained by the stability of the protrusion in question; IRTKS targets to brush border tips in both W4 cells and organoid crypts where microvilli are unstable and actively growing, while it targets to the base of microvilli in differentiated cells with stable BBs.

To explain the differences in microvillar tip versus base targeting, we speculate that IRTKS exists in two populations: one an open, active conformation promoting microvillar growth, and the other an autoinhibited, inactive state, perhaps functioning in BB maintenance or repair (Fig. 5-5). Autoinhibition is a common regulatory mechanism among BAR domain proteins and a previous study has shown that IRSp53 undergoes autoinhibition from its SH3 domain binding to an N-terminal PR (Kast et al., 2014). IRSp53 is the closest family member to IRTKS, and the two proteins have highly conserved I-BAR and SH3 domains (Millard et al., 2007), thus it is reasonable that the differential localization of IRTKS between the crypt and villus is a result of autoinhibition. The switch between these two states could be controlled by a binding partner with a ligand for the SH3 domain of IRTKS, which is how many autoinhibited proteins are regulated.

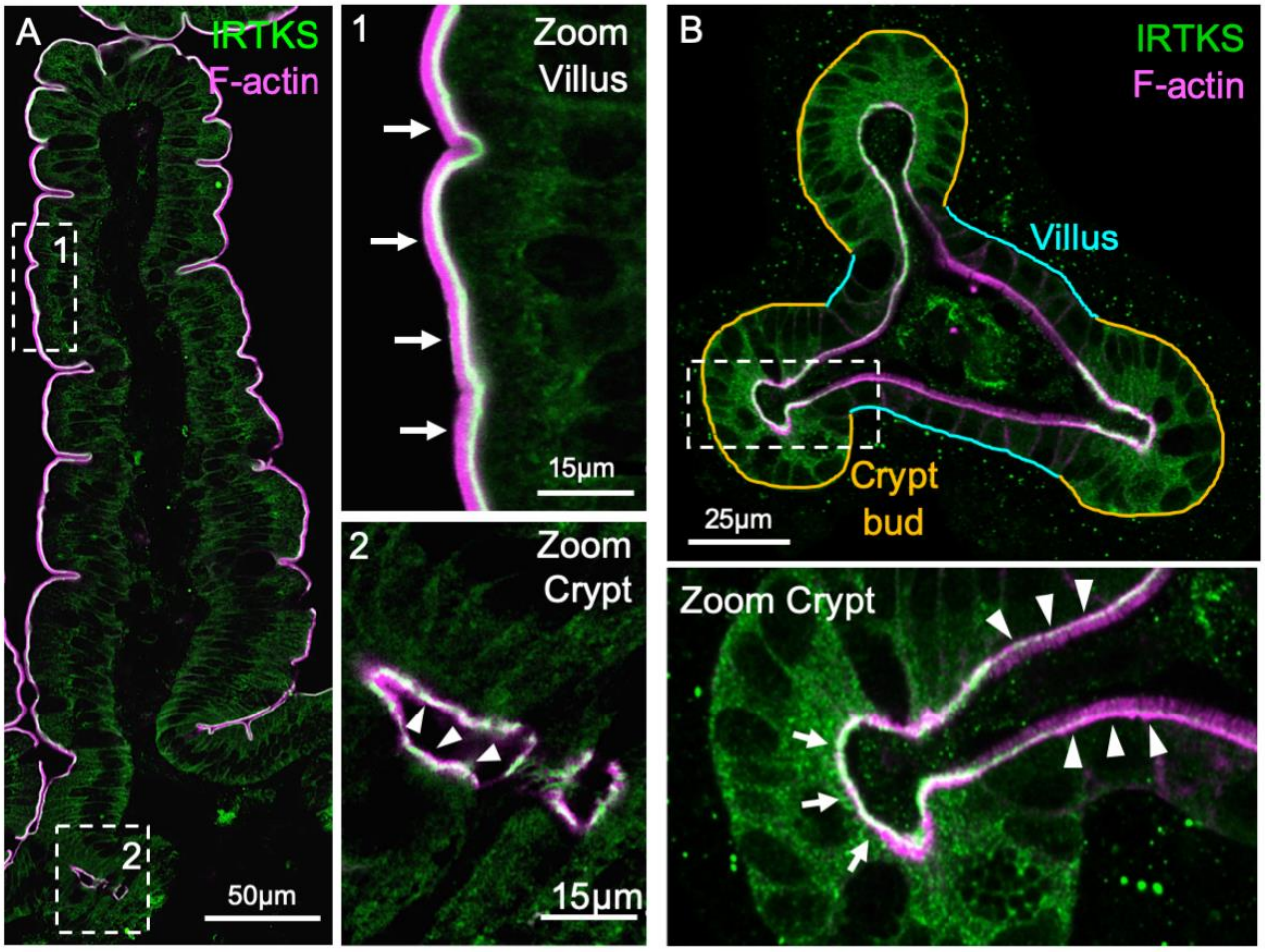

Figure 5-4: IRTKS endogenous localization in intestinal tissue and organoids. (A) Endogenous IRTKS (green) and phalloidin (magenta) labeling of frozen intestinal tissue. Dashed boxes indicate zooms. 1) zoom of the villar domain, arrows highlight IRTKS base localization; 2) zoom of the crypt domain, arrowheads highlight IRTKS tip localization. **(B)** Endogenous IRTKS (green) and phalloidin (magenta) labeling of an intestinal organoid. Dashed box indicates zoom of the crypt; arrows highlight IRTKS tip localization, arrowheads highlight IRTKS base localization.

Potential IRTKS constructs to determine intramolecular interactions

Future studies with different IRTKS constructs that will either force or prevent intramolecular interactions can be performed to establish if the differential localization of IRTKS is actually a result of autoinhibitory binding (Fig. 5-6). These constructs could contain 1) an IRTKS PR* construct with a loss of function mutation in the PR, 2) an IRTKS

ΔPR construct with a deleted PR, and 3) an IRTKS SAH construct with an added SAH between the PR and SH3 domains. The first two constructs should no longer bind to the SH3 domain, and the addition of the SAH domain in construct three will force the molecule into an extended conformation, and prevent it from folding (Peckham, 2011; Sweeney and Houdusse, 2010; Wolny et al., 2014).

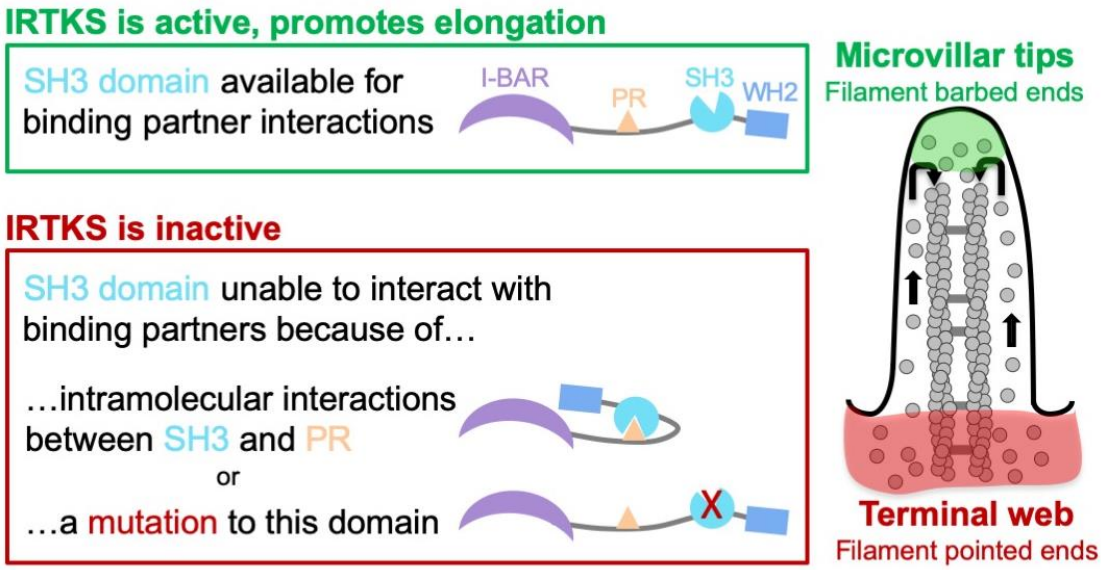

Figure 5-5: Proposed model of IRTKS regulation. IRTKS is in an open, active conformation at microvillar tips and a closed, inactive conformation at the base.

Two additional IRTKS constructs could be generated to force an intramolecular interaction, simulating autoinhibition. One way to accomplish this would be to utilize the EHEC effector $EspF_0$, which binds to the SH3 domain of IRTKS during EHEC infections (Vingadassalom et al., 2009) (Fig. 1-8). An NMR structure of this interaction has shown it to occur through the highest affinity possible (Aitio et al., 2010). We can take advantage of this high affinity interaction to generate an IRTKS construct replacing the canonical PR with the PR of $EspF_U$, thus generating a version of IRTKS locked in an autoinhibited state.

The final construct generated, IRTKS α-HD, could contain an alpha helical domain (α-HD) from the ERM protein Moesin. The α-HD interacts with itself in an antiparallel fashion; thus, the addition of this domain will force IRTKS into a folded state, blocking the SH3 domain and imitating an intramolecular interaction (Li et al., 2007; Mangeat et al., 1999; Niggli and Rossy, 2008).

Further characterization of these constructs could be obtained through expression in the IRTKS KO organoids proposed in the previous section. If the conformational state of IRTKS does indeed determine where the molecule targets, we would expect no differential localization occurring with the IRTKS constructs in a forced closed, or forced open, conformation. The three IRTKS constructs engineered to prevent intramolecular folding (Fig. 5-6) are predicted to show localization only at BB tips throughout both the crypt and villus. Because the SH3 domains will never be able to fold back and bind to the PR regions, SH3 binding partners will constantly be able to target the IRTKS molecules. As a result, the organoids would be expected to have slightly longer microvilli, such as those seen in the IRTKS preliminary data (Fig. 3A&B). In contrast, the two IRTKS constructs with forced intramolecular binding will likely localize to the BB base throughout both the organoid crypt and villus, opposite from the open constructs. It is also likely that preventing IRTKS from reaching the microvillar tips would cause the organoids to display a shortened BB phenotype, as seen in IRTKS SH3* (Fig. 3-4). This is because the inactive IRTKS molecule would no longer be able to interact with other molecules through the SH3 domain, which could prevent it from targeting to the growing microvillar tips. Significant mechanistic information can be gained from investigating the autoinhibitory state of IRTKS, and thus should be the focus of future work. If the differential localization is not a

result of autoinhibition, other potential binding partners of IRTKS should be examined to determine if a novel binging partner along the villar domain is what is controlling the localization of IRTKS.

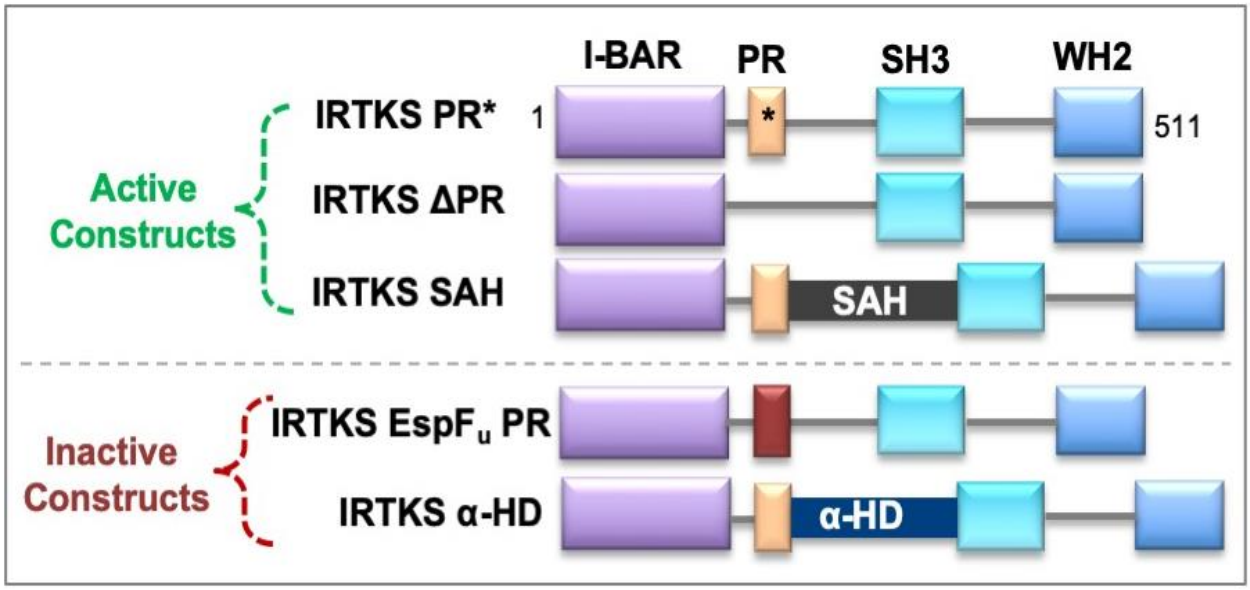

Figure 5-6: Schematic of proposed IRTKS constructs for future autoinhibition studies. Numbers indicate amino acids, * indicates point mutations P285,286,288A. SAH is the single α-helical domain, the red box indicates the PR domain from EspF$_u$ and the blue α-HD box indicates the α-helical domain. Domain aa: I-BAR 1-249, PR 281-303, SH3 339-402, WH2 483-511.

Utilizing CRSIPR/Cas9 for endogenous tagging

Overexpressing fluorescently tagged proteins in cell culture models provides a way to visualize the localization and function of specific molecules during live cell imaging. However, putting more protein in a cell than is normally expressed can generate unwanted artifacts. The CRSIPR/Cas9 system uses homologous recombination to generate cell lines with genomic insertions or deletions in a gene of interest. We can utilize this technology to insert a fluorescent tag in the IRTKS gene that would allow us to

visualize the molecule at endogenous levels. It would be beneficial to use WT intestinal organoids for the CRISPR/Cas9 endogenous tagging as they possess both undifferentiated crypt domains and mature villar domains.

The overexpression studies in the previous section will provide information as to whether or not autoinhibition is controlling the differential localization of IRTKS; however, they will not give insight into *why* IRTKS migrates from the tips to the base of microvilli. Endogenously tagging IRTKS in organoids will allow us use live imaging to visualize the molecule in real time as enterocytes migrate out of the crypt domain onto the villus. This would provide insight into the function of IRTKS in early microvillar growth as well as information on how IRTKS changes its localization, without the artifacts normally associated with overexpression. It is hypothesized that the tip to base transition of IRTKS occurs because the molecule is no longer needed to be tip localized on the villar domain as microvillar growth is complete. However, it begs the question as to why the protein is still expressed and localizing to the brush border. One reason might be for general microvillar maintenance after disruption or after brush border effacement from bacterial infections, like EHEC (de Groot et al., 2011; Vingadassalom et al., 2009). To determine if this is the case, the IRTKS tagged organoids could be used to generate brush border injury during live cell imaging. This would demonstrate if the IRTKS molecules at the brush border base along the villar domain localize back to the tips of microvilli to promote new growth. Studies using CRISPR/Cas9 to tag IRTKS in organoids would provide further insight into why IRTKS is differentially localized between the crypt and villar domains, as well as insight into the steps of early brush border formation.

Dissecting the Role of IRTKS in Brush Border Polarity Establishment

Epithelial cell polarity is a highly regulated process involving many signaling and actin regulatory molecules, particularly Rho family GTPases. The process of polarization and apical domain establishment is readily observed in intestinal epithelial W4 cells. In this cell line, the addition of doxycycline initiates the expression of FLAG-STRADα and the activation of LKB1, which causes an accumulation of PI(4,5)P2 at one end of a cell and the translocation of Mst4 to what will eventually be the apical membrane. This ultimately leads to ezrin phosphorylation, cell polarization, and brush border formation (Baas et al., 2003; Baas et al., 2004; Boudeau et al., 2003). Interestingly, when IRTKS is knocked down in W4 cells, the apical domain appears to expand (Fig. 3-4, 3-5). This suggests that IRTKS might play a role in epithelial polarity establishment, however where and how the molecule fits into the current W4 polarity pathway is not known.

In the IRTKS KD studies in Chapter III, it was shown that losing IRTKS led to brush borders with shortened microvilli (Fig. 3-4B). However, it was not addressed that IRTKS KD also causes the normally apical brush border to expand around the periphery of the cell, a phenomenon we defined and quantified as percent BB coverage (Fig. 5-7G). There are two possibilities that could lead to an expanded apical domain from loss of IRTKS, 1) there is an increase in the number of microvillar protrusions that cause the brush border to acquire more surface area of the cell, or 2) without IRTKS the W4 cells can no longer restrict their apical domain to the top third of the cell. Preliminary experiments were performed on W4 cells to examine these two possibilities further.

To determine if there is an increase in the number of microvillar protrusions in the IRTKS KD cells, individual microvilli were counted using EPS8 as a tip marker because

of its specificity (Fig. 3-6). Interestingly, the number of individual microvilli in the IRTKS KD cells, as well as the amount of actin that was quantified from mean brush border phalloidin intensity, were unchanged from the scramble control (Fig. 5-6 H, I). This suggests that the expanded apical domain is not caused by an increase in microvillar growth events around the perimeter of the W4 cells, and that the IRTKS KD and scramble cells have the same number of microvillar protrusions. We next sought to determine if the second possibility, that polarity establishment is lost without IRTKS, is what is occurring in the KD cells. Preliminary immunostaining was performed using the polarity marker Rab11a, which is a small GTPases that has been shown to help localize signaling proteins to the apical domain in intestinal cells (Sobajima et al., 2014). Interestingly, Rab11a localizes to the entire periphery of the expanded brush border in the KD cells (Fig. 5-7F). This suggests that the actual apical domain is physically expanding along with the brush border when IRTKS is no longer expressed.

It is logical for IRTKS to be a component of the epithelial polarity pathway as it has a Rac binding site within its I-BAR domain (Millard et al., 2007), which is a protein that is known to help establish the position of the apical domain in epithelial cells (Ngok et al., 2014). A dominant negative Rac causes a reversal in apical/ basal polarity in MDCK cells (O'Brien et al., 2001); thus, if IRTKS is helping establish the localization of Rac, the apical domain could be remodeled without it. Additionally, I-BAR domain proteins are thought to help restrict $PI(4,5)P_2$ to the appropriate areas of the cell through the electrostatic interactions with their I-BAR domains (Zhao et al., 2013). If IRTKS is no longer able to restrict $PI(4,5)P_2$ to the top third of the cell, an expanded apical domain could result.

Future studies will need to be performed to examine how the expanded apical domain forms in more detail and to determine where IRTKS fits into the polarity pathway.

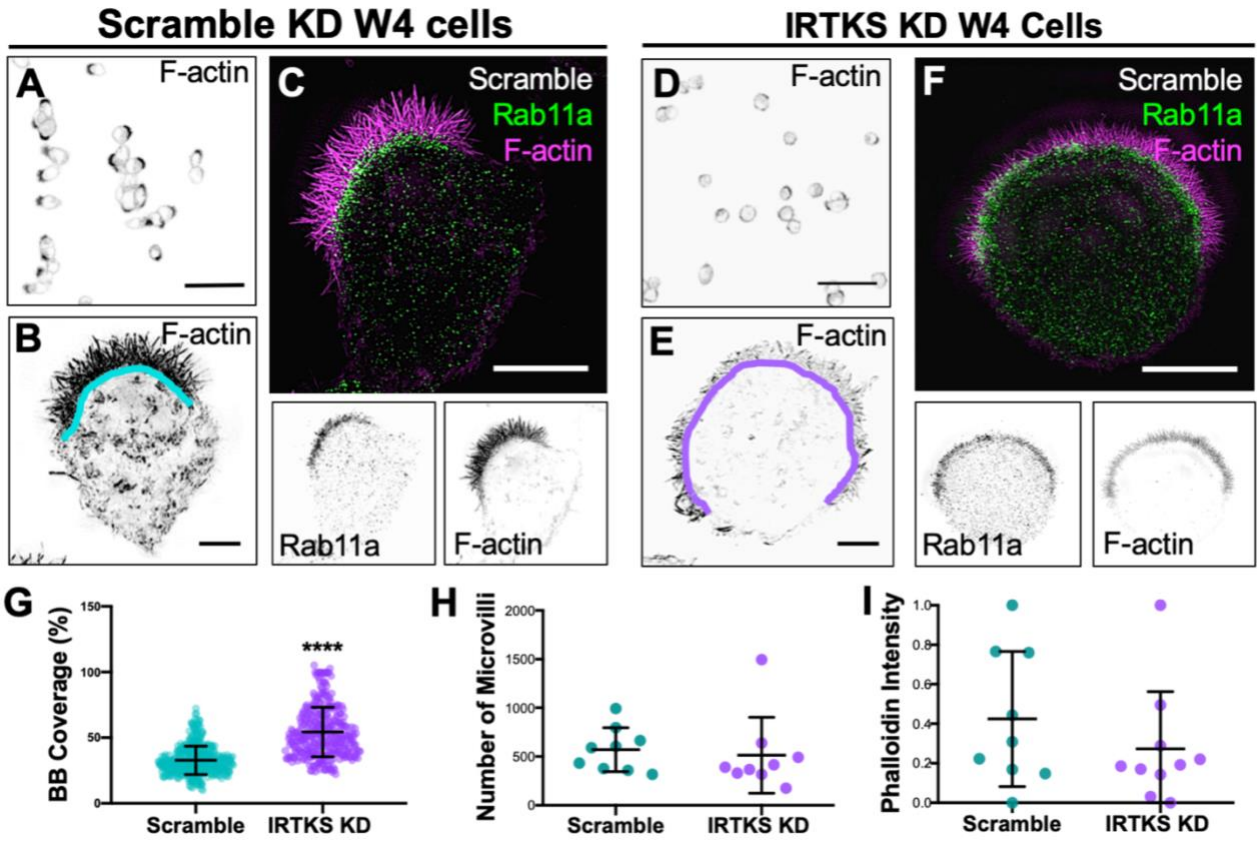

Figure 5-7: IRTKS KD in W4 cells leads to an expanded apical domain. **(A)** Phalloidin labeling of Scramble control W4 cells; image acquired using a 60x objective for a larger field of view. Scale bar, 20 μm. **(B)** Phalloidin staining in a scramble control W4 cell; teal line indicates the brush border coverage over ~30% of the cell. Scale bar, 5 μm. **(C)** Endogenous Rab11a (green) and phalloidin (magenta) labeling of a scramble control W4 cell; Rab11a staining highlights the apical domain. Scale bar, 5 μm. **(D)** Phalloidin labeling of IRTKS KD W4 cells; image acquired using a 60x objective for a larger field of view. Scale bar, 20 μm. **(B)** Phalloidin staining in an IRTKS KD W4 cell; purple line indicates the brush border coverage over ~70% of the cell. Scale bar, 5 μm. **(C)** Endogenous Rab11a (green) and phalloidin (magenta) labeling of an IRTKS KD W4 cell; Rab11a staining highlights the apical domain. Scale bar, 5 μm. **(G)** Quantification of percent BB coverage in scramble control and IRTKS KD cells. **(H)** Quantification of number of microvilli in scramble and IRTKS KD cells; microvilli were counted using EPS8 as a tip marker. (I) Quantification of the average phalloidin intensity between scramble and IRTKS KD cells.

Is IRSp53 a Member of the Intestinal Brush Border?

Functional redundancy of proteins is a defining feature of the intestinal brush border and is seen in many of the molecules we study in our lab. An interesting example of the redundancy of brush border proteins can be seen in the actin bundling proteins found within microvilli, villin, espin and fimbrin, where mice lacking one or more of these proteins are still able to assemble microvilli. Indeed, deletion of villin in mice had a minimal impact on brush border organization under normal conditions (Ferrary et al., 1999). Even more remarkably, a mouse model lacking all three major bundling proteins still assembled a functional brush border, although microvillar organization was perturbed (Revenu et al., 2012). Thus, the ability of IRTKS KD W4 cells (Fig. 3-4) and the IRTKS KO mouse (Fig. 5-2 and 5-3) to still form brush border indicates the presence of compensatory mechanisms.

In earlier sections, the potential for other brush border proteins to be compensating for IRTKS was briefly discussed, however a candidate molecule that was not mentioned was the I-BAR domain-containing protein IRSp53. IRTKS has a 59% sequence similarity with IRSp53 (Millard et al., 2007) and the two molecules share all of the domains previously identified as necessary for brush border assembly, including the I-BAR, SH3, and WH2 domains (Fig. 5-8A). IRSp53 is also expressed in the small intestine and appears to localize to the brush border in immunostaining by the Human Protein Atlas (Fig. 5-8C, D). Furthermore, IRSp53 has been implicated as one of the host molecules hijacked in EHEC actin pedestal formation, as it can bind to both Tir and $EspF_U$ to complete the signaling cascade towards branched actin polymerization (Crepin et al., 2010; de Groot et al., 2011). However, all of the studies of IRSp53 in EHEC pathogenesis

have been done outside of the physiological system, or in non-intestinal epithelial cells. Thus, the ability of IRSp53 to be hijacked for pedestal formation could just be a result of it being available in the cell lines used for these studies.

Additional preliminary evidence for the intestinal expression of IRSp53 was recently found through a proteomics screen in our lab. The BioID approach was utilized with the actin regulatory protein EPS8 to find potential tip localized proteins in W4 cells. BioID works by biotinylating proteins in the vicinity of a protein of interest, in our case EPS8, which can then be pulled down and sent to proteomics for identification (Roux et al., 2018). EPS8 was used because of its specificity at the tips of microvilli in W4 cells, which was hypothesized to provide a clean analysis of proteins specific to the brush border. Surprisingly, along with IRTKS, IRSp53 was identified as a protein biotinylated in the vicinity of EPS8. IRSp53 has been previously shown to bind to EPS8 through its SH3 domain in filopodial protrusions (Disanza et al., 2006; Funato et al., 2004), so the interaction is not surprising. However, one caveat of the BioID experiments performed in our lab is that W4 cells can generate filopodia when they are initially plated, so whether the EPS8 biotinylation of IRSp53 occurred in filopodia or within the brush border is unknown. Further BioID experiments will have to be performed with isolated brush borders or in a fully differentiated epithelial cell line to determine if IRSp53 is actually binding EPS8 within microvilli.

Additional future studies that will need to be performed with IRSp53 to determine whether it is normally localized to the brush border with IRTKS, upregulated in the absence of IRTKS to compensate for its loss, or playing a different role in intestinal

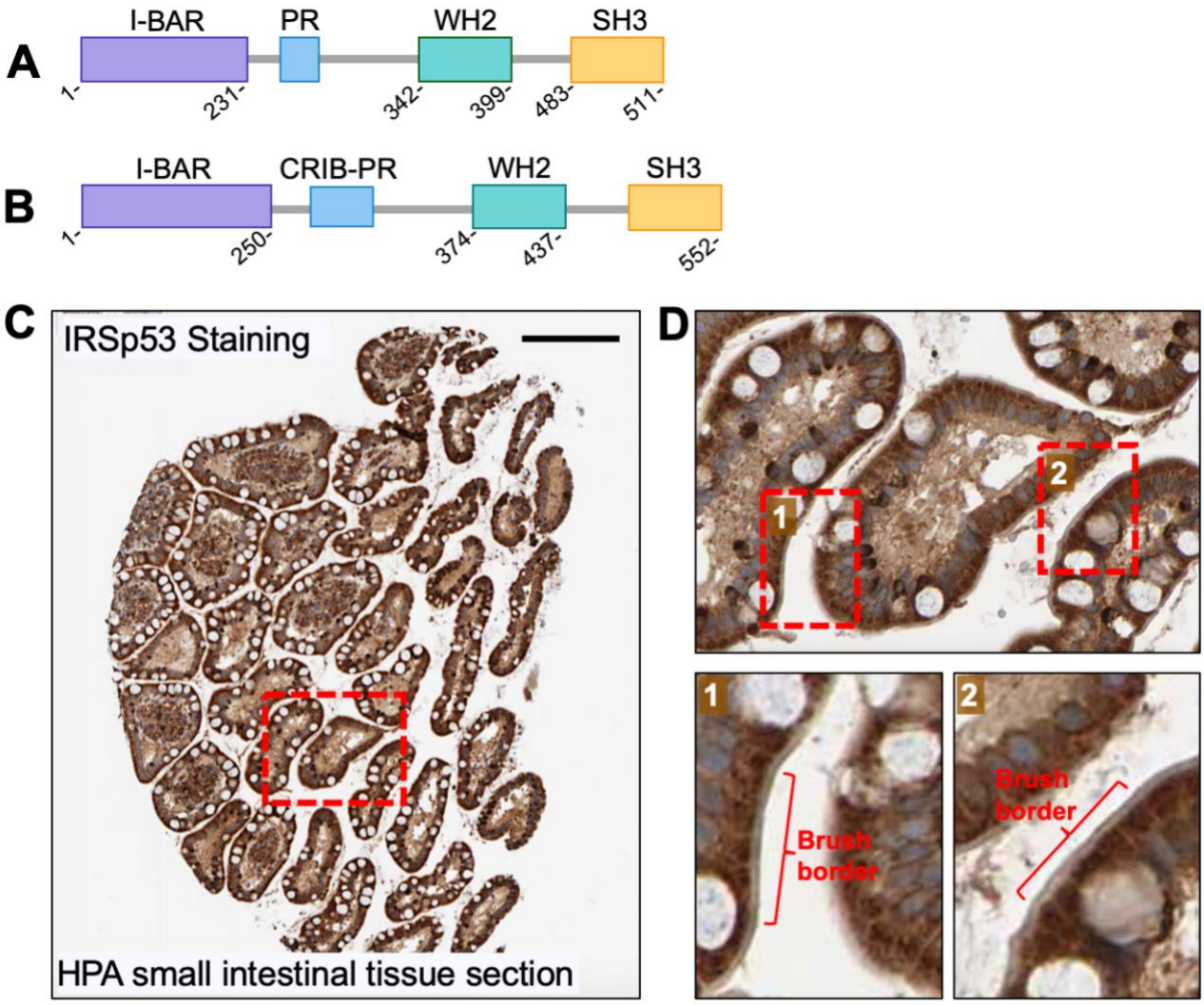

Figure 5-8: Small intestinal staining of IRSp53. **(A, B)** Domain diagrams of IRTKS (A) and IRSp53 (B) showing the similarities between the two proteins; numbers indicate amino acids. **(C, D)** IRSp53 staining from the Human Protein Atlas, darker brown indicates higher protein levels. Scale bar, 25 μm.

epithelial cells. One way to decipher this would be staining for IRSp53 in IRTKS KO tissue sections. This would tell us if and where IRSp53 is localized in the brush border, and if the expression of IRSp53 is increased in the absence of IRTKS, which would show its compensation. Another experiment would be to express an IRSp53 construct in IRTKS KO organoids to see if it can rescue brush border defects due to loss of IRTKS.

Mechanisms of PACSIN2 in Apical Endocytosis

Recent studies on PACSIN2 suggest the molecule plays a larger role in the internalization of caveolae than other forms of endocytosis (Kessels et al., 2006). It has been found to oligomerize around the neck of nascent caveolae for stabilization, before recruiting in the large GTPase Dynamin2 for excision from the membrane (Senju and Suetsugu, 2015). Caveolea are small, endocytic pits that bud inward from the plasma membrane (Parton, 1996) and, unlike clatherin-mediated endocytosis, they are uncoated with protein. They are important structural features in many mammalian cells and are thought to be inportant in lipid regulation and transcellular transport (Drab et al., 2001; Razani et al., 2002; Schubert et al., 2001). However, whether or not PACSIN2 localizes to caveola to promote their stabilization and excision in enterocytes is currently unknown.

Before examining the involvement of PACSIN2 in caveola formation, we first needed to determine the presence of caveolae at the enterocyte apical domain through preliminary staining of caveola proteins in WT intestinal tissue sections. We chose to satin for caveolin-1 and caveolin-2, which are two integral membrane proteins that form the main membrane component of caveolae (Hansen and Nichols, 2010). Indeed, both Caveolin-1 and Caveolin-2 localize to the base of the brush border, exactly where PACSIN2 localizes (Fig 5-9). This indicates that caveolae are forming at the intestinal apical domain, but more experiments need to be performed to show that PACSIN2 plays a role in their formation.

One way to show that PACSIN2 is involved in caveolar biogenesis is to perform immunofluorescence staining of Caveolin-1 and Caveolin-2 in PACSIN2 KO frozen tissue

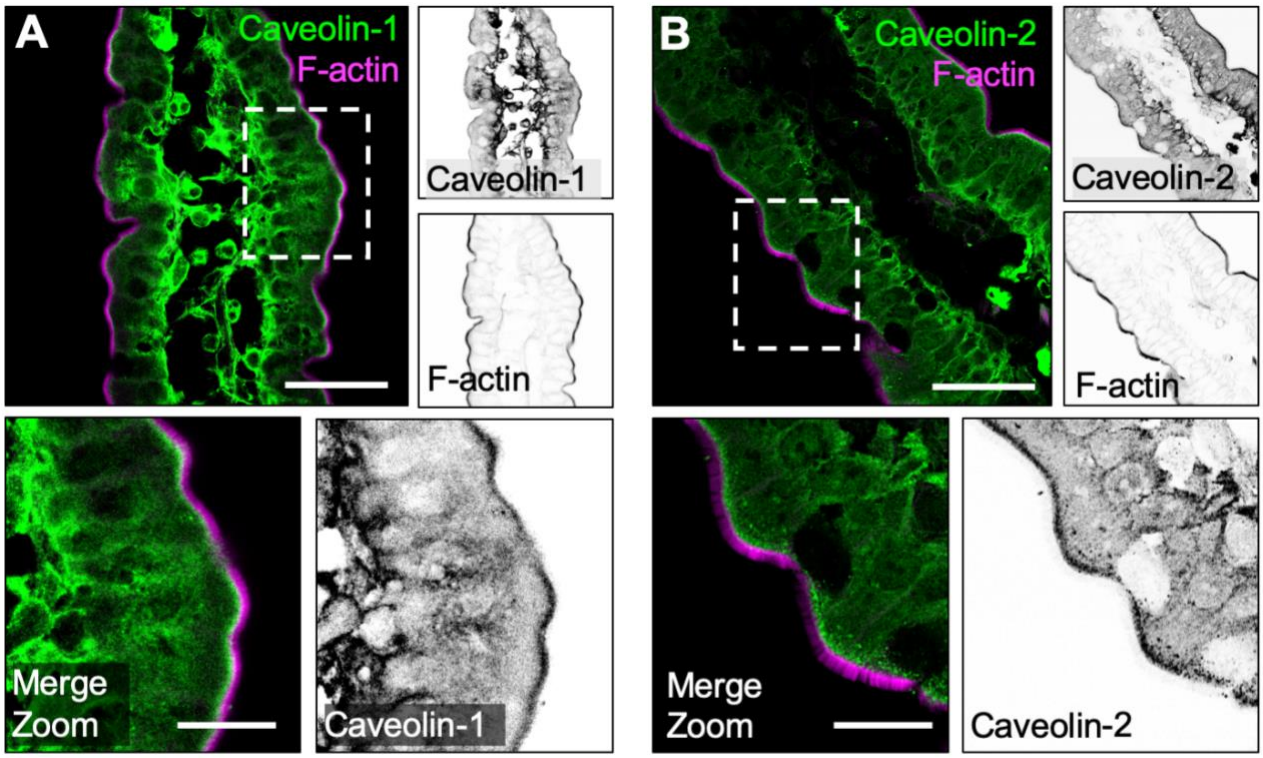

Figure 5-9: Caveolin-1 and Caveolin-2 localize to the enterocyte apical domain. (A) Endogenous Caveolin-1 (green) and phalloidin (magenta) labeling of frozen intestinal tissue. Dashed box indicates zoom the villar domain; scale bars, 25 μm in main panel, 10 μm in zoom. **(B)** Endogenous Caveolin-2 (green) and phalloidin (magenta) labeling of frozen intestinal tissue. Dashed box indicates zoom the villar domain; scale bars, 25 μm in main panel, 10 μm in zoom.

sections. We would hypothesize that there would be reduced staining of the Caveolin proteins in the KO tissue, as caveolae would no longer be stabilized at the apical domain without PACSIN2. Another method to directly test for the presence of caveolae is to KD both Caveolin-1 and PACSIN2 in W4 cells. If PACSIN2 is promoting the stabilization and excision of caveolae in the brush border, then we would expect the membrane tubules that form in the PACSIN2 KD W4 cells (Fig. 4-8E) would be absent or reduced in a Caveolin-1/ PACSIN2 double KD. Without caveolin-1 to initially form the caveolar vesicles, loss of PACSIN2 should have no effect on the plasma membrane tension and

thus no membrane tubules should form. However, if PACSIN2 is involved in the excision of non-caveolar vesicles at the apical domain, then the membrane tubules would still be expected to form. Additional future experiments should focus on the exact mechanism PACSIN2 uses for vesicle scission, and how it relates to the mechanism of PACSIN2 in complex with COBL in microvillar assembly.

Conclusions

The work presented here highlights roles for both I-BAR and F-BAR domain-containing proteins in brush border assembly and maintenance. We have established that the I-BAR domain protein IRTKS, along with the actin-binding protein EPS8, are necessary components of brush border assembly and required for microvillar elongation within the intestinal crypt domain (Chapter III). Additionally, we have established that the F-BAR domain protein PACSIN2 is controlling the membrane coverage of enterocyte microvilli by promoting dynamin-dependent endocytosis (Chapter IV). Future experiments highlighted in this section will be critical to further understand the mechanisms employed by IRTKS and PACSIN2 in brush border assembly. Following up on the IRTKS KO mouse data will be especially important to further analyze the need for the IRTKS/ EPS8 complex on microvillar growth *in vivo.* Moreover, further experiments performed that determine the type of endocytosis PACSIN2 is facilitating at the apical domain will help establish the link between membrane tension and microvillar morphology.

REFERENCES

Ahmed, S., Goh, W.I., and Bu, W. (2010). I-BAR domains, IRSp53 and filopodium formation. Semin Cell Dev Biol *21*, 350-356.

Ahuja, R., Pinyol, R., Reichenbach, N., Custer, L., Klingensmith, J., Kessels, M.M., and Qualmann, B. (2007). Cordon-bleu is an actin nucleation factor and controls neuronal morphology. Cell *131*, 337-350.

Aitio, O., Hellman, M., Kazlauskas, A., Vingadassalom, D.F., Leong, J.M., Saksela, K., and Permi, P. (2010). Recognition of tandem PxxP motifs as a unique Src homology 3-binding mode triggers pathogen-driven actin assembly. Proc Natl Acad Sci U S A *107*, 21743-21748.

Aitio, O., Hellman, M., Skehan, B., Kesti, T., Leong, J.M., Saksela, K., and Permi, P. (2012). Enterohaemorrhagic Escherichia coli exploits a tryptophan switch to hijack host f-actin assembly. Structure *20*, 1692-1703.

Apodaca, G. (2004). The uroepithelium: not just a passive barrier. Traffic *5*, 117-128.

Arasada, R., and Pollard, T.D. (2011). Distinct roles for F-BAR proteins Cdc15p and Bzz1p in actin polymerization at sites of endocytosis in fission yeast. Curr Biol *21*, 1450-1459.

Aspenstrom, P. (1997). A Cdc42 target protein with homology to the non-kinase domain of FER has a potential role in regulating the actin cytoskeleton. Curr Biol *7*, 479-487.

Aspenstrom, P. (2014). BAR domain proteins regulate Rho GTPase signaling. Small GTPases *5*, 7.

Avenarius, M.R., Krey, J.F., Dumont, R.A., Morgan, C.P., Benson, C.B., Vijayakumar, S., Cunningham, C.L., Scheffer, D.I., Corey, D.P., Muller, U.*, et al.* (2017). Heterodimeric capping protein is required for stereocilia length and width regulation. The Journal of cell biology *216*, 3861-3881.

Baas, A.F., Boudeau, J., Sapkota, G.P., Smit, L., Medema, R., Morrice, N.A., Alessi, D.R., and Clevers, H.C. (2003). Activation of the tumour suppressor kinase LKB1 by the STE20-like pseudokinase STRAD. EMBO J *22*, 3062-3072.

Baas, A.F., Kuipers, J., van der Wel, N.N., Batlle, E., Koerten, H.K., Peters, P.J., and Clevers, H.C. (2004). Complete polarization of single intestinal epithelial cells upon activation of LKB1 by STRAD. Cell *116*, 457-466.

Backhed, F., Ley, R.E., Sonnenburg, J.L., Peterson, D.A., and Gordon, J.I. (2005). Host-bacterial mutualism in the human intestine. Science *307*, 1915-1920.

Bacon, C., Endris, V., and Rappold, G. (2009). Dynamic expression of the Slit-Robo GTPase activating protein genes during development of the murine nervous system. J Comp Neurol *513*, 224-236.

Bailey, D.S., Freedman, A.R., Price, S.C., Chescoe, D., and Ciclitira, P.J. (1989). Early biochemical responses of the small intestine of coeliac patients to wheat gluten. Gut *30*, 78-85.

Bartles, J.R., Zheng, L., Li, A., Wierda, A., and Chen, B. (1998). Small espin: a third actin-bundling protein and potential forked protein ortholog in brush border microvilli. The Journal of cell biology *143*, 107-119.

Behlouli, A., Bonnet, C., Abdi, S., Bouaita, A., Lelli, A., Hardelin, J.P., Schietroma, C., Rous, Y., Louha, M., Cheknane, A*., et al.* (2014). EPS8, encoding an actin-binding protein of cochlear hair cell stereocilia, is a new causal gene for autosomal recessive profound deafness. Orphanet J Rare Dis *9*, 55.

Benesh, A.E., Nambiar, R., McConnell, R.E., Mao, S., Tabb, D.L., and Tyska, M.J. (2010). Differential localization and dynamics of class I myosins in the enterocyte microvillus. Mol Biol Cell *21*, 970-978.

Blood, P.D., and Voth, G.A. (2006). Direct observation of Bin/amphiphysin/Rvs (BAR) domain-induced membrane curvature by means of molecular dynamics simulations. Proc Natl Acad Sci U S A *103*, 15068-15072.

Bompard, G., Sharp, S.J., Freiss, G., and Machesky, L.M. (2005). Involvement of Rac in actin cytoskeleton rearrangements induced by MIM-B. Journal of cell science *118*, 5393-5403.

Bosch, M., Le, K.H., Bugyi, B., Correia, J.J., Renault, L., and Carlier, M.F. (2007). Analysis of the function of Spire in actin assembly and its synergy with formin and profilin. Mol Cell *28*, 555-568.

Boudeau, J., Baas, A.F., Deak, M., Morrice, N.A., Kieloch, A., Schutkowski, M., Prescott, A.R., Clevers, H.C., and Alessi, D.R. (2003). MO25alpha/beta interact with STRADalpha/beta enhancing their ability to bind, activate and localize LKB1 in the cytoplasm. EMBO J *22*, 5102-5114.

Boulant, S., Kural, C., Zeeh, J.C., Ubelmann, F., and Kirchhausen, T. (2011). Actin dynamics counteract membrane tension during clathrin-mediated endocytosis. Nat Cell Biol *13*, 1124-1131.

Bretscher, A., and Weber, K. (1979). Villin: the major microfilament-associated protein of the intestinal microvillus. Proc Natl Acad Sci U S A *76*, 2321-2325.

Bretscher, A., and Weber, K. (1980). Fimbrin, a new microfilament-associated protein present in microvilli and other cell surface structures. The Journal of cell biology *86*, 335-340.

Campellone, K.G. (2010). Cytoskeleton-modulating effectors of enteropathogenic and enterohaemorrhagic Escherichia coli: Tir, EspFU and actin pedestal assembly. FEBS J *277*, 2390-2402.

Campellone, K.G., Robbins, D., and Leong, J.M. (2004). EspFU is a translocated EHEC effector that interacts with Tir and N-WASP and promotes Nck-independent actin assembly. Dev Cell *7*, 217-228.

Carlier, M.F., Husson, C., Renault, L., and Didry, D. (2011). Control of actin assembly by the WH2 domains and their multifunctional tandem repeats in Spire and Cordon-Bleu. Int Rev Cell Mol Biol *290*, 55-85.

Carman, P.J., and Dominguez, R. (2018). BAR domain proteins-a linkage between cellular membranes, signaling pathways, and the actin cytoskeleton. Biophys Rev *10*, 1587-1604.

Chandrasekaran, R., Kenworthy, A.K., and Lacy, D.B. (2016). Clostridium difficile Toxin A Undergoes Clathrin-Independent, PACSIN2-Dependent Endocytosis. PLoS Pathog *12*, e1006070.

Chen, Z.B., Zhang, H.Y., Zhao, J.H., Zhao, W., Zhao, D., Zheng, L.F., Zhang, X.F., Liao, X.P., and Yi, X.N. (2012). Slit-Robo GTPase-activating proteins are differentially expressed in murine dorsal root ganglia: modulation by peripheral nerve injury. Anat Rec (Hoboken) *295*, 652-660.

Cooper, J.A., and Sept, D. (2008). New insights into mechanism and regulation of actin capping protein. Int Rev Cell Mol Biol *267*, 183-206.

Crawley, S.W., Mooseker, M.S., and Tyska, M.J. (2014a). Shaping the intestinal brush border. The Journal of cell biology *207*, 441-451.

Crawley, S.W., Shifrin, D.A., Jr., Grega-Larson, N.E., McConnell, R.E., Benesh, A.E., Mao, S., Zheng, Y., Zheng, Q.Y., Nam, K.T., Millis, B.A.*, et al.* (2014b). Intestinal brush border assembly driven by protocadherin-based intermicrovillar adhesion. Cell *157*, 433-446.

Crawley, S.W., Weck, M.L., Grega-Larson, N.E., Shifrin, D.A., Jr., and Tyska, M.J. (2016). ANKS4B Is Essential for Intermicrovillar Adhesion Complex Formation. Dev Cell *36*, 190-200.

Crepin, V.F., Girard, F., Schuller, S., Phillips, A.D., Mousnier, A., and Frankel, G. (2010). Dissecting the role of the Tir:Nck and Tir:IRTKS/IRSp53 signalling pathways in vivo. Mol Microbiol *75*, 308-323.

Croce, A., Cassata, G., Disanza, A., Gagliani, M.C., Tacchetti, C., Malabarba, M.G., Carlier, M.F., Scita, G., Baumeister, R., and Di Fiore, P.P. (2004). A novel actin barbed-end-capping activity in EPS-8 regulates apical morphogenesis in intestinal cells of Caenorhabditis elegans. Nat Cell Biol *6*, 1173-1179.

de Groot, J.C., Schluter, K., Carius, Y., Quedenau, C., Vingadassalom, D., Faix, J., Weiss, S.M., Reichelt, J., Standfuss-Gabisch, C., Lesser, C.F.*, et al.* (2011). Structural basis for complex formation between human IRSp53 and the translocated intimin receptor Tir of enterohemorrhagic E. coli. Structure *19*, 1294-1306.

de Kreuk, B.J., Anthony, E.C., Geerts, D., and Hordijk, P.L. (2012). The F-BAR protein PACSIN2 regulates epidermal growth factor receptor internalization. J Biol Chem *287*, 43438-43453.

de Kreuk, B.J., Nethe, M., Fernandez-Borja, M., Anthony, E.C., Hensbergen, P.J., Deelder, A.M., Plomann, M., and Hordijk, P.L. (2011). The F-BAR domain protein PACSIN2 associates with Rac1 and regulates cell spreading and migration. Journal of cell science *124*, 2375-2388.

de Kreuk, B.J., Schaefer, A., Anthony, E.C., Tol, S., Fernandez-Borja, M., Geerts, D., Pool, J., Hambach, L., Goulmy, E., and Hordijk, P.L. (2013). The human minor histocompatibility antigen 1 is a RhoGAP. PLoS One *8*, e73962.

Deibel, C., Kramer, S., Chakraborty, T., and Ebel, F. (1998). EspE, a novel secreted protein of attaching and effacing bacteria, is directly translocated into infected host cells, where it appears as a tyrosine-phosphorylated 90 kDa protein. Mol Microbiol *28*, 463-474.

Delacour, D., Salomon, J., Robine, S., and Louvard, D. (2016). Plasticity of the brush border - the yin and yang of intestinal homeostasis. Nat Rev Gastroenterol Hepatol *13*, 161-174.

Demeter, J., and Sazer, S. (1998). imp2, a new component of the actin ring in the fission yeast Schizosaccharomyces pombe. The Journal of cell biology *143*, 415-427.

Deng, W., Marshall, N.C., Rowland, J.L., McCoy, J.M., Worrall, L.J., Santos, A.S., Strynadka, N.C.J., and Finlay, B.B. (2017). Assembly, structure, function and regulation of type III secretion systems. Nat Rev Microbiol *15*, 323-337.

Disanza, A., Bisi, S., Winterhoff, M., Milanesi, F., Ushakov, D.S., Kast, D., Marighetti, P., Romet-Lemonne, G., Muller, H.M., Nickel, W.*, et al.* (2013). CDC42 switches IRSp53 from inhibition of actin growth to elongation by clustering of VASP. EMBO J *32*, 2735-2750.

Disanza, A., Carlier, M.F., Stradal, T.E., Didry, D., Frittoli, E., Confalonieri, S., Croce, A., Wehland, J., Di Fiore, P.P., and Scita, G. (2004). Eps8 controls actin-based motility by capping the barbed ends of actin filaments. Nat Cell Biol *6*, 1180-1188.

Disanza, A., Mantoani, S., Hertzog, M., Gerboth, S., Frittoli, E., Steffen, A., Berhoerster, K., Kreienkamp, H.J., Milanesi, F., Di Fiore, P.P.*, et al.* (2006). Regulation of cell shape by Cdc42 is mediated by the synergic actin-bundling activity of the Eps8-IRSp53 complex. Nat Cell Biol *8*, 1337-1347.

Dominguez, R. (2016). The WH2 Domain and Actin Nucleation: Necessary but Insufficient. Trends Biochem Sci *41*, 478-490.

Drab, M., Verkade, P., Elger, M., Kasper, M., Lohn, M., Lauterbach, B., Menne, J., Lindschau, C., Mende, F., Luft, F.C.*, et al.* (2001). Loss of caveolae, vascular dysfunction, and pulmonary defects in caveolin-1 gene-disrupted mice. Science *293*, 2449-2452.

Eberth, A., Lundmark, R., Gremer, L., Dvorsky, R., Koessmeier, K.T., McMahon, H.T., and Ahmadian, M.R. (2009). A BAR domain-mediated autoinhibitory mechanism for RhoGAPs of the GRAF family. Biochem J *417*, 371-377.

Fankhauser, C., Reymond, A., Cerutti, L., Utzig, S., Hofmann, K., and Simanis, V. (1995). The S. pombe cdc15 gene is a key element in the reorganization of F-actin at mitosis. Cell *82*, 435-444.

Fath, K.R., Obenauf, S.D., and Burgess, D.R. (1990). Cytoskeletal protein and mRNA accumulation during brush border formation in adult chicken enterocytes. Development *109*, 449-459.

Fauchereau, F., Herbrand, U., Chafey, P., Eberth, A., Koulakoff, A., Vinet, M.C., Ahmadian, M.R., Chelly, J., and Billuart, P. (2003). The RhoGAP activity of OPHN1, a new F-actin-binding protein, is negatively controlled by its amino-terminal domain. Mol Cell Neurosci *23*, 574-586.

Ferrary, E., Cohen-Tannoudji, M., Pehau-Arnaudet, G., Lapillonne, A., Athman, R., Ruiz, T., Boulouha, L., El Marjou, F., Doye, A., Fontaine, J.J.*, et al.* (1999). In vivo, villin is required for Ca(2+)-dependent F-actin disruption in intestinal brush borders. The Journal of cell biology *146*, 819-830.

Franck, Z., Footer, M., and Bretscher, A. (1990). Microinjection of villin into cultured cells induces rapid and long-lasting changes in cell morphology but does not inhibit cytokinesis, cell motility, or membrane ruffling. The Journal of cell biology *111*, 2475-2485.

Friedel, R.H., Seisenberger, C., Kaloff, C., and Wurst, W. (2007). EUCOMM--the European conditional mouse mutagenesis program. Brief Funct Genomic Proteomic *6*, 180-185.

Friederich, E., Huet, C., Arpin, M., and Louvard, D. (1989). Villin induces microvilli growth and actin redistribution in transfected fibroblasts. Cell *59*, 461-475.

Friedman, N.B. (1945). Cellular Dynamics in the Intestinal Mucosa: The Effect of Irradiation on Epithelial Maturation and Migration. J Exp Med *81*, 553-558.

Frost, A., De Camilli, P., and Unger, V.M. (2007). F-BAR proteins join the BAR family fold. Structure *15*, 751-753.

Funato, Y., Terabayashi, T., Suenaga, N., Seiki, M., Takenawa, T., and Miki, H. (2004). IRSp53/Eps8 complex is important for positive regulation of Rac and cancer cell motility/invasiveness. Cancer Res *64*, 5237-5244.

Gallop, J.L., Jao, C.C., Kent, H.M., Butler, P.J., Evans, P.R., Langen, R., and McMahon, H.T. (2006). Mechanism of endophilin N-BAR domain-mediated membrane curvature. EMBO J *25*, 2898-2910.

Garabedian, M.V., Stanishneva-Konovalova, T., Lou, C., Rands, T.J., Pollard, L.W., Sokolova, O.S., and Goode, B.L. (2018). Integrated control of formin-mediated actin assembly by a stationary inhibitor and a mobile activator. The Journal of cell biology *217*, 3512-3530.

Goh, S.L., Wang, Q., Byrnes, L.J., and Sondermann, H. (2012). Versatile membrane deformation potential of activated pacsin. PLoS One *7*, e51628.

Graziano, B.R., Yu, H.Y., Alioto, S.L., Eskin, J.A., Ydenberg, C.A., Waterman, D.P., Garabedian, M., and Goode, B.L. (2014). The F-BAR protein Hof1 tunes formin activity to sculpt actin cables during polarized growth. Mol Biol Cell *25*, 1730-1743.

Grega-Larson, N.E., Crawley, S.W., Erwin, A.L., and Tyska, M.J. (2015). Cordon bleu promotes the assembly of brush border microvilli. Mol Biol Cell *26*, 3803-3815.

Grega-Larson, N.E., Crawley, S.W., and Tyska, M.J. (2016). Impact of cordon-bleu expression on actin cytoskeleton architecture and dynamics. Cytoskeleton (Hoboken) *73*, 670-679.

Griffin, P.M., and Tauxe, R.V. (1991). The epidemiology of infections caused by Escherichia coli O157:H7, other enterohemorrhagic E. coli, and the associated hemolytic uremic syndrome. Epidemiol Rev *13*, 60-98.

Grimm-Gunter, E.M., Revenu, C., Ramos, S., Hurbain, I., Smyth, N., Ferrary, E., Louvard, D., Robine, S., and Rivero, F. (2009). Plastin 1 binds to keratin and is required for terminal web assembly in the intestinal epithelium. Mol Biol Cell *20*, 2549-2562.

Guerrier, S., Coutinho-Budd, J., Sassa, T., Gresset, A., Jordan, N.V., Chen, K., Jin, W.L., Frost, A., and Polleux, F. (2009). The F-BAR domain of srGAP2 induces membrane protrusions required for neuronal migration and morphogenesis. Cell *138*, 990-1004.

Guillot, C., and Lecuit, T. (2013). Mechanics of epithelial tissue homeostasis and morphogenesis. Science *340*, 1185-1189.

Hansen, C.G., Howard, G., and Nichols, B.J. (2011). Pacsin 2 is recruited to caveolae and functions in caveolar biogenesis. Journal of cell science *124*, 2777-2785.

Hansen, C.G., and Nichols, B.J. (2010). Exploring the caves: cavins, caveolins and caveolae. Trends Cell Biol *20*, 177-186.

Heath, R.J., and Insall, R.H. (2008). F-BAR domains: multifunctional regulators of membrane curvature. Journal of cell science *121*, 1951-1954.

Hegan, P.S., Giral, H., Levi, M., and Mooseker, M.S. (2012). Myosin VI is required for maintenance of brush border structure, composition, and membrane trafficking functions in the intestinal epithelial cell. Cytoskeleton (Hoboken) *69*, 235-251.

Helander, H.F., and Fandriks, L. (2014). Surface area of the digestive tract - revisited. Scand J Gastroenterol *49*, 681-689.

Henne, W.M., Kent, H.M., Ford, M.G., Hegde, B.G., Daumke, O., Butler, P.J., Mittal, R., Langen, R., Evans, P.R., and McMahon, H.T. (2007). Structure and analysis of FCHo2 F-BAR domain: a dimerizing and membrane recruitment module that effects membrane curvature. Structure *15*, 839-852.

Hertzog, M., Milanesi, F., Hazelwood, L., Disanza, A., Liu, H., Perlade, E., Malabarba, M.G., Pasqualato, S., Maiolica, A., Confalonieri, S.*, et al.* (2010). Molecular basis for the dual function of Eps8 on actin dynamics: bundling and capping. PLoS Biol *8*, e1000387.

Hirokawa, N., Tilney, L.G., Fujiwara, K., and Heuser, J.E. (1982). Organization of actin, myosin, and intermediate filaments in the brush border of intestinal epithelial cells. The Journal of cell biology *94*, 425-443.

Ho, N.K., Henry, A.C., Johnson-Henry, K., and Sherman, P.M. (2013). Pathogenicity, host responses and implications for management of enterohemorrhagic Escherichia coli O157:H7 infection. Can J Gastroenterol *27*, 281-285.

Huang, L.Y., Wang, Y.P., Wei, B.F., Yang, J., Wang, J.Q., Wu, B.H., Zhang, Z.Z., Hou, Y.Y., Sun, W.M., Hu, R.M.*, et al.* (2013). Deficiency of IRTKS as an adaptor of insulin receptor leads to insulin resistance. Cell Res *23*, 1310-1321.

Hueck, C.J. (1998). Type III protein secretion systems in bacterial pathogens of animals and plants. Microbiol Mol Biol Rev *62*, 379-433.

Husson, C., Renault, L., Didry, D., Pantaloni, D., and Carlier, M.F. (2011). Cordon-Bleu uses WH2 domains as multifunctional dynamizers of actin filament assembly. Mol Cell *43*, 464-477.

Itoh, T., Erdmann, K.S., Roux, A., Habermann, B., Werner, H., and De Camilli, P. (2005). Dynamin and the actin cytoskeleton cooperatively regulate plasma membrane invagination by BAR and F-BAR proteins. Dev Cell *9*, 791-804.

Ivanov, A.I., Hunt, D., Utech, M., Nusrat, A., and Parkos, C.A. (2005a). Differential roles for actin polymerization and a myosin II motor in assembly of the epithelial apical junctional complex. Mol Biol Cell *16*, 2636-2650.

Ivanov, A.I., Nusrat, A., and Parkos, C.A. (2005b). Endocytosis of the apical junctional complex: mechanisms and possible roles in regulation of epithelial barriers. Bioessays *27*, 356-365.

Jarin, Z., Tsai, F.C., Davtyan, A., Pak, A.J., Bassereau, P., and Voth, G.A. (2019). Unusual Organization of I-BAR Proteins on Tubular and Vesicular Membranes. Biophys J *117*, 553-562.

Jarvis, K.G., and Kaper, J.B. (1996). Secretion of extracellular proteins by enterohemorrhagic Escherichia coli via a putative type III secretion system. Infect Immun *64*, 4826-4829.

Kaplan, B.S., Meyers, K.E., and Schulman, S.L. (1998). The pathogenesis and treatment of hemolytic uremic syndrome. J Am Soc Nephrol *9*, 1126-1133.

Karch, H. (2001). The role of virulence factors in enterohemorrhagic Escherichia coli (EHEC)--associated hemolytic-uremic syndrome. Semin Thromb Hemost *27*, 207-213.

Kast, D.J., Yang, C., Disanza, A., Boczkowska, M., Madasu, Y., Scita, G., Svitkina, T., and Dominguez, R. (2014). Mechanism of IRSp53 inhibition and combinatorial activation by Cdc42 and downstream effectors. Nat Struct Mol Biol *21*, 413-422.

Kelley, C.F., Messelaar, E.M., Eskin, T.L., Wang, S., Song, K., Vishnia, K., Becalska, A.N., Shupliakov, O., Hagan, M.F., Danino, D.*, et al.* (2015). Membrane Charge Directs the Outcome of F-BAR Domain Lipid Binding and Autoregulation. Cell Rep *13*, 2597-2609.

Kenny, B., DeVinney, R., Stein, M., Reinscheid, D.J., Frey, E.A., and Finlay, B.B. (1997). Enteropathogenic E. coli (EPEC) transfers its receptor for intimate adherence into mammalian cells. Cell *91*, 511-520.

Kessels, M.M., Dong, J., Leibig, W., Westermann, P., and Qualmann, B. (2006). Complexes of syndapin II with dynamin II promote vesicle formation at the trans-Golgi network. Journal of cell science *119*, 1504-1516.

Kessels, M.M., and Qualmann, B. (2002). Syndapins integrate N-WASP in receptor-mediated endocytosis. EMBO J *21*, 6083-6094.

Kessels, M.M., and Qualmann, B. (2004). The syndapin protein family: linking membrane trafficking with the cytoskeleton. Journal of cell science *117*, 3077-3086.

Kessels, M.M., and Qualmann, B. (2006). Syndapin oligomers interconnect the machineries for endocytic vesicle formation and actin polymerization. J Biol Chem *281*, 13285-13299.

Khubchandani, S.R., Vohra, P., Chitale, A.R., and Sidana, P. (2011). Microvillous inclusion disease--an ultrastructural diagnosis: with a review of the literature. Ultrastruct Pathol *35*, 87-91.

Kitt, K.N., Hernandez-Deviez, D., Ballantyne, S.D., Spiliotis, E.T., Casanova, J.E., and Wilson, J.M. (2008). Rab14 regulates apical targeting in polarized epithelial cells. Traffic *9*, 1218-1231.

Knutton, S., Lloyd, D.R., and McNeish, A.S. (1987). Adhesion of enteropathogenic Escherichia coli to human intestinal enterocytes and cultured human intestinal mucosa. Infect Immun *55*, 69-77.

Korinek, W.S., Bi, E., Epp, J.A., Wang, L., Ho, J., and Chant, J. (2000). Cyk3, a novel SH3-domain protein, affects cytokinesis in yeast. Curr Biol *10*, 947-950.

Kostan, J., Salzer, U., Orlova, A., Toro, I., Hodnik, V., Senju, Y., Zou, J., Schreiner, C., Steiner, J., Merilainen, J.*, et al.* (2014). Direct interaction of actin filaments with F-BAR protein pacsin2. EMBO Rep *15*, 1154-1162.

Kovacs, E.M., Verma, S., Ali, R.G., Ratheesh, A., Hamilton, N.A., Akhmanova, A., and Yap, A.S. (2011). N-WASP regulates the epithelial junctional actin cytoskeleton through a non-canonical post-nucleation pathway. Nat Cell Biol *13*, 934-943.

Krey, J.F., Krystofiak, E.S., Dumont, R.A., Vijayakumar, S., Choi, D., Rivero, F., Kachar, B., Jones, S.M., and Barr-Gillespie, P.G. (2016). Plastin 1 widens stereocilia by transforming actin filament packing from hexagonal to liquid. The Journal of cell biology *215*, 467-482.

Krugmann, S., Jordens, I., Gevaert, K., Driessens, M., Vandekerckhove, J., and Hall, A. (2001). Cdc42 induces filopodia by promoting the formation of an IRSp53:Mena complex. Curr Biol *11*, 1645-1655.

Lai, Y., Rosenshine, I., Leong, J.M., and Frankel, G. (2013). Intimate host attachment: enteropathogenic and enterohaemorrhagic Escherichia coli. Cell Microbiol *15*, 1796-1808.

Lee, S.H., Kerff, F., Chereau, D., Ferron, F., Klug, A., and Dominguez, R. (2007). Structural basis for the actin-binding function of missing-in-metastasis. Structure *15*, 145-155.

Li, J., He, Y., Lu, Q., and Zhang, M. (2016). Mechanistic Basis of Organization of the Harmonin/USH1C-Mediated Brush Border Microvilli Tip-Link Complex. Dev Cell *36*, 179-189.

Li, J., He, Y., Weck, M.L., Lu, Q., Tyska, M.J., and Zhang, M. (2017). Structure of Myo7b/USH1C complex suggests a general PDZ domain binding mode by MyTH4-FERM myosins. Proc Natl Acad Sci U S A *114*, E3776-E3785.

Li, Q., Nance, M.R., Kulikauskas, R., Nyberg, K., Fehon, R., Karplus, P.A., Bretscher, A., and Tesmer, J.J. (2007). Self-masking in an intact ERM-merlin protein: an active role for the central alpha-helical domain. J Mol Biol *365*, 1446-1459.

Lichte, B., Veh, R.W., Meyer, H.E., and Kilimann, M.W. (1992). Amphiphysin, a novel protein associated with synaptic vesicles. EMBO J *11*, 2521-2530.

Licois, D., Reynaud, A., Federighi, M., Gaillard-Martinie, B., Guillot, J.F., and Joly, B. (1991). Scanning and transmission electron microscopic study of adherence of Escherichia coli O103 enteropathogenic and/or enterohemorrhagic strain GV in enteric infection in rabbits. Infect Immun *59*, 3796-3800.

Lim, K.B., Bu, W., Goh, W.I., Koh, E., Ong, S.H., Pawson, T., Sudhaharan, T., and Ahmed, S. (2008). The Cdc42 effector IRSp53 generates filopodia by coupling membrane protrusion with actin dynamics. J Biol Chem *283*, 20454-20472.

Loomis, P.A., Kelly, A.E., Zheng, L., Changyaleket, B., Sekerkova, G., Mugnaini, E., Ferreira, A., Mullins, R.D., and Bartles, J.R. (2006). Targeted wild-type and jerker espins reveal a novel, WH2-domain-dependent way to make actin bundles in cells. Journal of cell science *119*, 1655-1665.

Loomis, P.A., Zheng, L., Sekerkova, G., Changyaleket, B., Mugnaini, E., and Bartles, J.R. (2003). Espin cross-links cause the elongation of microvillus-type parallel actin bundles in vivo. The Journal of cell biology *163*, 1045-1055.

Macnab, R.M. (2003). How bacteria assemble flagella. Annu Rev Microbiol *57*, 77-100.

Mangeat, P., Roy, C., and Martin, M. (1999). ERM proteins in cell adhesion and membrane dynamics: Authors' correction. Trends Cell Biol *9*, 289.

Manor, U., Disanza, A., Grati, M., Andrade, L., Lin, H., Di Fiore, P.P., Scita, G., and Kachar, B. (2011). Regulation of stereocilia length by myosin XVa and whirlin depends on the actin-regulatory protein Eps8. Curr Biol *21*, 167-172.

Masuda, M., and Mochizuki, N. (2010). Structural characteristics of BAR domain superfamily to sculpt the membrane. Semin Cell Dev Biol *21*, 391-398.

Mattila, P.K., Pykalainen, A., Saarikangas, J., Paavilainen, V.O., Vihinen, H., Jokitalo, E., and Lappalainen, P. (2007). Missing-in-metastasis and IRSp53 deform PI(4,5)P2-rich membranes by an inverse BAR domain-like mechanism. The Journal of cell biology *176*, 953-964.

McConnell, R.E., Benesh, A.E., Mao, S., Tabb, D.L., and Tyska, M.J. (2011). Proteomic analysis of the enterocyte brush border. American journal of physiology Gastrointestinal and liver physiology *300*, G914-926.

McDonald, N.A., and Gould, K.L. (2016). Linking up at the BAR: Oligomerization and F-BAR protein function. Cell Cycle *15*, 1977-1985.

McDonald, N.A., Takizawa, Y., Feoktistova, A., Xu, P., Ohi, M.D., Vander Kooi, C.W., and Gould, K.L. (2016). The Tubulation Activity of a Fission Yeast F-BAR Protein Is Dispensable for Its Function in Cytokinesis. Cell Rep *14*, 534-546.

McMahon, H.T., Wigge, P., and Smith, C. (1997). Clathrin interacts specifically with amphiphysin and is displaced by dynamin. FEBS Lett *413*, 319-322.

Mejillano, M.R., Kojima, S., Applewhite, D.A., Gertler, F.B., Svitkina, T.M., and Borisy, G.G. (2004). Lamellipodial versus filopodial mode of the actin nanomachinery: pivotal role of the filament barbed end. Cell *118*, 363-373.

Michael Danielsen, E., and Hansen, G.H. (2016). Small molecule pinocytosis and clathrin-dependent endocytosis at the intestinal brush border: Two separate pathways into the enterocyte. Biochim Biophys Acta *1858*, 233-243.

Millard, T.H., Bompard, G., Heung, M.Y., Dafforn, T.R., Scott, D.J., Machesky, L.M., and Futterer, K. (2005). Structural basis of filopodia formation induced by the IRSp53/MIM homology domain of human IRSp53. EMBO J *24*, 240-250.

Millard, T.H., Dawson, J., and Machesky, L.M. (2007). Characterisation of IRTKS, a novel IRSp53/MIM family actin regulator with distinct filament bundling properties. Journal of cell science *120*, 1663-1672.

Milosevic, I., Giovedi, S., Lou, X., Raimondi, A., Collesi, C., Shen, H., Paradise, S., O'Toole, E., Ferguson, S., Cremona, O.*, et al.* (2011). Recruitment of endophilin to clathrin-coated pit necks is required for efficient vesicle uncoating after fission. Neuron *72*, 587-601.

Mim, C., Cui, H., Gawronski-Salerno, J.A., Frost, A., Lyman, E., Voth, G.A., and Unger, V.M. (2012). Structural basis of membrane bending by the N-BAR protein endophilin. Cell *149*, 137-145.

Mim, C., and Unger, V.M. (2012). Membrane curvature and its generation by BAR proteins. Trends Biochem Sci *37*, 526-533.

Mogilner, A., and Rubinstein, B. (2005). The physics of filopodial protrusion. Biophys J *89*, 782-795.

Moon, H.W., Whipp, S.C., Argenzio, R.A., Levine, M.M., and Giannella, R.A. (1983). Attaching and effacing activities of rabbit and human enteropathogenic Escherichia coli in pig and rabbit intestines. Infect Immun *41*, 1340-1351.

Mooseker, M.S. (1985). Organization, chemistry, and assembly of the cytoskeletal apparatus of the intestinal brush border. Annu Rev Cell Biol *1*, 209-241.

Mooseker, M.S., Graves, T.A., Wharton, K.A., Falco, N., and Howe, C.L. (1980). Regulation of microvillus structure: calcium-dependent solation and cross-linking of actin filaments in the microvilli of intestinal epithelial cells. The Journal of cell biology *87*, 809-822.

Mooseker, M.S., and Tilney, L.G. (1975). Organization of an actin filament-membrane complex. Filament polarity and membrane attachment in the microvilli of intestinal epithelial cells. The Journal of cell biology *67*, 725-743.

Ngok, S.P., Lin, W.H., and Anastasiadis, P.Z. (2014). Establishment of epithelial polarity--GEF who's minding the GAP? Journal of cell science *127*, 3205-3215.

Nicholson-Fish, J.C., Kokotos, A.C., Gillingwater, T.H., Smillie, K.J., and Cousin, M.A. (2015). VAMP4 Is an Essential Cargo Molecule for Activity-Dependent Bulk Endocytosis. Neuron *88*, 973-984.

Niggli, V., and Rossy, J. (2008). Ezrin/radixin/moesin: versatile controllers of signaling molecules and of the cortical cytoskeleton. Int J Biochem Cell Biol *40*, 344-349.

Noris, M., and Remuzzi, G. (2005). Hemolytic uremic syndrome. J Am Soc Nephrol *16*, 1035-1050.

O'Brien, L.E., Jou, T.S., Pollack, A.L., Zhang, Q., Hansen, S.H., Yurchenco, P., and Mostov, K.E. (2001). Rac1 orientates epithelial apical polarity through effects on basolateral laminin assembly. Nat Cell Biol *3*, 831-838.

Obrig, T.G. (2010). Escherichia coli Shiga Toxin Mechanisms of Action in Renal Disease. Toxins (Basel) *2*, 2769-2794.

Oh, Y., Schreiter, J., Nishihama, R., Wloka, C., and Bi, E. (2013). Targeting and functional mechanisms of the cytokinesis-related F-BAR protein Hof1 during the cell cycle. Mol Biol Cell *24*, 1305-1320.

Ohta, K., Higashi, R., Sawaguchi, A., and Nakamura, K. (2012). Helical arrangement of filaments in microvillar actin bundles. J Struct Biol *177*, 513-519.

Otsuki, M., Itoh, T., and Takenawa, T. (2003). Neural Wiskott-Aldrich syndrome protein is recruited to rafts and associates with endophilin A in response to epidermal growth factor. J Biol Chem *278*, 6461-6469.

Padrick, S.B., and Rosen, M.K. (2010). Physical mechanisms of signal integration by WASP family proteins. Annu Rev Biochem *79*, 707-735.

Parton, R.G. (1996). Caveolae and caveolins. Curr Opin Cell Biol *8*, 542-548.

Peckham, M. (2011). Coiled coils and SAH domains in cytoskeletal molecular motors. Biochem Soc Trans *39*, 1142-1148.

Peter, B.J., Kent, H.M., Mills, I.G., Vallis, Y., Butler, P.J., Evans, P.R., and McMahon, H.T. (2004). BAR domains as sensors of membrane curvature: the amphiphysin BAR structure. Science *303*, 495-499.

Pinette, J.A., Mao, S., Millis, B.A., Krystofiak, E.S., Faust, J.J., and Tyska, M.J. (2019). Brush border protocadherin CDHR2 promotes the elongation and maximized packing of microvilli in vivo. Mol Biol Cell *30*, 108-118.

Plomann, M., Lange, R., Vopper, G., Cremer, H., Heinlein, U.A., Scheff, S., Baldwin, S.A., Leitges, M., Cramer, M., Paulsson, M.*, et al.* (1998). PACSIN, a brain protein that is upregulated upon differentiation into neuronal cells. Eur J Biochem *256*, 201-211.

Pollard, T.D., and Borisy, G.G. (2003). Cellular motility driven by assembly and disassembly of actin filaments. Cell *112*, 453-465.

Pollock, L.M., and McDermott, B.M., Jr. (2015). The cuticular plate: a riddle, wrapped in a mystery, inside a hair cell. Birth Defects Res C Embryo Today *105*, 126-139.

Postema, M.M., Grega-Larson, N.E., Meenderink, L.M., and Tyska, M.J. (2019). PACSIN2-dependent apical endocytosis regulates the morphology of epithelial microvilli. Mol Biol Cell, mbcE19060352.

Postema, M.M., Grega-Larson, N.E., Neininger, A.C., and Tyska, M.J. (2018). IRTKS (BAIAP2L1) Elongates Epithelial Microvilli Using EPS8-Dependent and Independent Mechanisms. Curr Biol *28*, 2876-2888 e2874.

Prevost, C., Zhao, H., Manzi, J., Lemichez, E., Lappalainen, P., Callan-Jones, A., and Bassereau, P. (2015). IRSp53 senses negative membrane curvature and phase separates along membrane tubules. Nat Commun *6*, 8529.

Prost, J., Barbetta, C., and Joanny, J.F. (2007). Dynamical control of the shape and size of stereocilia and microvilli. Biophys J *93*, 1124-1133.

Pykalainen, A., Boczkowska, M., Zhao, H., Saarikangas, J., Rebowski, G., Jansen, M., Hakanen, J., Koskela, E.V., Peranen, J., Vihinen, H.*, et al.* (2011). Pinkbar is an epithelial-specific BAR domain protein that generates planar membrane structures. Nat Struct Mol Biol *18*, 902-907.

Qualmann, B., and Kelly, R.B. (2000). Syndapin isoforms participate in receptor-mediated endocytosis and actin organization. The Journal of cell biology *148*, 1047-1062.

Qualmann, B., Kessels, M.M., and Kelly, R.B. (2000). Molecular links between endocytosis and the actin cytoskeleton. The Journal of cell biology *150*, F111-116.

Qualmann, B., Roos, J., DiGregorio, P.J., and Kelly, R.B. (1999). Syndapin I, a synaptic dynamin-binding protein that associates with the neural Wiskott-Aldrich syndrome protein. Mol Biol Cell *10*, 501-513.

Quinlan, M.E., Heuser, J.E., Kerkhoff, E., and Mullins, R.D. (2005). Drosophila Spire is an actin nucleation factor. Nature *433*, 382-388.

Ramesh, P., Baroji, Y.F., Reihani, S.N., Stamou, D., Oddershede, L.B., and Bendix, P.M. (2013). FBAR syndapin 1 recognizes and stabilizes highly curved tubular membranes in a concentration dependent manner. Sci Rep *3*, 1565.

Rao, Y., Ma, Q., Vahedi-Faridi, A., Sundborger, A., Pechstein, A., Puchkov, D., Luo, L., Shupliakov, O., Saenger, W., and Haucke, V. (2010). Molecular basis for SH3 domain regulation of F-BAR-mediated membrane deformation. Proc Natl Acad Sci U S A *107*, 8213-8218.

Razani, B., Wang, X.B., Engelman, J.A., Battista, M., Lagaud, G., Zhang, X.L., Kneitz, B., Hou, H., Jr., Christ, G.J., Edelmann, W.*, et al.* (2002). Caveolin-2-deficient mice show evidence of severe pulmonary dysfunction without disruption of caveolae. Mol Cell Biol *22*, 2329-2344.

Revenu, C., Ubelmann, F., Hurbain, I., El-Marjou, F., Dingli, F., Loew, D., Delacour, D., Gilet, J., Brot-Laroche, E., Rivero, F.*, et al.* (2012). A new role for the architecture of microvillar actin bundles in apical retention of membrane proteins. Mol Biol Cell *23*, 324-336.

Ritter, B., Modregger, J., Paulsson, M., and Plomann, M. (1999). PACSIN 2, a novel member of the PACSIN family of cytoplasmic adapter proteins. FEBS Lett *454*, 356-362.

Robinson, C.M., Sinclair, J.F., Smith, M.J., and O'Brien, A.D. (2006). Shiga toxin of enterohemorrhagic Escherichia coli type O157:H7 promotes intestinal colonization. Proc Natl Acad Sci U S A *103*, 9667-9672.

Roffers-Agarwal, J., Xanthos, J.B., and Miller, J.R. (2005). Regulation of actin cytoskeleton architecture by Eps8 and Abi1. BMC Cell Biol *6*, 36.

Roignot, J., Peng, X., and Mostov, K. (2013). Polarity in mammalian epithelial morphogenesis. Cold Spring Harb Perspect Biol *5*.

Roux, K.J., Kim, D.I., Burke, B., and May, D.G. (2018). BioID: A Screen for Protein-Protein Interactions. Curr Protoc Protein Sci *91*, 19 23 11-19 23 15.

Saarikangas, J., Kourdougli, N., Senju, Y., Chazal, G., Segerstrale, M., Minkeviciene, R., Kuurne, J., Mattila, P.K., Garrett, L., Holter, S.M.*, et al.* (2015). MIM-Induced Membrane Bending Promotes Dendritic Spine Initiation. Dev Cell *33*, 644-659.

Saarikangas, J., Zhao, H., Pykalainen, A., Laurinmaki, P., Mattila, P.K., Kinnunen, P.K., Butcher, S.J., and Lappalainen, P. (2009). Molecular mechanisms of membrane deformation by I-BAR domain proteins. Curr Biol *19*, 95-107.

Sakamuro, D., Elliott, K.J., Wechsler-Reya, R., and Prendergast, G.C. (1996). BIN1 is a novel MYC-interacting protein with features of a tumour suppressor. Nat Genet *14*, 69-77.

Sato, T., and Clevers, H. (2013a). Growing self-organizing mini-guts from a single intestinal stem cell: mechanism and applications. Science *340*, 1190-1194.

Sato, T., and Clevers, H. (2013b). Primary mouse small intestinal epithelial cell cultures. Methods Mol Biol *945*, 319-328.

Sato, T., Vries, R.G., Snippert, H.J., van de Wetering, M., Barker, N., Stange, D.E., van Es, J.H., Abo, A., Kujala, P., Peters, P.J.*, et al.* (2009). Single Lgr5 stem cells build crypt-villus structures in vitro without a mesenchymal niche. Nature *459*, 262-265.

Schubert, W., Frank, P.G., Razani, B., Park, D.S., Chow, C.W., and Lisanti, M.P. (2001). Caveolae-deficient endothelial cells show defects in the uptake and transport of albumin in vivo. J Biol Chem *276*, 48619-48622.

Scita, G., Confalonieri, S., Lappalainen, P., and Suetsugu, S. (2008). IRSp53: crossing the road of membrane and actin dynamics in the formation of membrane protrusions. Trends Cell Biol *18*, 52-60.

Sekerkova, G., Richter, C.P., and Bartles, J.R. (2011). Roles of the espin actin-bundling proteins in the morphogenesis and stabilization of hair cell stereocilia revealed in CBA/CaJ congenic jerker mice. PLoS Genet *7*, e1002032.

Sekerkova, G., Zheng, L., Loomis, P.A., Changyaleket, B., Whitlon, D.S., Mugnaini, E., and Bartles, J.R. (2004). Espins are multifunctional actin cytoskeletal regulatory proteins in the microvilli of chemosensory and mechanosensory cells. J Neurosci *24*, 5445-5456.

Self, T., Sobe, T., Copeland, N.G., Jenkins, N.A., Avraham, K.B., and Steel, K.P. (1999). Role of myosin VI in the differentiation of cochlear hair cells. Dev Biol *214*, 331-341.

Senju, Y., Itoh, Y., Takano, K., Hamada, S., and Suetsugu, S. (2011). Essential role of PACSIN2/syndapin-II in caveolae membrane sculpting. Journal of cell science *124*, 2032-2040.

Senju, Y., Rosenbaum, E., Shah, C., Hamada-Nakahara, S., Itoh, Y., Yamamoto, K., Hanawa-Suetsugu, K., Daumke, O., and Suetsugu, S. (2015). Phosphorylation of PACSIN2 by protein kinase C triggers the removal of caveolae from the plasma membrane. Journal of cell science *128*, 2766-2780.

Senju, Y., and Suetsugu, S. (2015). Possible regulation of caveolar endocytosis and flattening by phosphorylation of F-BAR domain protein PACSIN2/Syndapin II. Bioarchitecture *5*, 70-77.

Shifrin, D.A., Jr., McConnell, R.E., Nambiar, R., Higginbotham, J.N., Coffey, R.J., and Tyska, M.J. (2012). Enterocyte microvillus-derived vesicles detoxify bacterial products and regulate epithelial-microbial interactions. Curr Biol *22*, 627-631.

Shin, J.B., Longo-Guess, C.M., Gagnon, L.H., Saylor, K.W., Dumont, R.A., Spinelli, K.J., Pagana, J.M., Wilmarth, P.A., David, L.L., Gillespie, P.G.*, et al.* (2010). The R109H variant of fascin-2, a developmentally regulated actin crosslinker in hair-cell stereocilia, underlies early-onset hearing loss of DBA/2J mice. J Neurosci *30*, 9683-9694.

Simunovic, M., Prevost, C., Callan-Jones, A., and Bassereau, P. (2016). Physical basis of some membrane shaping mechanisms. Philos Trans A Math Phys Eng Sci *374*.

Sivadon, P., Bauer, F., Aigle, M., and Crouzet, M. (1995). Actin cytoskeleton and budding pattern are altered in the yeast rvs161 mutant: the Rvs161 protein shares common domains with the brain protein amphiphysin. Mol Gen Genet *246*, 485-495.

Skau, C.T., and Waterman, C.M. (2015). Specification of Architecture and Function of Actin Structures by Actin Nucleation Factors. Annu Rev Biophys *44*, 285-310.

Sobajima, T., Yoshimura, S., Iwano, T., Kunii, M., Watanabe, M., Atik, N., Mushiake, S., Morii, E., Koyama, Y., Miyoshi, E.*, et al.* (2014). Rab11a is required for apical protein localisation in the intestine. Biol Open *4*, 86-94.

Sorre, B., Callan-Jones, A., Manzi, J., Goud, B., Prost, J., Bassereau, P., and Roux, A. (2012). Nature of curvature coupling of amphiphysin with membranes depends on its bound density. Proc Natl Acad Sci U S A *109*, 173-178.

Specian, R.D., and Neutra, M.R. (1981). The surface topography of the colonic crypt in rabbit and monkey. The American journal of anatomy *160*, 461-472.

Steegmaier, M., Klumperman, J., Foletti, D.L., Yoo, J.S., and Scheller, R.H. (1999). Vesicle-associated membrane protein 4 is implicated in trans-Golgi network vesicle trafficking. Mol Biol Cell *10*, 1957-1972.

Stelzner, M., Helmrath, M., Dunn, J.C., Henning, S.J., Houchen, C.W., Kuo, C., Lynch, J., Li, L., Magness, S.T., Martin, M.G.*, et al.* (2012). A nomenclature for intestinal in vitro cultures. American journal of physiology Gastrointestinal and liver physiology *302*, G1359-1363.

Sudhaharan, T., Sem, K.P., Liew, H.F., Yu, Y.H., Goh, W.I., Chou, A.M., and Ahmed, S. (2016). The Rho GTPase Rif signals through IRTKS, Eps8 and WAVE2 to generate dorsal membrane ruffles and filopodia. Journal of cell science *129*, 2829-2840.

Suetsugu, S., and Gautreau, A. (2012). Synergistic BAR-NPF interactions in actin-driven membrane remodeling. Trends Cell Biol *22*, 141-150.

Suetsugu, S., Toyooka, K., and Senju, Y. (2010). Subcellular membrane curvature mediated by the BAR domain superfamily proteins. Semin Cell Dev Biol *21*, 340-349.

Sumoy, L., Pluvinet, R., Andreu, N., Estivill, X., and Escarceller, M. (2001). PACSIN 3 is a novel SH3 domain cytoplasmic adapter protein of the pacsin-syndapin-FAP52 gene family. Gene *262*, 199-205.

Svitkina, T.M., Bulanova, E.A., Chaga, O.Y., Vignjevic, D.M., Kojima, S., Vasiliev, J.M., and Borisy, G.G. (2003). Mechanism of filopodia initiation by reorganization of a dendritic network. The Journal of cell biology *160*, 409-421.

Sweeney, H.L., and Houdusse, A. (2010). Myosin VI rewrites the rules for myosin motors. Cell *141*, 573-582.

Takeda, T., Robinson, I.M., Savoian, M.M., Griffiths, J.R., Whetton, A.D., McMahon, H.T., and Glover, D.M. (2013). Drosophila F-BAR protein Syndapin contributes to coupling the plasma membrane and contractile ring in cytokinesis. Open Biol *3*, 130081.

Takei, K., Slepnev, V.I., Haucke, V., and De Camilli, P. (1999). Functional partnership between amphiphysin and dynamin in clathrin-mediated endocytosis. Nat Cell Biol *1*, 33-39.

Takemura, K., Hanawa-Suetsugu, K., Suetsugu, S., and Kitao, A. (2017). Salt Bridge Formation between the I-BAR Domain and Lipids Increases Lipid Density and Membrane Curvature. Sci Rep *7*, 6808.

Tang, V.W., and Brieher, W.M. (2012). alpha-Actinin-4/FSGS1 is required for Arp2/3-dependent actin assembly at the adherens junction. The Journal of cell biology *196*, 115-130.

Thomas, N.J., Messina, J.J., DeBruin, W.J., and Carcillo, J.A. (2005). Cardiac failure in hemolytic uremic syndrome and rescue with extracorporeal life support. Pediatr Cardiol *26*, 104-106.

Tilney, L.G., and Cardell, R.R. (1970). Factors controlling the reassembly of the microvillous border of the small intestine of the salamander. The Journal of cell biology *47*, 408-422.

Tocchetti, A., Soppo, C.B., Zani, F., Bianchi, F., Gagliani, M.C., Pozzi, B., Rozman, J., Elvert, R., Ehrhardt, N., Rathkolb, B.*, et al.* (2010). Loss of the actin remodeler Eps8 causes intestinal defects and improved metabolic status in mice. PLoS One *5*, e9468.

Tsujita, K., Suetsugu, S., Sasaki, N., Furutani, M., Oikawa, T., and Takenawa, T. (2006). Coordination between the actin cytoskeleton and membrane deformation by a novel membrane tubulation domain of PCH proteins is involved in endocytosis. The Journal of cell biology *172*, 269-279.

Tsujita, K., Takenawa, T., and Itoh, T. (2015). Feedback regulation between plasma membrane tension and membrane-bending proteins organizes cell polarity during leading edge formation. Nat Cell Biol *17*, 749-758.

Tu, Y., Liang, L., Frank, S.J., and Wu, C. (2001). Src homology 3 domain-dependent interaction of Nck-2 with insulin receptor substrate-1. Biochem J *354*, 315-322.

Tumbarello, D.A., Kendrick-Jones, J., and Buss, F. (2013). Myosin VI and its cargo adaptors - linking endocytosis and autophagy. Journal of cell science *126*, 2561-2570.

Vallance, B.A., Chan, C., Robertson, M.L., and Finlay, B.B. (2002). Enteropathogenic and enterohemorrhagic Escherichia coli infections: emerging themes in pathogenesis and prevention. Can J Gastroenterol *16*, 771-778.

Vallen, E.A., Caviston, J., and Bi, E. (2000). Roles of Hof1p, Bni1p, Bnr1p, and myo1p in cytokinesis in Saccharomyces cerevisiae. Mol Biol Cell *11*, 593-611.

van der Flier, L.G., and Clevers, H. (2009). Stem cells, self-renewal, and differentiation in the intestinal epithelium. Annu Rev Physiol *71*, 241-260.

van Dongen, J.M., Visser, W.J., Daems, W.T., and Galjaard, H. (1976). The relation between cell proliferation, differentiation and ultrastructural development in rat intestinal epithelium. Cell and tissue research *174*, 183-199.

Vehlow, A., Soong, D., Vizcay-Barrena, G., Bodo, C., Law, A.L., Perera, U., and Krause, M. (2013). Endophilin, Lamellipodin, and Mena cooperate to regulate F-actin-dependent EGF-receptor endocytosis. EMBO J *32*, 2722-2734.

Vignjevic, D., Kojima, S., Aratyn, Y., Danciu, O., Svitkina, T., and Borisy, G.G. (2006). Role of fascin in filopodial protrusion. The Journal of cell biology *174*, 863-875.

Vingadassalom, D., Kazlauskas, A., Skehan, B., Cheng, H.C., Magoun, L., Robbins, D., Rosen, M.K., Saksela, K., and Leong, J.M. (2009). Insulin receptor tyrosine kinase substrate links the E. coli O157:H7 actin assembly effectors Tir and EspF(U) during pedestal formation. Proc Natl Acad Sci U S A *106*, 6754-6759.

Wang, Q., Navarro, M.V., Peng, G., Molinelli, E., Goh, S.L., Judson, B.L., Rajashankar, K.R., and Sondermann, H. (2009). Molecular mechanism of membrane constriction and tubulation mediated by the F-BAR protein Pacsin/Syndapin. Proc Natl Acad Sci U S A *106*, 12700-12705.

Wayt, J., and Bretscher, A. (2014). Cordon Bleu serves as a platform at the basal region of microvilli, where it regulates microvillar length through its WH2 domains. Mol Biol Cell *25*, 2817-2827.

Weck, M.L., Crawley, S.W., Stone, C.R., and Tyska, M.J. (2016). Myosin-7b Promotes Distal Tip Localization of the Intermicrovillar Adhesion Complex. Curr Biol *26*, 2717-2728.

Willet, A.H., McDonald, N.A., Bohnert, K.A., Baird, M.A., Allen, J.R., Davidson, M.W., and Gould, K.L. (2015). The F-BAR Cdc15 promotes contractile ring formation through the direct recruitment of the formin Cdc12. The Journal of cell biology *208*, 391-399.

Wilson, W., Scott, R.B., Pinto, A., and Robertson, M.A. (2001). Intractable diarrhea in a newborn infant: microvillous inclusion disease. Can J Gastroenterol *15*, 61-64.

Wolny, M., Batchelor, M., Knight, P.J., Paci, E., Dougan, L., and Peckham, M. (2014). Stable single alpha-helices are constant force springs in proteins. J Biol Chem *289*, 27825-27835.

Wong, K., Ren, X.R., Huang, Y.Z., Xie, Y., Liu, G., Saito, H., Tang, H., Wen, L., Brady-Kalnay, S.M., Mei, L.*, et al.* (2001). Signal transduction in neuronal migration: roles of

GTPase activating proteins and the small GTPase Cdc42 in the Slit-Robo pathway. Cell *107*, 209-221.

Wu, T., Shi, Z., and Baumgart, T. (2014). Mutations in BIN1 associated with centronuclear myopathy disrupt membrane remodeling by affecting protein density and oligomerization. PLoS One *9*, e93060.

Yamagishi, A., Masuda, M., Ohki, T., Onishi, H., and Mochizuki, N. (2004). A novel actin bundling/filopodium-forming domain conserved in insulin receptor tyrosine kinase substrate p53 and missing in metastasis protein. J Biol Chem *279*, 14929-14936.

Yamazaki, D., Oikawa, T., and Takenawa, T. (2007). Rac-WAVE-mediated actin reorganization is required for organization and maintenance of cell-cell adhesion. Journal of cell science *120*, 86-100.

Yan, S., Lv, Z., Winterhoff, M., Wenzl, C., Zobel, T., Faix, J., Bogdan, S., and Grosshans, J. (2013). The F-BAR protein Cip4/Toca-1 antagonizes the formin Diaphanous in membrane stabilization and compartmentalization. Journal of cell science *126*, 1796-1805.

Yeh, T.C., Ogawa, W., Danielsen, A.G., and Roth, R.A. (1996). Characterization and cloning of a 58/53-kDa substrate of the insulin receptor tyrosine kinase. J Biol Chem *271*, 2921-2928.

Yi, C.R., and Goldberg, M.B. (2009). Enterohemorrhagic Escherichia coli raises the I-BAR. Proc Natl Acad Sci U S A *106*, 6431-6432.

Yu, I.M., Planelles-Herrero, V.J., Sourigues, Y., Moussaoui, D., Sirkia, H., Kikuti, C., Stroebel, D., Titus, M.A., and Houdusse, A. (2017). Myosin 7 and its adaptors link cadherins to actin. Nat Commun *8*, 15864.

Zaidel-Bar, R., Joyce, M.J., Lynch, A.M., Witte, K., Audhya, A., and Hardin, J. (2010). The F-BAR domain of SRGP-1 facilitates cell-cell adhesion during C. elegans morphogenesis. The Journal of cell biology *191*, 761-769.

Zampini, V., Ruttiger, L., Johnson, S.L., Franz, C., Furness, D.N., Waldhaus, J., Xiong, H., Hackney, C.M., Holley, M.C., Offenhauser, N.*, et al.* (2011). Eps8 regulates hair bundle length and functional maturation of mammalian auditory hair cells. PLoS Biol *9*, e1001048.

Zhao, H., Michelot, A., Koskela, E.V., Tkach, V., Stamou, D., Drubin, D.G., and Lappalainen, P. (2013). Membrane-sculpting BAR domains generate stable lipid microdomains. Cell Rep *4*, 1213-1223.

Zhao, H., Pykalainen, A., and Lappalainen, P. (2011). I-BAR domain proteins: linking actin and plasma membrane dynamics. Curr Opin Cell Biol *23*, 14-21.

Zheng, L., Sekerkova, G., Vranich, K., Tilney, L.G., Mugnaini, E., and Bartles, J.R. (2000). The deaf jerker mouse has a mutation in the gene encoding the espin actin-bundling proteins of hair cell stereocilia and lacks espins. Cell *102*, 377-385.

Zhu, C., Das, S.L., and Baumgart, T. (2012). Nonlinear sorting, curvature generation, and crowding of endophilin N-BAR on tubular membranes. Biophys J *102*, 1837-1845.

Zimmerberg, J., and Kozlov, M.M. (2006). How proteins produce cellular membrane curvature. Nat Rev Mol Cell Biol *7*, 9-19.